EXPERIMENTAL INVESTIGATION INTO THE AERODYNAMIC GROUND EFFECT OF A TAILLESS CHEVRON AND LAMBDA-SHAPED UCAVS

THESIS

Won In, Captain, USAF
AFIT/GAE/ENY/06-M16

DEPARTMENT OF THE AIR FORCE
AIR UNIVERSITY

AIR FORCE INSTITUTE OF TECHNOLOGY

Wright-Patterson Air Force Base, Ohio

AFIT/GAE/ENY/06-M16

EXPERIMENTAL INVESTIGATION INTO THE AERODYNAMIC GROUND EFFECT OF A TAILLESS CHEVRON AND LAMBDA-SHAPED UCAVS

THESIS

Presented to the Faculty

Department of Aeronautics and Astronautics

Graduate School of Engineering and Management

Air Force Institute of Technology

Air University

Air Education and Training Command

In Partial Fulfillment of the Requirements for the

Degree of Master of Science in Aeronautical Engineering

Won In, BSE

Captain, USAF

March 2006

AFIT/GAE/ENY/06-M16

EXPERIMENTAL INVESTIGATION INTO THE AERODYNAMIC GROUND EFFECT OF A TAILLESS CHEVRON AND LAMBDA SHAPED UCAVS

Won In, BSE
Captain, USAF

Approved:

/signed/

_____ _____
Dr. Milton E. Franke (Chairman) date

/signed/

_____ _____
Dr. Mark F. Reeder (Member) date

/signed/

_____ _____
Lt Col Eric J. Stephen (Member) date

Abstract

As future aircraft migrate toward tailless, blended wing body configurations, aircraft designers are faced with a lack of experimental data that represent these types of configurations. A wind tunnel investigation was conducted to identify the ground effect region of two unmanned combat air vehicle (UCAV) models. The AFIT low-speed wind tunnel (LSWT) and ground plane were used to study the forces and moments on the UCAV models in ground effect. The Chevron and Lambda planforms used in this study were originally tested in full-scale for stability and control without ground effects. A static ground plane was used in this study. Hot-wire results showed a minimal difference between the transducer velocity and the hot-wire measured velocity and these differences were accounted for as wind tunnel blockage. In addition to hot-wire results, flow visualization results revealed the AFIT LSWT had an adequate testing environment for the use of the ground plane. The ground effect regions for the Chevron and Lambda UCAVs were characterized by an increase in lift and drag, and a decrease in lift-to-drag ratio.

To my parents and sisters for their love and support in every endeavor of my life and to my wife and two sons for their patience and encouragement throughout this entire project.

Acknowledgements

I would like to thank the Air Vehicles Directorate of the Air Force Research Lab for their support and resources for this project. Also, I would like to thank my thesis advisor, Dr. Franke for his vision and guidance. I would like to also express my sincere gratitude to Dwight Gehring, AFIT/ENY, and Ryan Plumley, AFRL/VAAA, for their work. Mr. Gehring was instrumental in the set-up, calibration, and operation of the AFIT LSWT. Mr. Plumley assisted with coordination of meetings and information flow between AFIT and VAAA that was vital to the successful completion of this study. Additionally, Randy Miller, AFIT/ENY, deserves the credit for the set-up and operation of the FaroArm Platinum with Laser ScanArm for digitization and rapid prototyping of the Lambda UCAV model and Vincent Parisi, AFRL/HECV, for his initial assistance with the 3-D digitization process. I want to thank Dr. Reeder for his assistance with the analysis of the wind tunnel data reduction code and results along with LtCol Stephen, USAF, and 1Lt Westfeld, USAF, for assisting with Lambda analysis of the vortex lattice method and CFD analysis in FLUENT respectively. Lastly, I want to thank God for His guidance and strength throughout this entire project.

Won In

Table of Contents

Page

List of Figures

Page

Page

Page

List of Tables

Page

Page

List of Symbols

Symbol	Name
a	speed of sound
A	axial force (body axis)
A_1	balance axial sensor
AR	aspect ratio
b	wing span
C	tunnel test area
C_D	drag coefficient
CG	center of gravity
C_L	lift coefficient
C_m	pitch moment coefficient
C_P	pressure coefficient
c_r	wing root chord
D	drag force (wind axis)
h	height above ground
k	induced drag constant
L	lift force (wind axis)
l	roll moment
l_1	balance roll moment sensor
L/D	lift-to-drag ratio
M	Mach number
m	pitch moment
N	normal force (body axis)
N_1 & N_2	balance normal sensors
P	test room pressure
q_∞	free stream dynamic pressure
R	Ideal gas constant
Re	Reynolds number
S*	side force (wind axis)
S	wing area
S_1 & S_2	balance side sensors
T	test room temperature
U	boundary layer velocity
U_∞	free stream velocity
UCAV	unmanned combat air vehicle
Y	side force (body axis)
α, AOA	angle of attack ($\alpha = \theta$)
γ	ratio of specific heats (c_p / c_T)
μ	air viscocity
ρ	air density
ϕ	induced drag factor
ψ	yaw angle

EXPERIMENTAL INVESTIGATION INTO THE AERODYNAMIC GROUND EFFECT OF A TAILLESS CHEVRON AND LAMBDA-SHAPED UCAV

I. Introduction

Section 1 – Ground Effect

Since the early days of aviation, pilots have experienced a ground effect phenomenon while operating their aircraft very close to the ground. During take-off or landing, an aircraft will experience improved efficiency near the ground in the form of increased lift and decrease in induced drag. However, this poses a problem because most aircraft are not designed for this flight condition and pilots have to manually adjust for each type of aircraft (1).

A typical aircraft is in-ground-effect (IGE) when it is within one wingspan of the ground (2). The amount ground effect experienced by an aircraft is partially dependent on the amount of induced drag. When the height of an aircraft is below one wingspan of the ground, the induced drag significantly decreases due to the wingtip vortices interacting with the ground (2). During normal flight, wingtip vortices are cylindrical in shape, but while in interference with the ground, they tend to flatten out at the trailing end which increases the effective wingspan and aspect ratio. Since aspect ratio has a strong inverse effect on induced drag, an aircraft flying very near the ground will experience a reduction in induced drag therefore reducing the total drag of the aircraft (2).

In addition, an increase in lift and pitching moment are characteristics of an aircraft in ground effect. The increase in lift along with the reduction of drag

significantly increases the lift-to-drag ratio, which increases the overall aircraft efficiency. (1).

Section 2 – Unmanned Air Vehicles

Since the beginning of aviation, the engineers and scientists have been intrigued by the concept of unmanned flight. The first unmanned air vehicles (UAV) were built to be used as guided missiles. The Kettering "Bug" and Sperry aerial torpedo were the first two combat UAVs but were never used in operation due to their inaccuracy. As technology advanced, researchers investigated the use of radio and eventually television control links to correct the navigation issues (1). Significant advances during the last quarter-century in computing capabilities, electronics miniaturization, communications, guidance, navigation, and control have allowed for successful flight operations of the Global Hawk and Predator UAVs. The UAVs such as the Global Hawk and Predator are currently being used daily in conflicts around the world (3).

Current development of unmanned flight is in the unmanned combat air vehicle (UCAV). Today, the primary program for UCAV exploration is the joint unmanned combat air systems (J-UCAS) program involving a joint program with the Defense Advanced Research Projects Agency (DARPA), Air Force, and Navy. The J-UCAS program is designed to demonstrate the technical feasibility, military utility and operational value for a networked system of high performance, weaponized unmanned air vehicles. The J-UCAS program's goal are to effectively and affordably prosecute 21st century combat missions, including Suppression of Enemy Air Defenses (SEAD),

surveillance, and precision strike within the emerging global command and control architecture. (4)

The two leading UCAVs of the J-UCAS program are the Boeing X-45 and the Northrop Grumman X-47. The X-45 will combine advance air vehicle hardware, including integrated sensors, communication, navigation equipment and low-observability features with the J-UCAS Common Operating System to demonstrate the capabilities of the J-UCAS system in realistic mission scenarios. (4) Both the X-45 and the X-47 have an unconventional configuration to include a tailless blended wing body with swept wings. Although, today's advanced control systems allow for such unconventional designs, the ground effect phenomenon still poses problems (1).

Section 3 – UAVs and Ground Effect

The location and the extent of the ground effect region is of particular interest for UAVs because of the fact that they are unmanned. Pilots use sight and feel to adjust accordingly for increase in flight performance when operating a conventional aircraft near the ground. During landings, a pilot will normally flare the aircraft to ensure that the rear landing gear makes contact with the flightline first. A pilot makes small adjustments to the aircraft attitude for the drag reduction and increase in lift while in the ground effect region (1). The pilot for a UAV operates the aircraft from a Ground Control Station (GCS) and uses real time video and sensors for feedback information. The remote operator or UAV pilot cannot feel the effects of the ground during take off and landing and relies entirely on the automatic control system. To ensure UAV's safe take-offs and landings, it is essential to identify the ground effect region. Normally, the ground effect

region is not factored into the landing control system design since the ground effect region is a small portion of time compared to the entire glide slope to land. However, with sufficient data from flight tests or wind tunnel tests, the control engineer will make gain adjustments to account for the ground effect region (5).

Unmanned flight research suffered numerous mishaps near the ground. One of particular interest was on 22 April 1996, when the Lockheed Martin/Boeing RQ-3A DarkStar's fight control system did not accurately account for ground effect. It 'porpoised' during take-off, pitched up, and stalled due to over-correction by ailerons (6).

Section 4 – Boeing AFRL/VAAA UCAV Program

In an effort to expand the database for unconventional aircraft, Capt. Shad Reed of the Air Vehicles Directorate (VAAA) of the Air Force Research Laboratory (AFRL) conducted a low-speed wind tunnel stability and control investigation on three advanced UCAV configuration. The test program defined the stability and control characteristics of moderately swept, low aspect ratio, tailless, blended wing body planforms. The three planforms tested were two arrow type, Chevron and Lambda planforms, and one diamond type, Diamond planform. Their characteristics are found in reference 7. Of the three advance configurations tested, the Chevron planform had the highest maximum lift coefficient, highest lift-to-drag ratio, and lowest minimum drag coefficient. However, Reed concluded that due to the Chevron planform's lack of fuselage, subsystem integration would be difficult since engines, weapons, and other components are normally located in the fuselage. A ground effects test for the Chevron planform is still

of interest because improved technology can solve the apparent subsystem integration problems identified by Reed (7).

Lambda planform was also included in this ground effect study because it was concluded to have adequate stability by Reed. Lambda planform's configuration also will allow more conventional subsystem integration. This combination of aerodynamic characteristics and ease of integration makes Lambda planform configuration the most viable of the three planforms tested by Reed (7).

II. Literature Review

Section 1 – Ground Effect Theory

From the beginning of flight, aircraft designers realized an increase in lift while in close proximity to the ground. Engineers conducted numerous wind tunnel and flight test studies around the world in order to investigate ground effect.

In 1922, Wieselsberger developed his theoretical equation for estimating the induced drag reduction of aircraft near the ground. He used Prandl's three-dimensional wing theory and the reflection method to establish a relatively simple relationship between induced drag and height above ground (8). His famous equation became the standard for predicting ground effect and was verified throughout the 1930s and 1940s in references 9 and 10.

Another theoretical approach for estimating the decrease in induced drag due to the ground is McCormick's induced drag factor. In his section on ground roll and takeoff distance, McCormick derived Equation [1] by replacing a rectangular wing with a simple horseshoe vortex modeled with its image so the vertical velocity components cancel each other out simulating the ground. The height was the distance between the reflection plane to the horseshoe vortices. McCormick used the Biot-Savart Law to estimate the velocity induced at a point from each horseshoe vortex. This led him to identify a ratio between the induced drag in ground effect and the induced drag out-of-ground effect (11).

$$\phi = \frac{\left[16\left(h/b\right)\right]^2}{1+\left[16\left(h/b\right)\right]^2} \tag{1}$$

A ground effect is normally experienced at heights above ground less than one wingspan, and the effect is increased exponentially as the aircraft flies below half of a wingspan as demonstrated in references 12, 13, and 14. Equation (1) provides a prediction for ground effect when multiplied by the induced drag,. Figure1 is a plot of McCormick's induced drag factor (1).

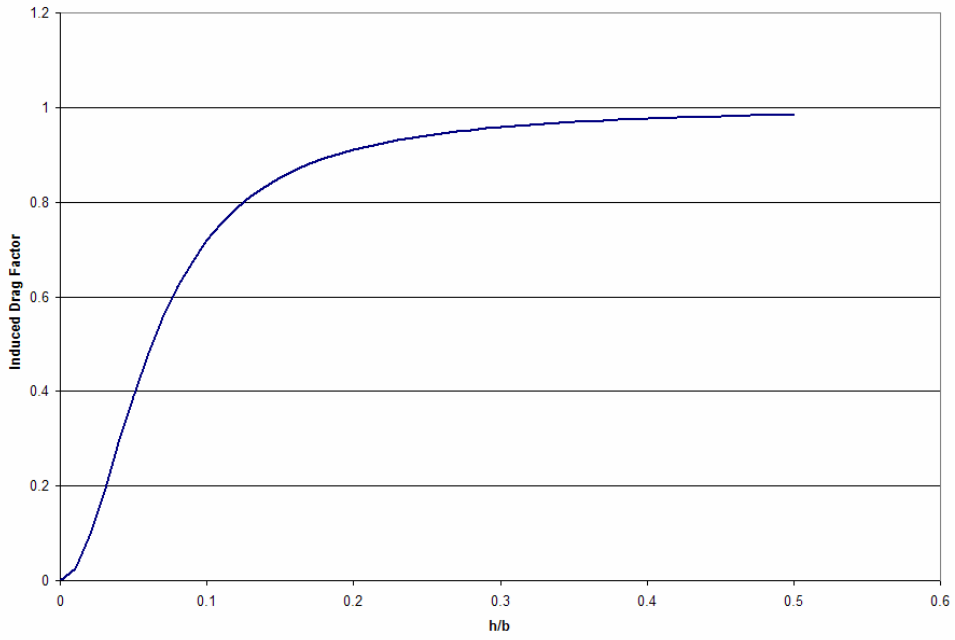

Figure 1: McCormick's Induced Drag Factor

Equation (2) below shows the relationship of the total drag coefficient, C_D, with respect to the parasite drag, C_{D0}, due to skin friction and form drag, McCormick's

induced drag factor, ϕ, combined coefficient of induced drag and viscous drag, k, and lift coefficient, C_L (1).

$$C_D = C_{D0} + \phi k C_L^2$$

(2)

Section 2 – Planform Shapes

An innovative configuration work has been done by Adamczak related to UAV planforms (29). This investigation gathered force and moment data on a Lambda wing planform with a cylindrical fuselage and ogive forebody at low and transonic speeds. Flow visualization revealed a tendency for the flow to separate at the mid span wing kink. Gatlin and McGrath (30) conducted a comprehensive investigation of the low speed longitudinal characteristics of twenty-one new planform shapes. Aerodynamic force and moment data were taken from 0º to +70 º AOAs at a dynamic pressure of 30 psf. All tested planforms were cut from a 0.25 inch thick steel plate and have beveled leading edges (7).

As mentioned in section I, little experimental data exists on configurations that resemble the configuration tested in this study. Ross, Fears, and Moul (31-33), conducted studies that are applicable set of experimental data. Their research focused on combinations of aspect ratio, planform shape and leading edge sweep. The research showed a slight increase in lift with an increase in aspect ratio (7).

The primary difference between the configurations studied by Ross, et al., and the configurations presented in this study is the thickness effect. The study conducted by Ross, et al., focused on the gross effects of planform and configuration using crude balance housings to represent fuselage effects and beveled flat plates for the wing surfaces. The current test is focussed on the combined effects of planform, and thickness using notional fuselage shapes for the wings. Because little experimental data exists for configuration of this class, designers are currently forced to extrapolate data from other sources which can lead to poor designs. The data gathered in this test program will provide aircraft designers with a valuable experimental database which can be used to estimate the system level performance impacts of configuration design variables, such as wing sweep, planform, fuselage shape and aspect ratio (7).

Section 3 – Static vs. Dynamic Wind Tunnel Testing

The ground effects experimental methods have become more sophisticated during the past several decades. One of the first wind tunnel investigations was Raymond's study at the Massachusetts Institute of Technology in 1921 (15). He analyzed ground effect by testing three different airfoils in a wind tunnel by using a flat plate for a ground plane. He also attempted to create an imaginary ground plane condition by a reflection method. Both methods revealed similar results except at high angles of attack. Raymond's test confirmed that when near the ground, an airfoil will increase in lift and decrease in induced drag (1).

As testing continued, Raymond's flat plate method took the name of static wind tunnel testing. A static wind tunnel test involves a fixed ground plane height with fixed

model. Moving the model closer to the ground plane is normally how various heights above ground are simulated. In order to validate these tests, test pilots flew ground effect testing routes, called 'fly-by' patterns. To determine the location of the ground effect region, altitude and angle of attack were held constant. However, in 1967, William Schweikhard developed a method for measuring the ground effects of an aircraft as it approached a runway (16). A test pilot would maintain a constant angle of attack and power setting, but would let the sink rate vary. This flight test technique ensured that lift, drag, and pitching moment were constant just before approaching the ground. Once in the ground effect region, flight test engineers measured changes in flight path angle, velocity, or control surface deflection. They found that this technique saved time and data analysis over standard fly-by or static tests (16).

In an effort to reduce high flight test costs, engineers developed dynamic test methods for ground effect in a wind tunnel. A dynamic wind tunnel test method attempts to better simulate a landing approach or a take-off by manually or mechanically moving the model towards the ground plane. Chang et al. found a disparity between static tests and landing data in regards to dynamic wind tunnel testing (17). He tested delta wings of 60, 70, and 75 deg sweep, the XB-70, and the F-104A statically and dynamically. He, along with Baker et al., concluded that the static wind tunnel results for the delta wings and XB-70 significantly over predicted the change in lift due to ground effect at heights of $h/b < 0.4$ (12). However, he also stated that the amount of difference between static and dynamic results decreased as aspect-ratio increased as in Figure 2 (1).

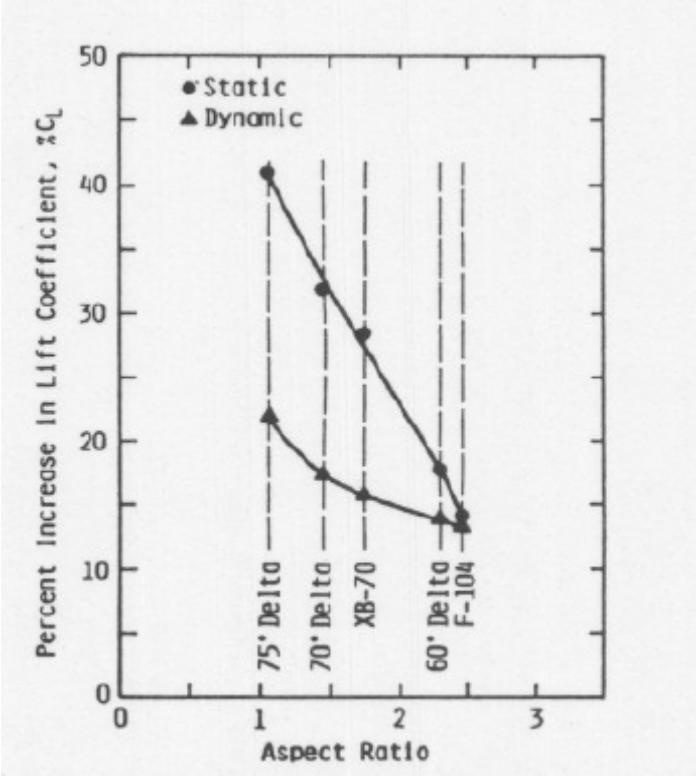

Figure 2: Incremental C_L vs. AR for static and dynamic ground effect at h/b=0.3 (12)

Additionally, Corda, et al. (18) performed a dynamic ground effect tests on the F-15. Their results are mentioned because the Chevron and Lambda UCAVs have similar aspect ratios to that of the F-15. They are relevant to the following equation of the dynamic ground effect tests for the delta wings presented in Figure 3:

$$\%\Delta C_{L,GE} = \left(\frac{0.2}{AR} + 0.04\right) * 100 \qquad (3)$$

Equation (3) quantifies the relationship between percent increase in lift coefficient due to ground effect and aspect ratio of a wing. Based on this prediction the Chevron and Lambda UCAVs should experience a 10.9% and 11.3% increase in lift respectively due

to ground effect. More importantly, this relationship presented in Figure 3 suggests that static ground effect tests for the Chevron and Lambda UCAVs should produce similar results as dynamic tests (1).

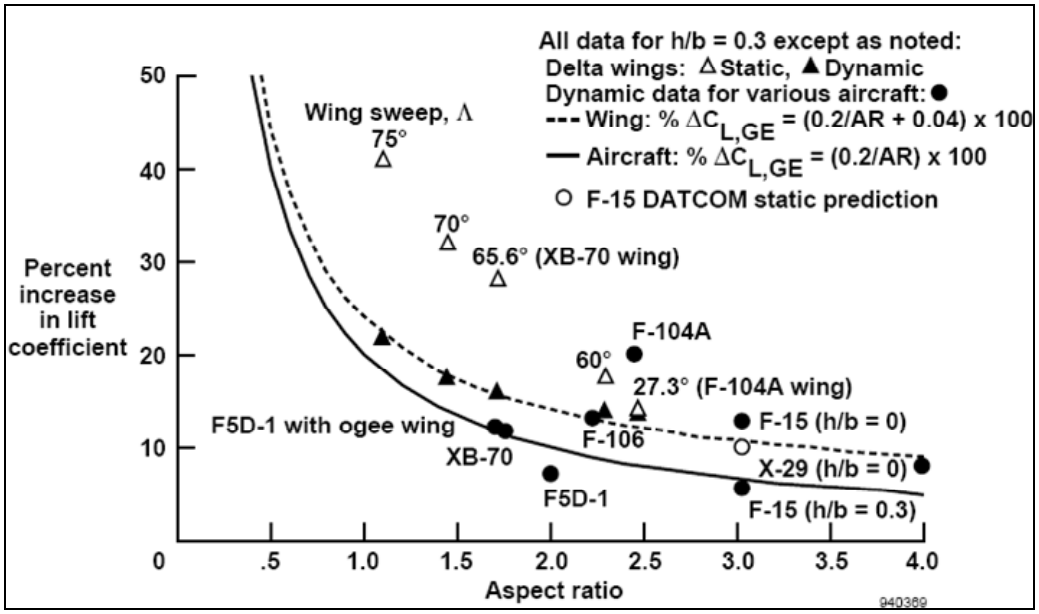

Figure 3: Percent Increase in C_L in Ground Effect vs. AR for Various Aircraft (18)

One of the common tools used to predict and verify ground effect tests is the U.S. Air Force Data Compendium (DATCOM) (19). This analytical code uses equations, charts, and flight data to predict stability and control characteristics of an aircraft (1).

Section 3.1 – Adverse Ground Effect

Although ground effect is normally characterized by an increase in lift and a decrease in drag, not all aircraft configurations experience these beneficial traits. Lee, et al. (13) reported an increase in lift along with an increase in drag as height above ground decreased (1).

Lee, et al. performed dynamic and static wind tunnel tests on models of a 60 deg delta wing, F-106, and XB-70-1. They varied Re from $3x10^5$ to $7.5x10^5$ and height above ground from h/b=1.6 to h/b=0.2 for all three models. No emphasis was placed on the increasing lift or drag because the primary focus was on the differences between the static and dynamic test results. The C_D vs. (h/b) plot for the F-106 in Figure 4 represents their results (1).

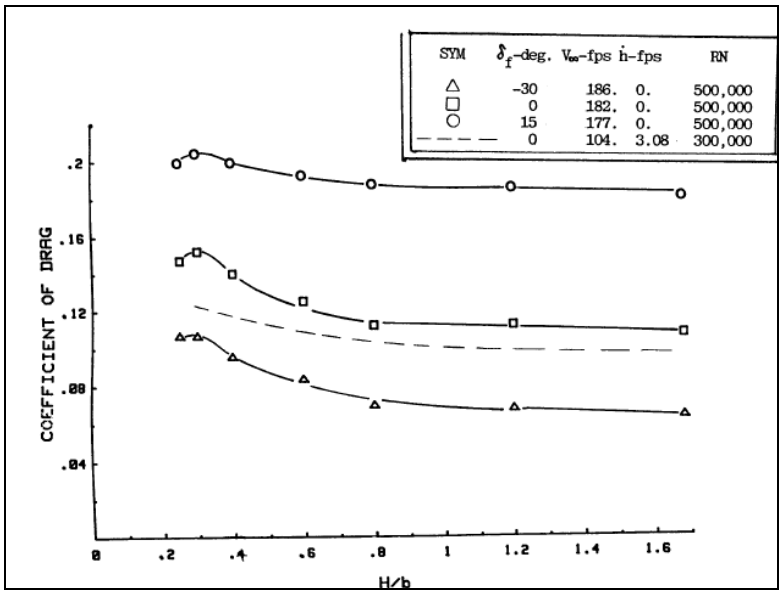

Figure 4: Ground Effect for the F-106 at an AOA = 14 deg (13)

Even though Lee, et al. did not show any L/D results, Jones (1) extrapolated static data from their C_D vs. (h/b) plots (similar to Figure 4) and C_L vs. (h/b) for each model to analyze the trends. Jones concluded that the 60 deg delta wing experienced a subtle decrease in L/D. Also, the F-106 and XB-70-1 both experienced a decrease and a slight increase in L/D at the lowest height above ground. The decreasing trend of C_D between

h/b=0.3 and 0.2 in Figure 4 was common for the XB-70-1 and explained the increasing trend in L/D (1).

Section 4 – Boundary Layer Removal

The boundary layer build-up across the top surface is one of the limitations using a ground plane in a wind tunnel for ground effect study. Boundary layers form on any surface where a moving fluid has direct contact and cause an unrealistic test condition in wind tunnels. A boundary layer removal system is typically utilized to resolve this issue (1).

One of the methods of removing the boundary layer in a wind tunnel is to use a moving-belt ground plane. A moving-belt ground plane would better simulate an aircraft flying over the ground where the belt would spin at the same velocity of the air, which in turn does not allow the boundary layer to form` (1).

While it seems that boundary layer removal with a moving-belt ground plane is essential to achieving proper flight dynamics, two different studies were conducted that showed the necessity of a moving-belt ground plane depends on the maximum lift coefficient of the air vehicle (1). Turner (20) investigated the use of conventional ground planes for ground effect in wind tunnel testing. More specifically, he examined the possible use of endless-belt ground planes and determined the conditions where it would be necessary to have a moving ground plane. He concluded that the use of a moving-belt ground plane depended on spanwise lift coefficient and height above ground (20).

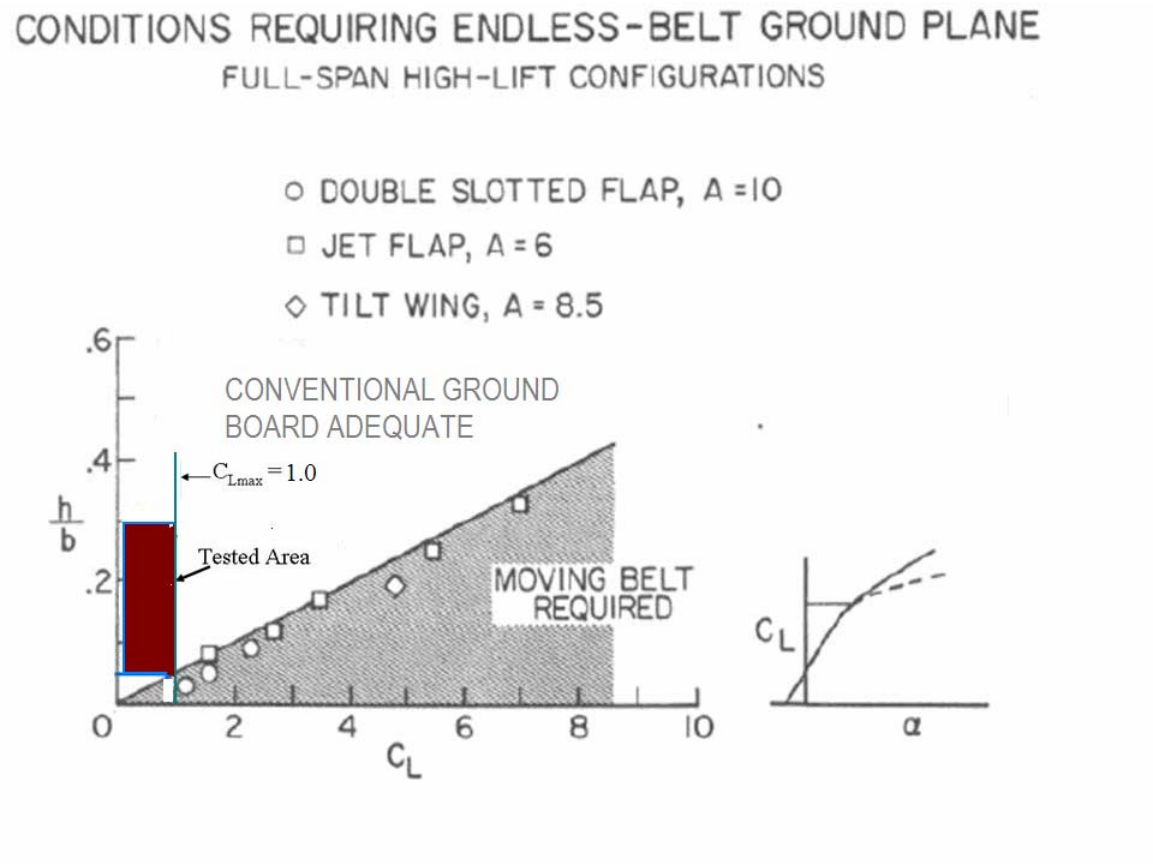

Figure 5: Conditions Requiring an Endless-belt Ground Plane (20)

The shaded box in Figure 5 indicates the region tested in this study, and the C_L max line is 1.0 compared to 0.9 in Reed's study (7). According to Turner, a moving-belt ground plane was not required for this experiment.

Kemmerly and Paulson, Jr. did a similar study investigating the use of a conventional ground plane (21). Their study evaluated an F-18 and delta wing models, and they concluded that if the condition in Equation (4) was satisfied, then an engineer must use a moving-belt ground plane to study ground effects (1).

$$\frac{(h/b)}{C_L} < 0.05 \qquad (4)$$

According to the heights used in this study and the maximum lift coefficient according to Reed, a conventional flat-plate ground plane without a moving-belt was adequate to properly measure ground effects, Table 1 and Table 2 shows that Equation (4) was not satisfied (1).

Table 1: Justification for a Flat-plate Ground Plane for Chevron UCAV Planform (1)

Chevron UCAV Planform			
h/b	C_L max	(h/b) / C_L max	< 0.05
0.3	1.0	0.3	No
0.15	1.0	0.15	No
0.1	1.0	0.1	No
0.05	1.0	0.05	No

Table 2: Justification for a Flat-plate Ground Plane for Lambda UCAV Planform

Lambda UCAV Planform			
h/b	C_L max	(h/b) / C_L max	< 0.05
0.33	1.0	0.33	No
0.16	1.0	0.16	No
0.11	1.0	0.11	No
0.05	1.0	0.05	No

Section 5 – Goals of the Experimental Effort

Reed stated that the Chevron planform performed the best with respect to aerodynamics and longitudinal/lateral stability but the Lambda planform had a combination of aerodynamic characteristics and ease of integration. A ground effect

analysis in this study will further the investigation of the aerodynamics of an advanced aircraft configuration.

The goal of this effort is to:

- identify the ground effect region of the Chevron and Lambda planforms with respect to height above the ground;
- use analytical tools to help understand the experimental results of the Chevron and Lambda planforms
- verify Chevron and Lambda planforms' aerodynamic out-of-ground effect data with Reed's study.
- expand the existing aerodynamic database for moderately swept, low aspect ratio, tailless, blended wing body UAVs

III. Experimental Set-up & Procedures

The following chapter will explain the various resources and materials used to test the Chevron and Lambda UCAV models in ground effect in addition to an outline of the wind tunnel testing procedures.

Section 1 – Wind Tunnel

Section 1.1 – Equipment

The UCAV wind tunnel investigations were done at the AFIT LSWT fabricated by the New York Blower Company. The AFIT LSWT is an open circuit subsonic wind tunnel with test section measuring 31"x 44". It includes an ACF/PLF Class IV fan with a Toshiba Premium Efficiency (EQP III) fan motor controlled by the Siemens (13710) Adjustable Frequency Tunnel Controller. The fan motor and controller specifications can be found in Table 3 (1). Figure 6 illustrates the complete schematic of the AFIT LSWT.

Table 3: Fan and Controller Specifications (1)

Specifications	
Fan Motor	**Controller**
3 phase induction	
4 Poles	
60 Hz	
230/460 Volts	460 Volts
444/222 Amps	315 Amps
200 Brake Horsepower	250 max HP
1785 RPM Operating Speed	
150 mph - Theoretical Max	
148 mph - Tested Max	

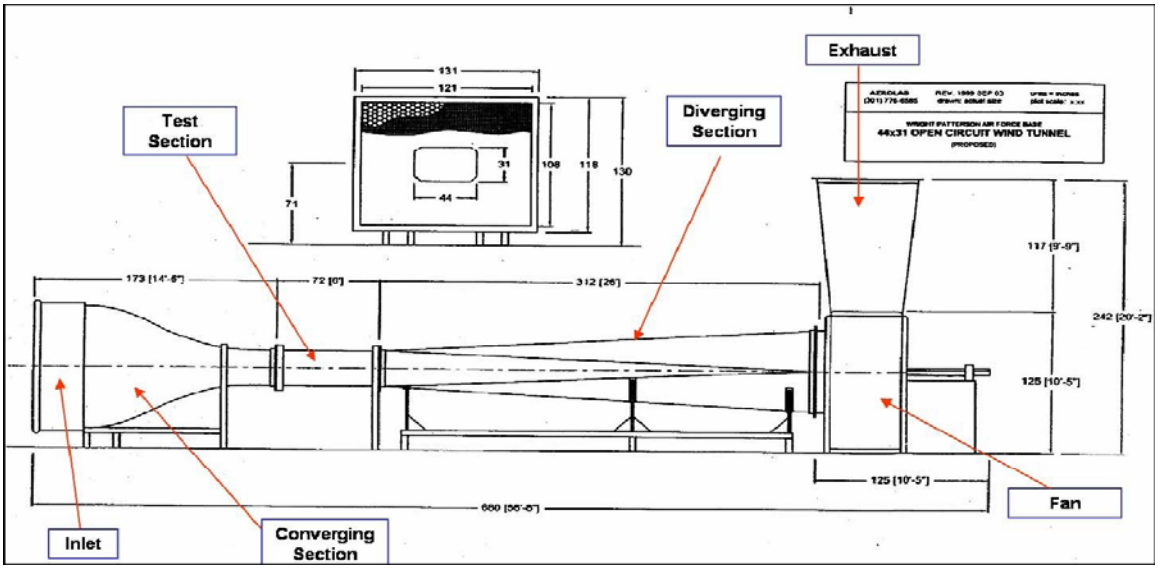

Figure 6: Wind Tunnel Schematic (22)

The AFIT LSWT is an Eiffel-type, open circuit configuration with a closed test section and is capable of generating test section velocities upto 148 mph at atmospheric pressure with its fan. The tunnel fan draws ambient air through the 122-in wide by 111-in tall by 70-in deep intake plenum, which has an internal quarter-inch aluminum honeycomb flow-straightener and steel mesh anti-turbulence screens. After the flow passes the last anti-turbulence screen it passes through the convergent section of the tunnel, which is 95.5-in long and has a contraction ratio of 9.5:1 (1).

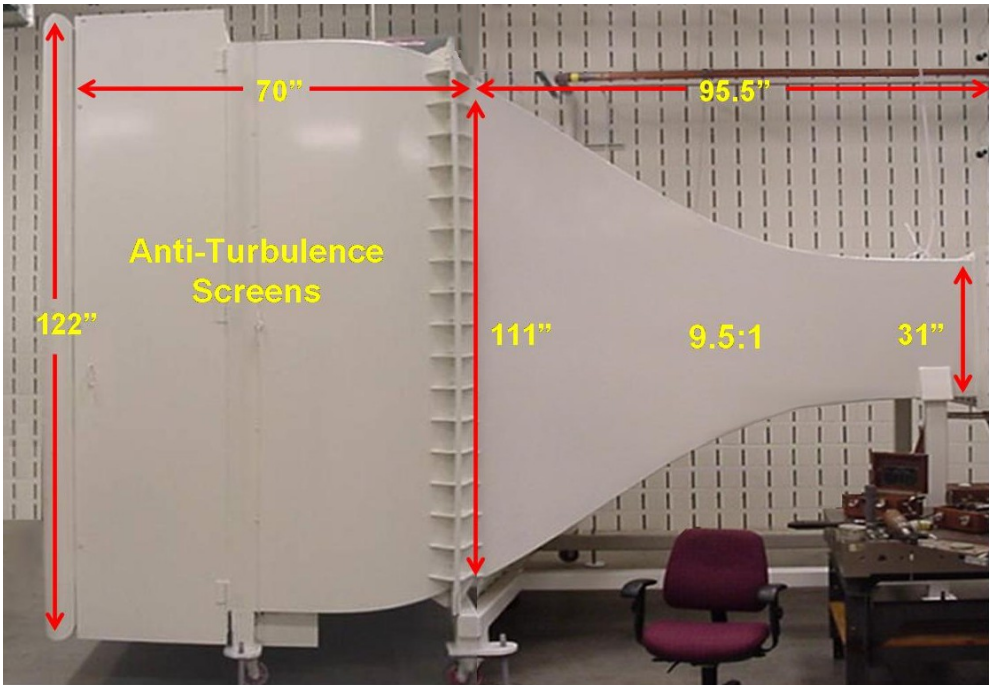

Figure 7: Wind Tunnel Intake and Convergent Sections with Dimensions (23)

After the convergent section, the flow passes through the test section. The test section is octagonal in shape for elimination of the corner interference effects and has dimensions of 31.5-in tall, 44-in wide, and 72-in long. The span-to-tunnel width ratio for Chevron UCAV model is 0.37 and for Lambda UCAV model is 0.33, which are well below the recommended value of 0.8 (24). In addition, the ground plane frontal area is 6.7% of the test-section cross-sectional area, which is below the recommended value of 7.5% (24).

The model support system consisted of a sting support that is positioned in the test section through a slot in the traverse circular plate. This remote controlled device can vary the angle of attack of the model from -25^{o} to $+25^{o}$. For yaw angle, the traverse

circular plate can rotate along with the entire sting mechanism and can be rotated from -20° to +20° (1).

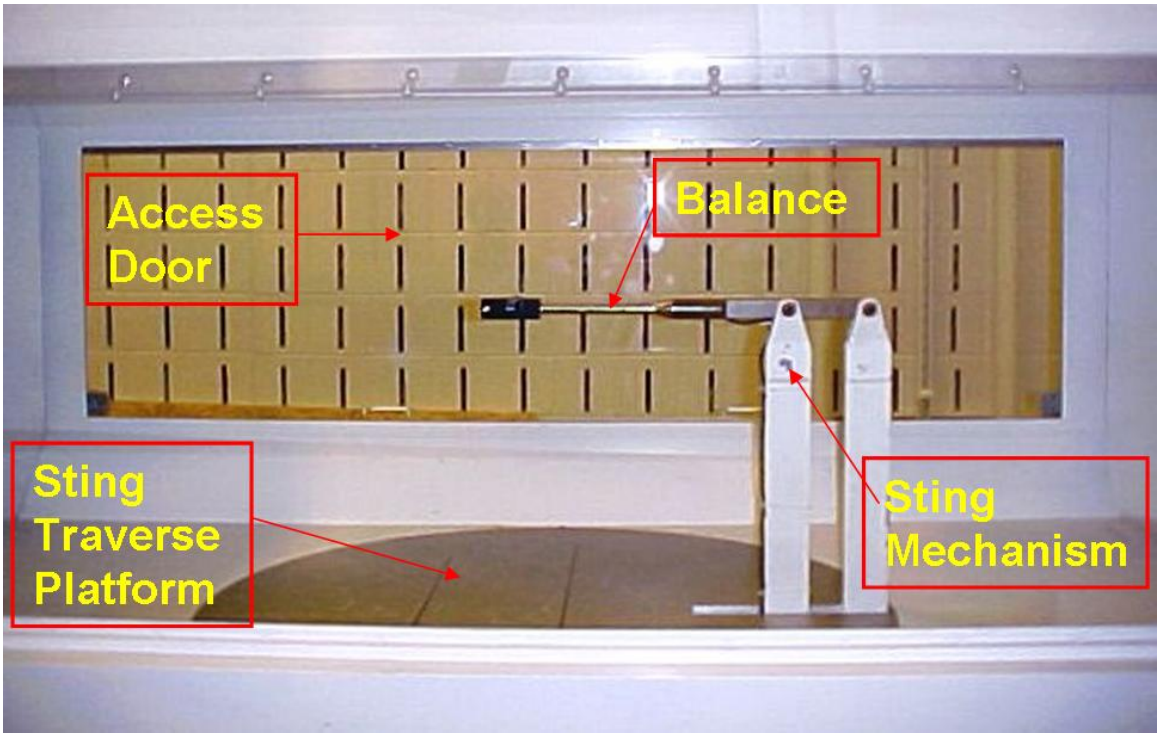

Figure 8: Wind Tunnel Test Section and Components (22)

The balance used for this test was the AFIT-100 lbf balance (S/N 16080), an internal six-component balance manufactured by Able Corporation. See the complete capacity of strain gage rosettes listed in Table 4 (1).

Table 4: AFIT-100 lbf Balance Maximum Loads (S/N 16080)

Component	Maximum Load
Normal Force (N1)	100 lbs
Pitch Moment (N2)	100 in-lbs
Side Force (S1)	50 lbs
Yaw Moment (S2)	50 in-lbs
Axial Force (A1)	50 lbs
Roll Moment (L1)	40 in-lbs

After the flow travels through the test section, it enters the 26-ft long divergent section. The divergent section includes a model catcher in case of any component failure. Once through the divergent section, the flow travels through the fan and exits vertically up through the exhaust pipe (1).

Section 1.2 – Procedure

A static weight calibration was carried out first. Known calibration weights were attached to the balance and the calibration constants were adjusted in the data collection software by matching the loads on the balance to the loads registered in the software. Linearity was verified by ensuring that the balance weights converted from the voltages corresponded linearly to the increases in weights attached. LabView Virtual Instrument© interface was used to control all tunnel parameters to include angle of attack, yaw angle, and tunnel speed. The analog backups of angle of attack and sideslip angle were also monitored with sting mounted optical encoders in addition to the interface control parameters. The analog measurements for velocity were from a pressure transducer and a pitot-static tube. These analog measurements were the main guide for tunnel velocity throughout all the test runs (1).

The measured data from the balance was stored in the format of two normal force components (N_1 & N_2), two side force components (S_1 & S_2), an axial force component (A_1), and a roll moment component (ℓ_1). The resistance was measured across the wire filament while the voltage was continuously applied to the strain gage rosette. The

applied load elongated the wire increasing the resistance. Output voltages from the increased resistance were equated to strain and force through a series of calibration equations. A conventional coordinate system was used in the tunnel with +x-direction pointing towards the intake, +y-direction pointing out towards the right access door looking from aft to forward of the test section, and +z-direction pointing down towards the tunnel floor. See Figure 9 for an illustration of the coordinate system (1).

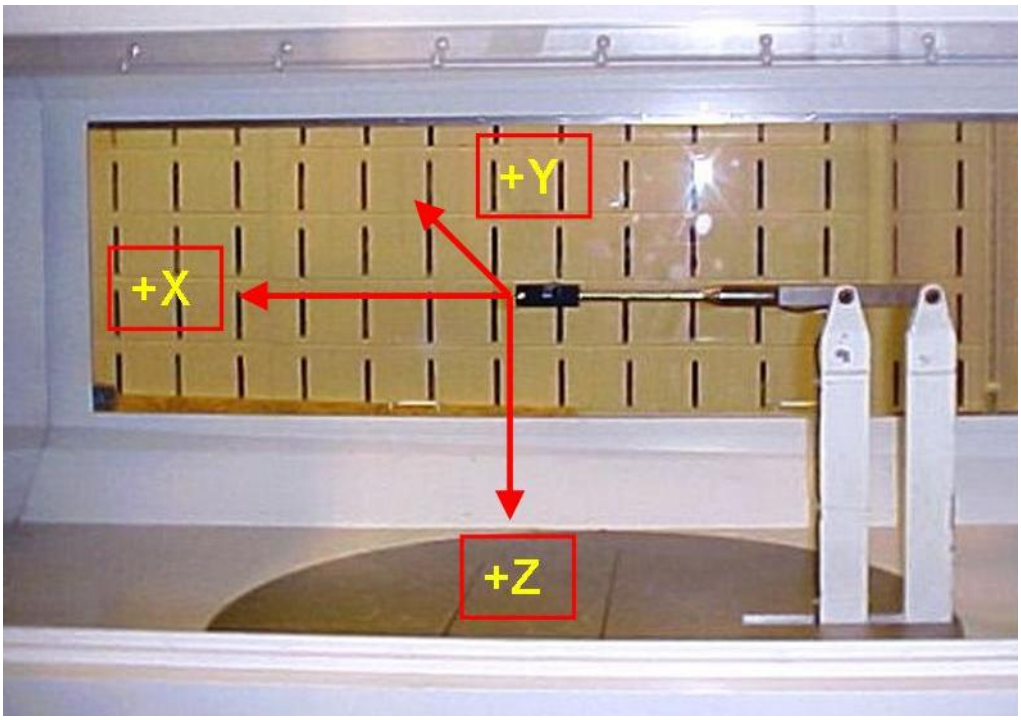

Figure 9: Test Section Coordinates (23)

After the balance was calibrated, the Chevron UCAV half-scale model was mounted to the balance using two 2-56 screws. Because of the symmetrical wing planform of the Chevron UCAV model, the balance was in line with the longitudinal x-axis and at the y- and z-axis centers of gravity. For the Lambda UCAV model the balance was in line with the longitudinal x-axis centers of gravity only due to left and

right symmetry. The Lambda UCAV scaled model was mounted similarly after the Chevron model tests were done (1).

The Chevron and Lambda UCAV models were tested separately in two different flight conditions: Out-of-Ground-Effect (OGE) and In-Ground-Effect (IGE). The OGE tests examined the longitudinal forces and moments on the UCAV in free stream, whereas the IGE tests explored the ground effect condition where the ground plane was placed at four different heights. The proposed test conditions called for four different wind tunnel speeds, 40, 60, 80, and 100 mph, each with angle of attack sweeping from -10 deg to +20 deg. However, these conditions were not met for some of the test runs due to interference between the model/sting mechanism and the ground plane for the highest ground plane conditioin, plane 4 with h/b = 0.05. Table 5 and Table 6 show the Chevron and Lambda models' actual test matrix for each of their test runs respectively. A tare or wind-off runs were completed to calculate the effect of the UCAVs' static weight on the balance. These effects were necessary to remove the static weight effects on the axial sensor, which affects the drag coefficient calculation (1).

Table 5: Experimental Test Matrix for Chevron UCAV Model

Tunnel Speed (mph)	UCAV only .	Plane 1 h/b = 0.3	Plane 2 h/b = 0.15	Plane 3 h/b = 0.10	Plane 4 h/b = 0.05
40	$-10° < \alpha < +20°$	$-10° < \alpha < +20°$	$-10° < \alpha < +20°$	$-10° < \alpha < +20°$	$-4° < \alpha < +13°$
60	$-10° < \alpha < +20°$	$-10° < \alpha < +20°$	$-10° < \alpha < +20°$	$-10° < \alpha < +20°$	$-4° < \alpha < +13°$
80	$-10° < \alpha < +20°$	$-10° < \alpha < +20°$	$-10° < \alpha < +20°$	$-10° < \alpha < +20°$	$-4° < \alpha < +13°$
100	$-10° < \alpha < +20°$	$-10° < \alpha < +20°$	$-10° < \alpha < +20°$	$-10° < \alpha < +20°$	$-4° < \alpha < +13°$

Table 6: Experimental Test Matrix for Lambda UCAV Model

Tunnel Speed (mph)	UCAV only .	Plane 1 h/b = 0.33	Plane 2 h/b = 0.16	Plane 3 h/b = 0.11	Plane 4 h/b = 0.05
40	$-10° < \alpha < +20°$	$-10° < \alpha < +20°$	$-10° < \alpha < +20°$	$-10° < \alpha < +20°$	$-4° < \alpha < +13°$
60	$-10° < \alpha < +20°$	$-10° < \alpha < +20°$	$-10° < \alpha < +20°$	$-10° < \alpha < +20°$	$-4° < \alpha < +13°$
80	$-10° < \alpha < +20°$	$-10° < \alpha < +20°$	$-10° < \alpha < +20°$	$-10° < \alpha < +20°$	$-4° < \alpha < +13°$
100	$-10° < \alpha < +20°$	$-10° < \alpha < +20°$	$-10° < \alpha < +20°$	$-10° < \alpha < +20°$	$-4° < \alpha < +13°$

The test matrix in Table 5 and Table 6 shows that for h/b = 0.05, angle of attack range was reduced from $-10° < \alpha < +20°$ to $-4° < \alpha < +13°$ due to the previously mentioned interference between models and the ground plane.

Section 1.3 – Data Analysis

A data acquisition program was set up within the control computer to store the data in a tab delimited text file at a rate of two Hz sampling rate. For the alpha sweeps, the flow velocity was increased until the desired speed was reached. After ensuring that the balance data stabilized, the model was pitched down to its lowest alpha setting and data were acquired for 30 sec. The angle of attack was then increased in increments of 2 deg and held for another 10 sec each. This was repeated until either the angle of attack reached +20 deg or the ground plane interfered with the sting mechanism.

A MATLAB® code, written by DeLuca (23), Gebbie (22), and altered for the AFIT-1 balance by Parga (25) and Jones (1) was altered for the AFIT-100 lb balance and used to reduce the acquired force and moment data. The data reduction program imported the tare file and corresponding experimental test files. It corrected for blockage, tare and

balance interaction and combined the similar measured forces and moments and averaged them to a single test point for each angle of attack. For more details regarding the MATLAB® data reduction program, see references 22, 23, and 25.

After the MATLAB® program reduced the data, an EXCEL® output file was created for each test run conditions that consisted of Mach number, Reynolds number, dynamic pressure, velocity, angle of attack, lift, drag, roll moment, pitching moment, yaw moment, and side force coefficients for the range of angle of attack specified in Table 5 and Table 6. Standard aerodynamic plots were then created from these output files. See Appendix D for additional ground effect plots and Appendix E for corresponding data tables. Also, see Appendix C for a sample calculation of the data reduction (1).

Section 2 – UCAV Models

As mentioned previously in chapter II, the wing planforms used in this study were originally tested by Reed of AFRL/VAAA for stability and controls study. The original models were built by Dynamic Engineering, Inc. in 1996 and tested in the Boeing St. Louis Low and in the AFRL wind tunnel facilities. They were built out of Ren 450, a woodlike epoxy resin board, and 7075-T6 aluminum. The Chevron and Lambda models' dimensions can be found in Table 7 and Table 8 (7).

Table 7: Original and Scaled Chevron UCAV Model Properties (1)

Chevron UCAV Dimensions		
	Original Model	Scaled Model
Material	Ren 450 & Aluminum	Photopolymer Plastic
Wing Area, in^2	364.87	87.4
Span, in	32	16
Root Chord, in	14.85	7.42
MAC, in	13.35	5.2
Asect Ratio	2.81	2.93
Leading Edge Sweep, deg	45	45

Table 8: Original and Scaled Lamda UCAV Model Properties

Lamda UCAV Dimensions		
	Original Model	Scaled Model
Material	Ren 450 & Aluminum	Photopolymer Plastic
Wing Area, in^2	366.91	78.16
Span, in	32	14.63
Root Chord, in	22.79	10.63
MAC, in	14.46	6.33
Asect Ratio	2.791	2.35
Leading Edge Sweep, deg	50	50

Figure 10: Original Chevron UCAV (1)

Figure 11: Original Lamda UCAV Proof Model

The original Chevron model and Lambda proof model (shown in Figure 10 and Figure 11 respectively) have 32-in wingspans, making them just small enough to fit it the AFIT 31" x 44" LSWT. Because their wingtips would be too close to the test section walls to produce accurate results, half-scaled models were created. The original electronic drawings could not be found, so the original models were digitized. The Chevron UCAV half-scaled model was built by Jones and its details of the digitization and rapid-prototyping process can be found in reference 1. Engineers and technicians of AFRL/Human Effectiveness Branch (HECV) and a technician of AFIT/ENY assisted the author to use a 3-D digitizer to make the half-scaled Lambda UCAV model (1).

Figure 12: FaroArm – Platinum with FARO Laser ScanArm

The digitizer set up included the FaroArm – Platinum along with FARO Laser ScanArm as shown in Figure 12. After laser calibration, the pivoting arm was moved so that the laser scaned the bottom and top surfaces of the Lambda proof model. The cross-sections were then formed from the scanned surfaces and transposed into an IGES file. The transposed IGES file was then imported into the drawing program Solid Works©. Only top and bottom surfaces of the Lambda planform's right wing were scanned since it had

left and right symmetry. The Lambda planform's right wing surfaces were mirrored across the centerline along the integrated fulselage to make the model. Initially, half-scale Lambda model was planned to be made, but due to the printable area limitation of the AFIT 3-D rapid prototyping machine, a 0.457 scale model was made instead for the Lambda planform. Once the Lambda scaled model was in Solid Works©, the hole for the balance was added. The Lambda model center of gravity (CG) was located 4.75 inches forward from the back edge of the mounting hole. The Solid Works© Chevron and Lambda models are illustrated in Figure 13 and Figure 14 respectively. A scaling factor of half-scale was orinally to allow for the model to be small enough to fit into the wind tunnel, but large enough to compare and gather aerodynamic data (1).

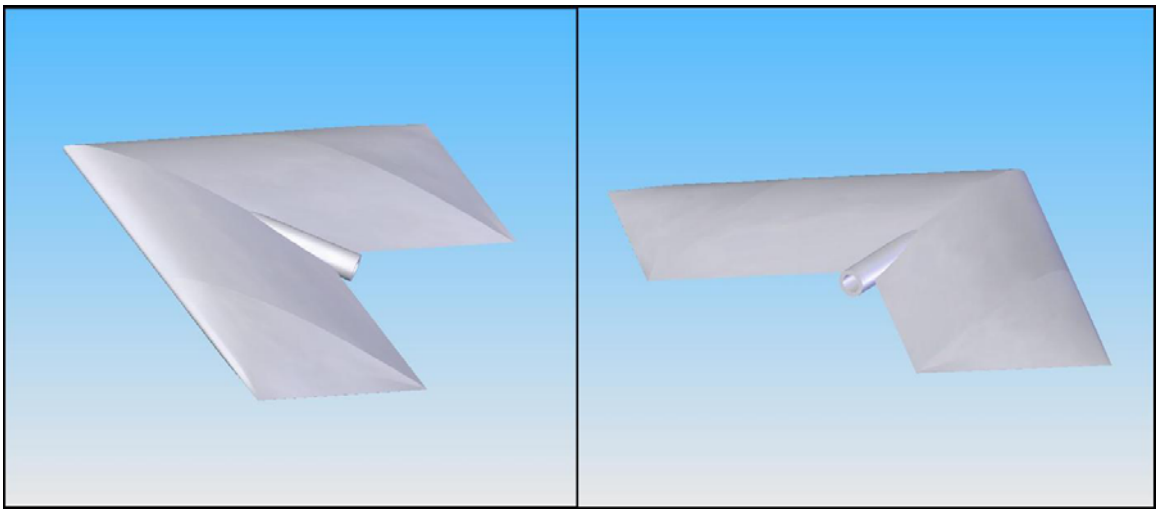

Figure 13: Solid Works Drawings of the $\frac{1}{2}$-scaled Chevron UCAV (1)

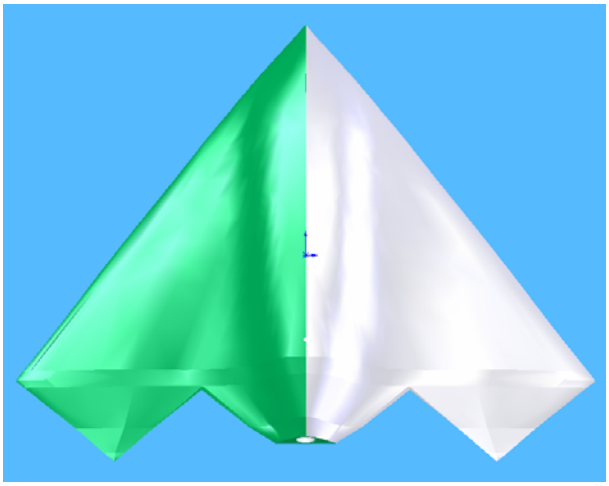

Figure 14: Solid Works Drawings of the 0.457-scaled Lamda UCAV

The final step in producing the scaled Lambda model was converting the Solid Works© file into .stl format and then printing it with the AFIT/ENY 3-D rapid prototyping machine. The Stratasys Objet EDEN 333 rapid prototyping machine utilizes eight small jets that lay down UV plastic (also known as photopolymer plastic) material and a gel-like UV plastic for support material in 0.0006-in layers. The eight jets traverse across the printed region in 2-in strips followed by a UV light which cures the plastic simultaneously (26). The Full Cure 700 series photopolymer plastic model material can be machined, drilled, and chrome-plated; used as a mold; and absorb paint (27). The images of the scaled models of the rapid prototyped Chevron and Lambda planforms are shown in Figure 15, Figure 16 and Figure 17, Figure 18 respectively (1).

Figure 15: $\frac{1}{2}$-Scaled Chevron UCAV Model (1)

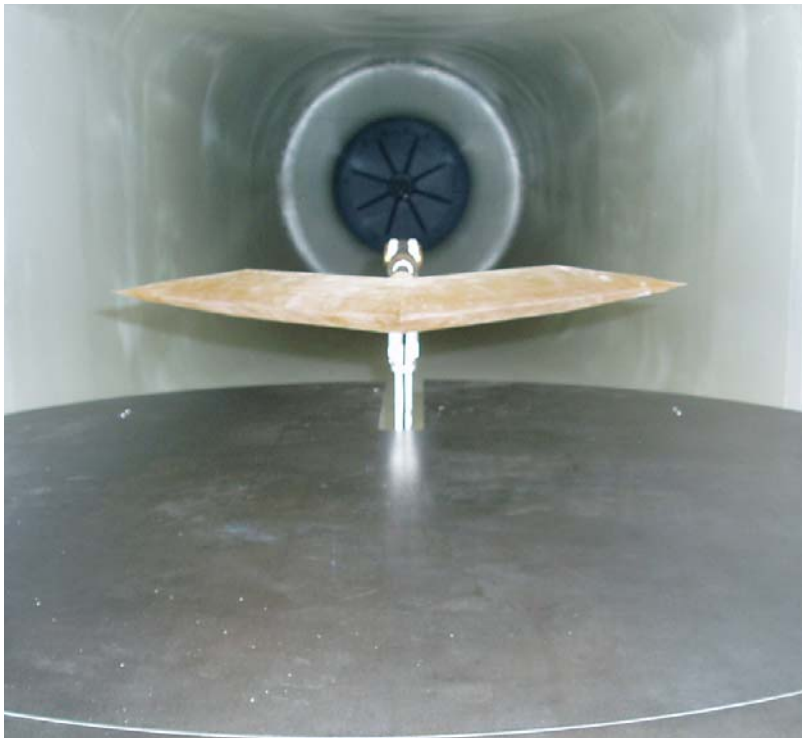

Figure 16: $\frac{1}{2}$-Scaled Chevron UCAV in Test Section (1)

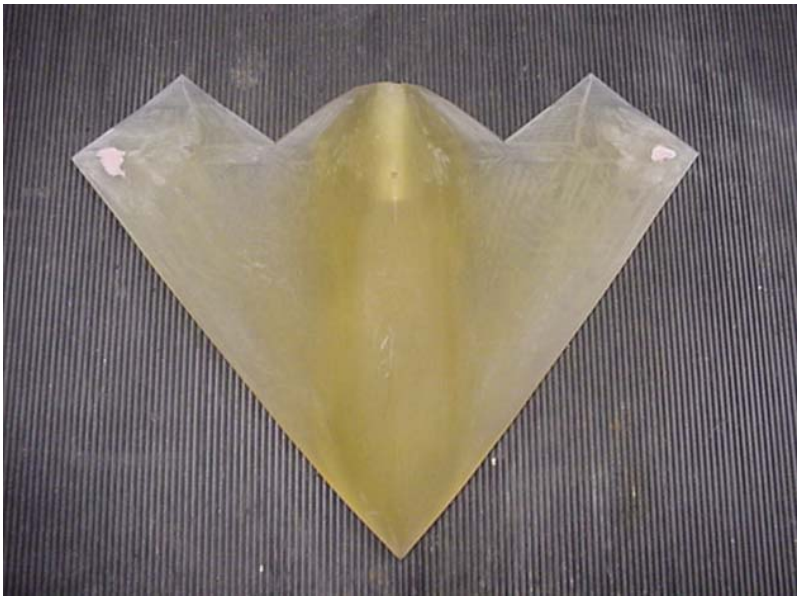

Figure 17: 0.457-Scaled Lamda UCAV Model

Figure 18: 0.457-Scaled Lamda UCAV in Test Section

Section 3 – Ground Plane Description

In order to properly represent the model flying close to the ground, a ground plane was built by Jones in his study and was used in his wind tunnel investigation. The ground plane consisted of two plates and eight cylindrical legs. The plates were made of hot-rolled steel and the legs were make of cold-rolled steel. The ground plane plate's and legs' dimensions are shown in Table 9 and pictures are shown in Figure 19 and Figure 20 (1).

Figure 19: Ground Plane (1)

Figure 20: Ground Plane and Model in Test Section (1)

Table 9: Ground Plane Dimensions (1)

Ground Plane Dimensions		
Plate		
	thickness, in	0.25
	diameter/width, in	35.313
	max length, in	44.313
Legs		
	diameter, in	1.5
	length, in	
	height 1	9.77
	height 2	12.17
	height 3	12.97
	height 4	13.77

Section 3.1 – Predicting the Leg Heights

Not having the flexibility of altering the model height with the sting mechanism, the ground plane height was changed to vary the height above ground. Four different sets of legs were interchanged for each height to vary the ground plane height. The ground plane heights were selected by Jones (1) to ensure the greatest effect from the ground on the model. Table 10 shows the four heights chosen and corresponding h/b for both Chevron and Lambda UCAV models (1). The height was measured from the interface between the sting mechanism and the 100 lb. balance. This reference, which is located at the back edge of each model's mounting hole, was 2.5 in aft of Chevron model's CG and 4.75 in aft of Lambda model's CG. Refer to reference 1 for further details on the ground plane descriptions.

Table 10: Ground Plane Heights and Corresponding h/b for Chevron and Lambda UCAV Models

GP Designator	height	Chevron h/b	Lambda h/b
Plane 1	10.02	0.3	0.33
Plane 2	12.42	0.15	0.16
Plane 3	14.02	0.1	0.11
Plane 4	14.22	0.05	0.05

Section 4 – Hot-wire Anemometry

A hot-wire anemometry experiment was used to determine the difference between the transducer velocity which was taken forward of the model and the actual velocity at the model. Also, it was used to study the blockage effects due to the ground plane. The

following describes the equipment, procedure, and data analysis of the hot-wire anemometry experiment (1).

Section 4.1 – Equipment

The AFIT LSWT is equipped with a Dantec-Dynamics Streamline 90N10 Constant Temperature Anemometer (CTA). It is fully motorized and programmable with a 3-axis traversing system. A single wire 55 P11 probe type was used with the vertical attachment. Figure 21 illustrates a probe with the single wire parallel to the y-axis (1).

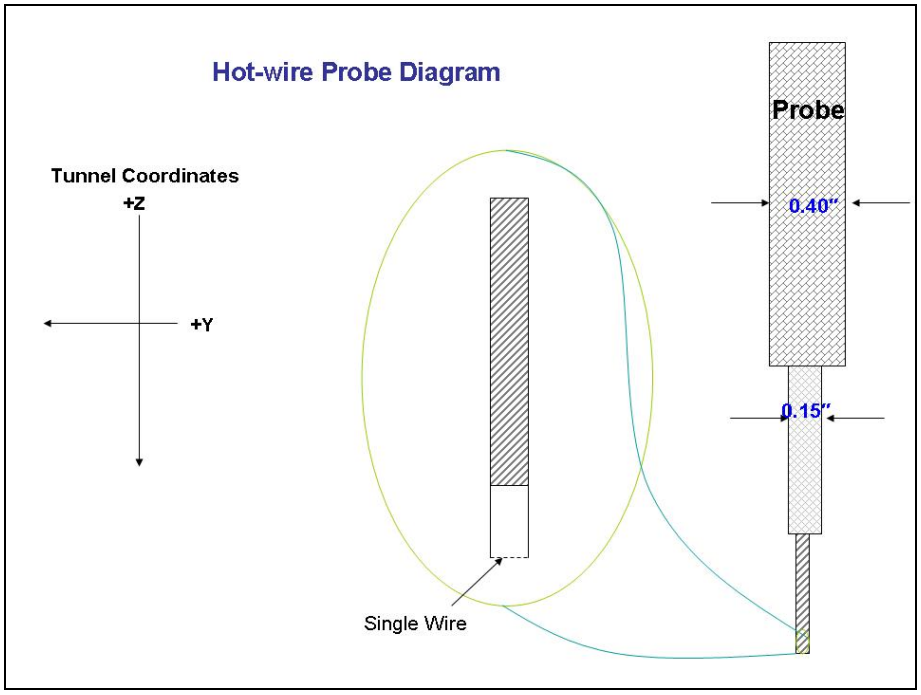

Figure 21: Schematic of Hot-wire Probe Configuration (1)

The maximum range of the probe is 19.7 inches in the y-direction (horizontal) and z-direction (vertical). In addition, it has the capability to traverse longitudinally in the x-

direction approximately 3 ft. The Dantec hot-wire anemometer came with a data acquisition program called Streamware® which was used to collect, process, and format raw experimental data (1).

Section 4.2 – Procedure

The hot-wire anemometer was first calibrated using the Dantec automatic calibrator system. See details of the hot-wire anemometer calibration process in reference 1.

For the hot-wire anemometry experiment, the top Plexiglas window was replaced by one with slotted grooves specifically designed for the hot-wire measurement. All slots were plugged except for the longitudinal station of interest. Figure 22 illustrates slot number 1 open for hot-wire velocity measurements and slot numbers 2 to 6 plugged.

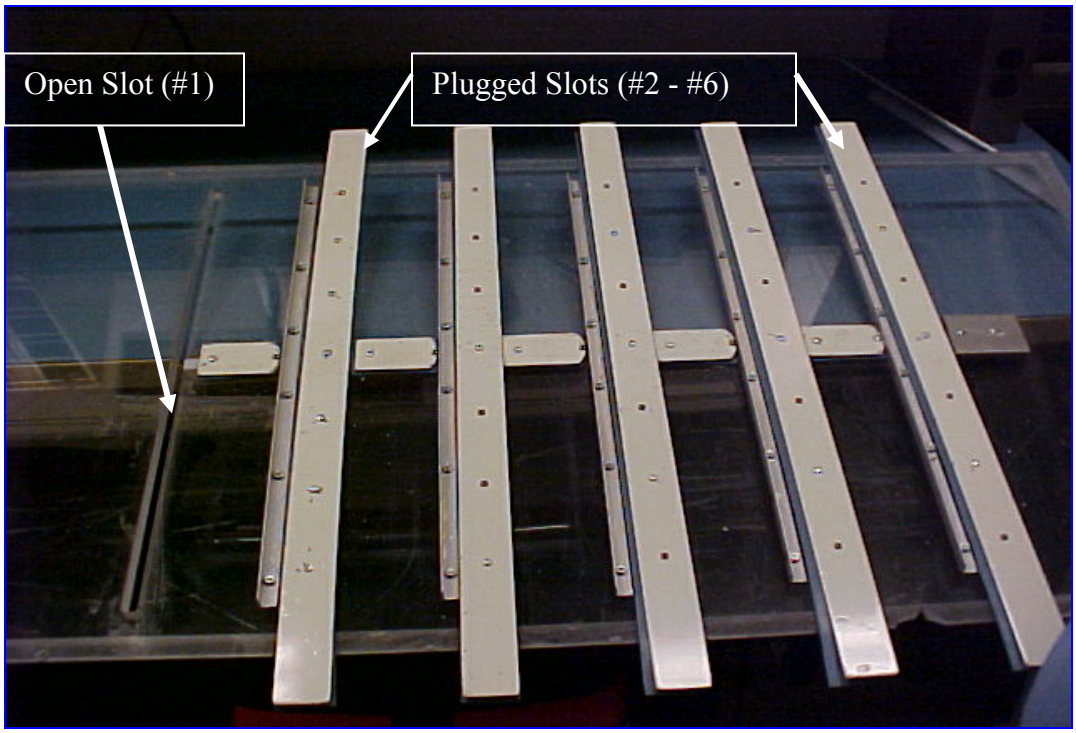

Figure 22: Removable Plexiglas Top for Hot-wire Anemometry (22)

Slot number 2 and 3 were used for this experiment because they were the closest stations to the Chevron and Lambda model CGs respectively. Velocity measurements were made at speeds 40, 60, 80, and 100 mph for three conditions: without the ground plane, at the lowest ground plane height, and the highest ground plane height (1). For detailed description of the hot-wire probe test grid see reference 1.

See Figure 23 for the illustration of the nominal probe grid test pattern.

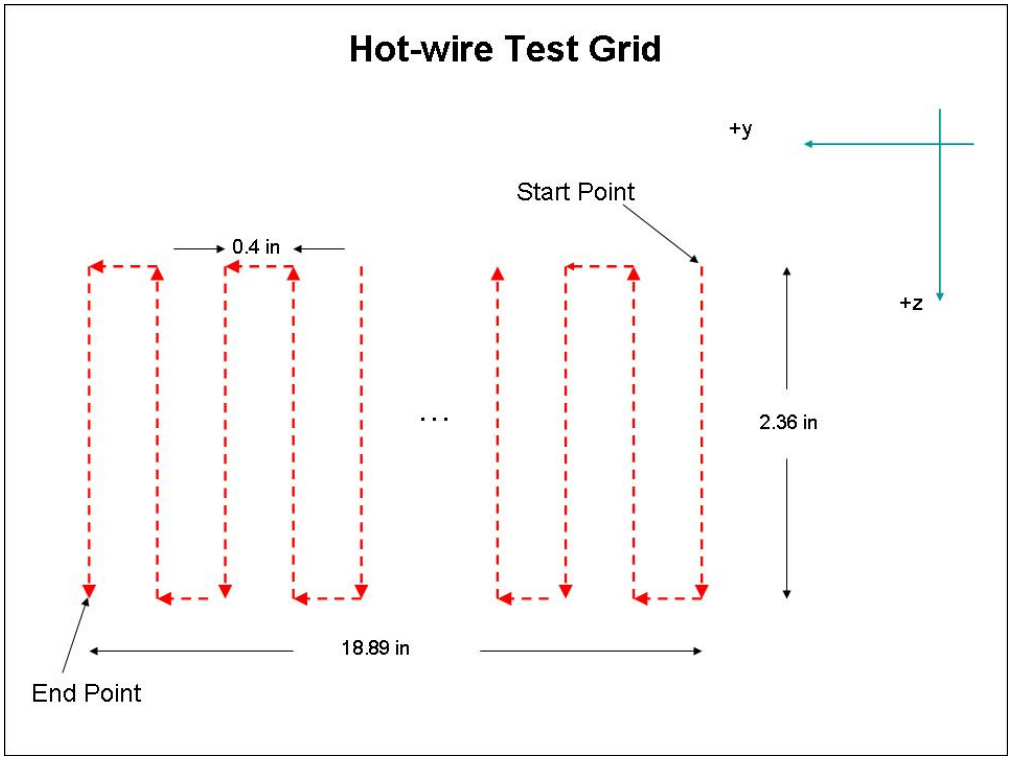

Figure 23: Hot-wire Test Grid (1)

Section 4.3 – Data Analysis

The Dantec Streamware® software stored the experimental data files from each test run as a Comma Separated File (.csv). The software converted the raw test data, from voltages into mean velocities at each test point. The mean velocities were compared to the transducer indicated velocities to anotate the differences (1).

IV. Results & Analysis

This chapter presents the results from the wind tunnel experiments for the Chevron and Lambda UCAV models. The hot-wire anemometry and ground effects results will be presented.

Section 1 – Hot-wire Anemometry

The results from the hot-wire anemometry experiment showed minimal differences in the velocities measured by the pressure transducer and the hot-wire anemometer. Figure 24 illustrates the transducer measured velocity compared to the hot-wire measured velocity for the OGE test condition.

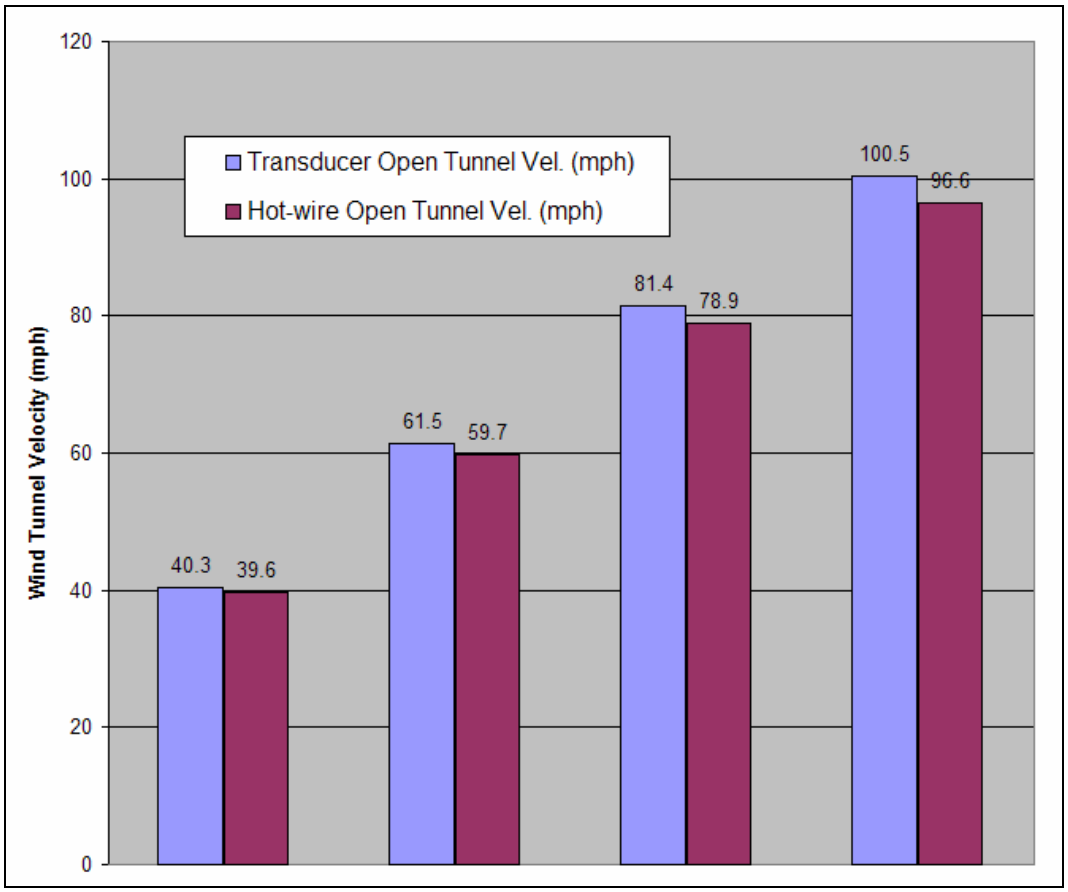

Figure 24: Open Tunnel Hot-wire and Transducer Velocity Comparison

One observation from Figure 24 is the averaged 3 % difference in the open tunnel hot-wire velocities compared to the transducer velocities at each test condition. The difference in velocities was likely due to a slight tapering out of the cross section area from the front to the back of the test section. The cross section area increased 1.15% from where the transducer was located to where the hot-wire measurements were made. This increase in the cross section area accounts for slight decrease in velocities from the transducer to the hot-wire. These velocity differences were accounted for in the MATLAB© data reduction code as a velocity correction.

To measure the blockage correction due to the ground plane, the wind tunnel velocity was held constant for each test velocities of 40, 60, 80, and 100 mph while the hot-wire measured the corresponding tunnel velocities. The ground plane heights of h/b = 0.3 and h/b = 0.05 were used to obtain the blockage measurements. Figure 25 illustrates the comparison of the velocities of the open tunnel, the ground plane 1 and the ground plane 4 hot-wire measurements.

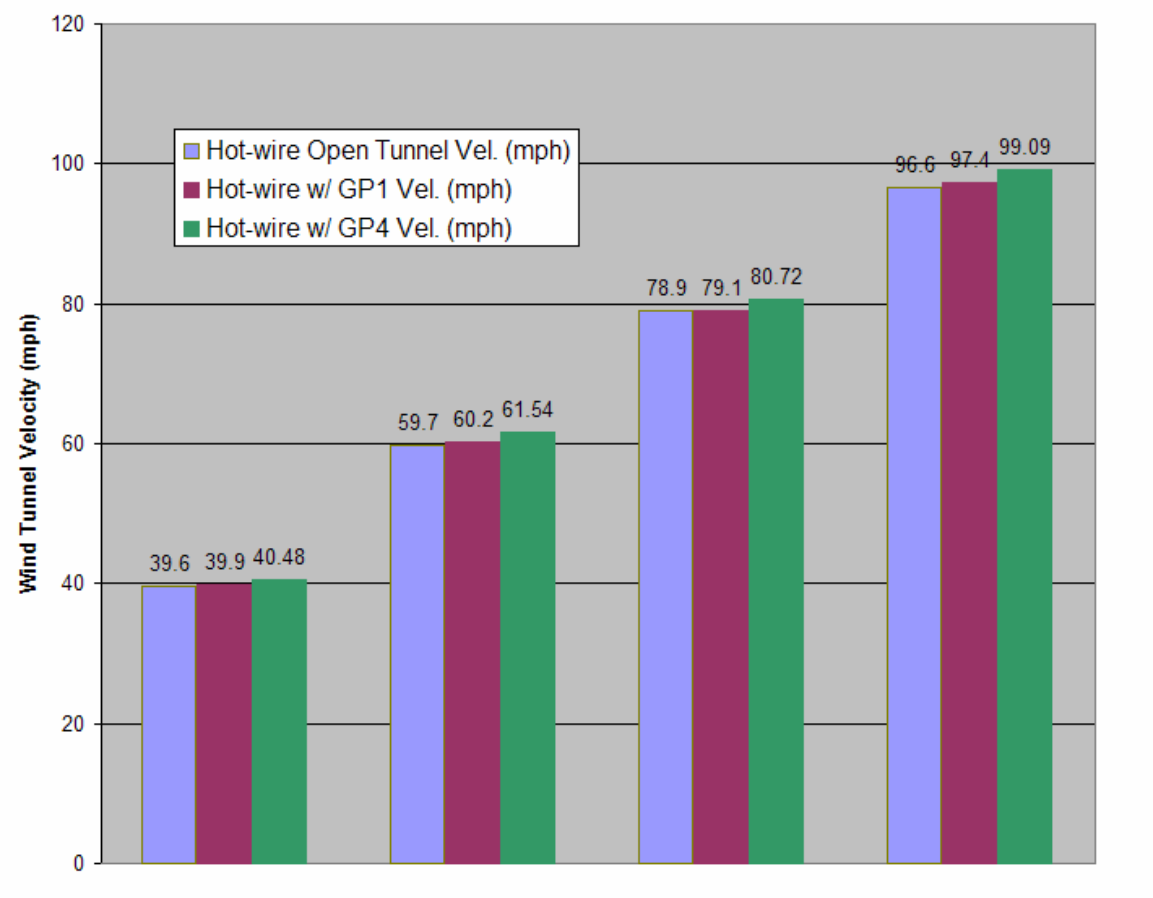

Figure 25: Velocity comparison of the open tunnel hot-wire and the ground plane (GP) 1 and 4 hot-wire measuments

Compared to the open tunnel test section, the airflow was forced to speed up around the ground plane to satisfy the conservation of mass. The associated increase in velocity was accounted for by the blockage correction factors. Blockage correction factors are ratios between the open tunnel and ground plane velocities. As shown in Equation (5), the total blockage correction facor is the velocity ratios between the open tunnel velocity with respect to the ground plane multiplied by the transducer velocity with respect to the open tunnel velocity (1).

$$\frac{GP}{Tr} = \frac{OT}{Tr} * \frac{GP}{OT} \tag{5}$$

Table 11 summarizes the correction factors for varying ground plane height and velocity test conditions.

Table 11: Velocity Correction Factors Used for Blockage

Correction Factors	40 mph	60 mph	80 mph	100 mph
OT-to-Tr	0.983	0.971	0.969	0.961
Plane 1-to-OT	1.007	1.008	1.002	1.008
Plane 2-to-OT	1.016	1.022	1.015	1.019
Plane 3-to-OT	1.019	1.026	1.019	1.022
Plane 4-to-OT	1.022	1.031	1.023	1.026

Section 2 – Ground Effect Tests

The following is the wind tunnel ground effect data collected during this study on the Chevron and Lambda UCAV models. The ground effect region was identified from the lift and drag coefficient with respect to the longitudinal axis. Tables 12 and 13

display the flight parameters of the Chevron and Lambda UCAV models respectively at the various test conditions. The wind tunnel velocities in Tables 12 and 13 are corrected values accounting for the blockage correction vs. the velocity labeled 40, 60, 80, and 100 mph on the figures illustrated in this results chapter and in the Appendix B and corresponding Re on the figures are also from Tables 12 and 14 for Chevron and Lambda UCAV models. The Re for Reed's OGE data for original Chevron and Lambda UCAVs were calculated from root chords referenced in Tables 7 and 8 and Reed's test velocity of 117 mph.

Table 12: Chevron UCAV Summary of Flight Conditions

U_∞^* (mph)		Mach No.		q_c (lbf / ft^2)		Re_c	
OGE	IGE P4	OGE	IGE P4	OGE	IGE P4	OGE	IGE P4
39.37	40.23	0.051	0.053	3.77	3.99	2.17E+05	2.25E+05
58.32	60.11	0.076	0.079	8.28	8.91	3.22E+00	3.36E+05
77.63	79.43	0.101	0.104	14.67	15.55	4.28E+05	4.44E+05
96.21	98.71	0.125	0.129	22.53	24.02	5.31E+05	5.51E+05
* = corrected velocity							

Table 13: Lambda UCAV Summary of Flight Conditions

U_∞^* (mph)		Mach No.		q_c (lbf / ft^2)		Re_c	
OGE	IGE P4	OGE	IGE P4	OGE	IGE P4	OGE	IGE P4
39.36	40.22	0.052	0.053	3.77	3.97	3.11E+05	3.20E+05
58.31	60.10	0.076	0.079	8.28	8.86	4.61E+05	4.78E+05
77.61	79.41	0.101	0.104	14.66	15.46	6.13E+05	6.32E+05
96.19	98.69	0.125	0.129	22.53	23.88	7.60E+05	7.85E+05
* = corrected velocity							

Section 2.1 – Repeatability

The main purpose for performing repeat runs was to ensure that the test conditions and the performance of the test apparatus did not change during the course of

this study. In addition, checking the repeatability of the data provides confirmation that the data gathered at the end of a test can be compared with data gathered at the beginning of the test. Repeatability also provides the opportunity to check the uncertainty in the experimental data.

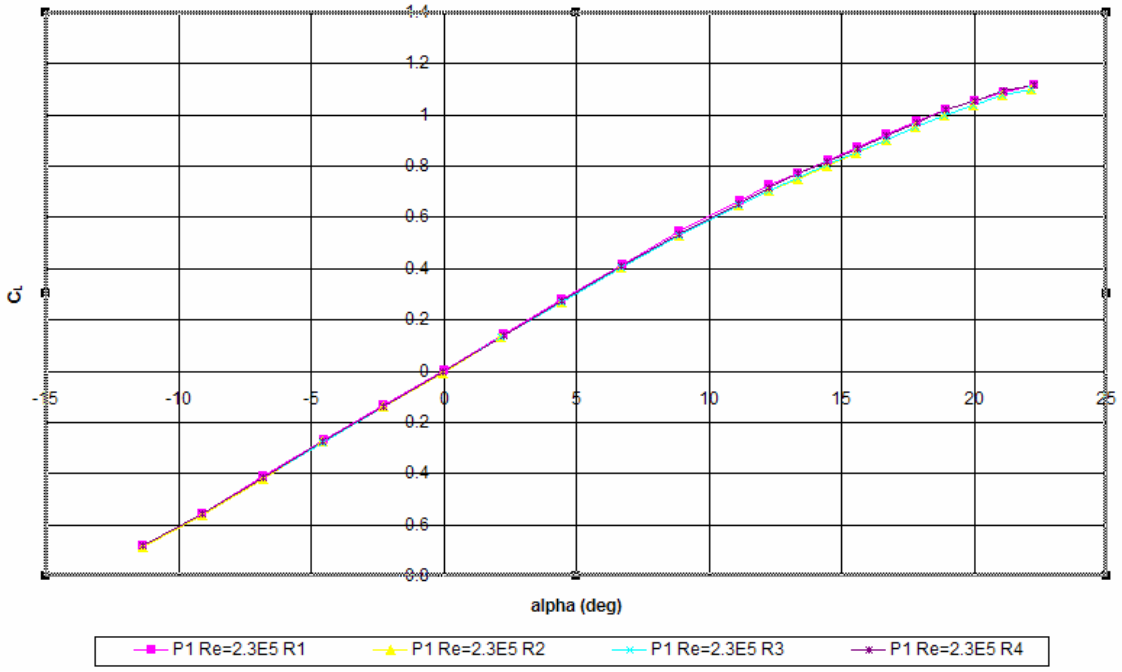

Figure 26: Chevron C_L vs. alpha Repeatability at P1 (h/b = 0.3) 40

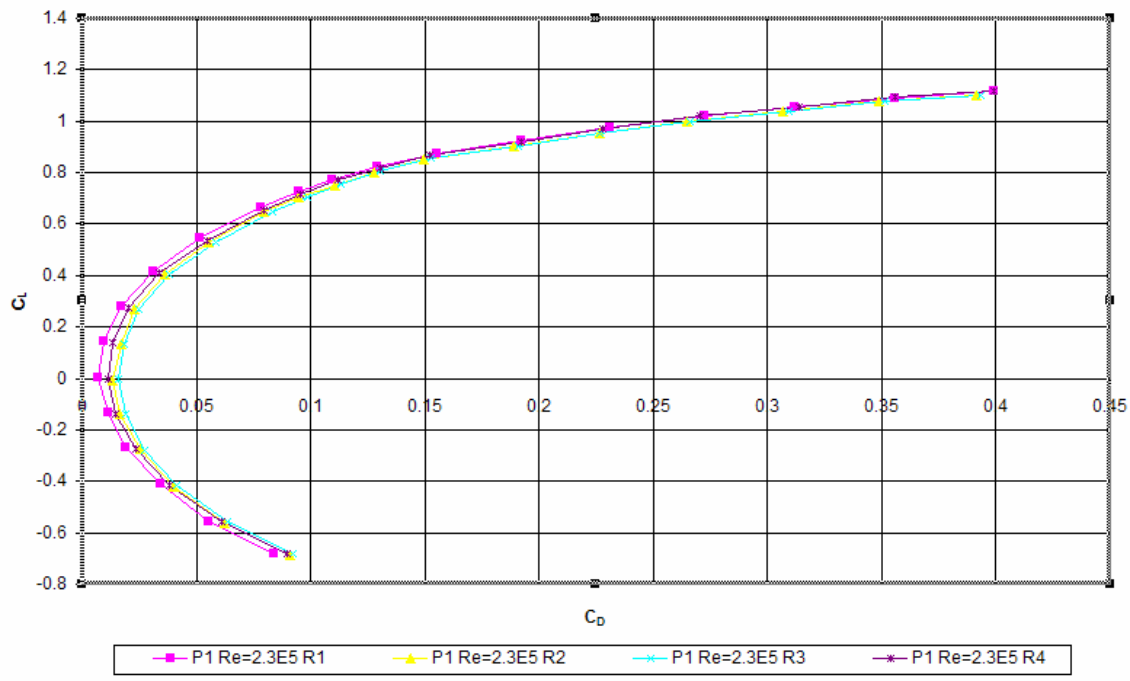

Figure 27: Chevron C_L vs. C_D Repeatability at P1 (h/b = 0.3) 40 mph

Section 2.1.1 – AFIT SLWT Repeatability

Several Chevron UCAV model runs were made during the test entry. Figure 26 shows good repeatability characteristics of the lift coefficient with 1.5% to 3.8% variation. The drag coefficient repeatability illustrated in Figure 27 reveal some variation between runs 1 and 2 with 0.01% for 6 deg AOA to 43% for 2 deg AOA. Due to small values of drag coefficients, any small variation results in high percent variation as in 43% for 2 deg AOA between runs 1 and 2.

Section 2.2 – Out of Ground Effect Runs

The purpose of the open tunnel tests without the ground plane was to establish OGE data. In addition, OGE results can be verified against longitudinal characteristics Reed (7) identified in his study.

Section 2.2.1 – Lift Coefficient Variation

Figures 28 and 29 show similarities between the lift coefficients measured with the original Chevron and Lambda UCAVs along with their respective scale models.

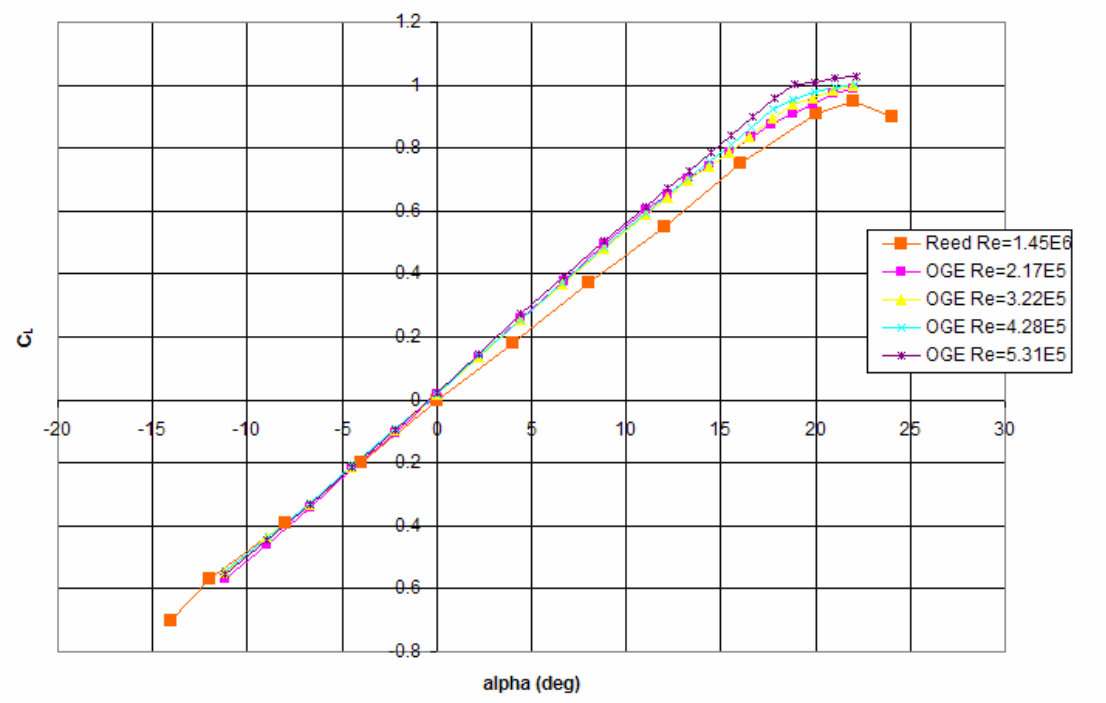

Figure 28: Chevron UCAV Aerodynamic Comparison - C_L vs. alpha

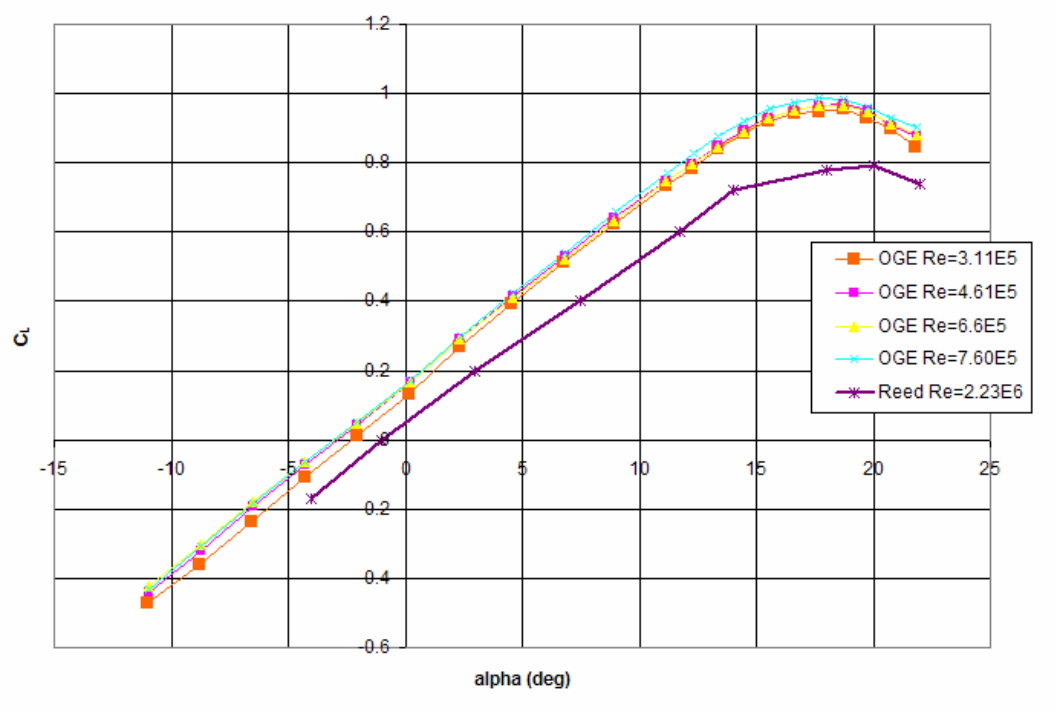

Figure 29: Lambda UCAV Aerodynamic Comparison - C_L vs. alpha

The lift curve slopes approximated from Figures 28 and 29 for Chevron and Lambda models are 0.053 per deg and 0.047 respectively, and are relatively similar for both tests. The C_L for Lambda model varied more than that from Reed's C_L and may be because the original Lambda model was not available and had to use the original proof model made of foam. The scale model may not be an exact scale replica of the original Lamba model, because the proof model's condition was poor with rough surfaces, crushed nose and wing tips as shown in Figure 11. Some surfaces of the Lambda proof model had to be estimated for the 3-D modeling process.

Section 2.2.2 – Lift Coefficient vs Drag Coefficient Variation

The Chevron model's OGE results agreed well with Reed's OGE results. For the Lambda model, the drag coefficient difference was greater than that of the Chevron UCAV model's for the same reason mentioned for the lift coefficient. Figure 30 is the drag polars of the original Chevron UCAV and the scale model at each test speed and Figure 31 is of the Lamda UCAV and scale model drag polars.

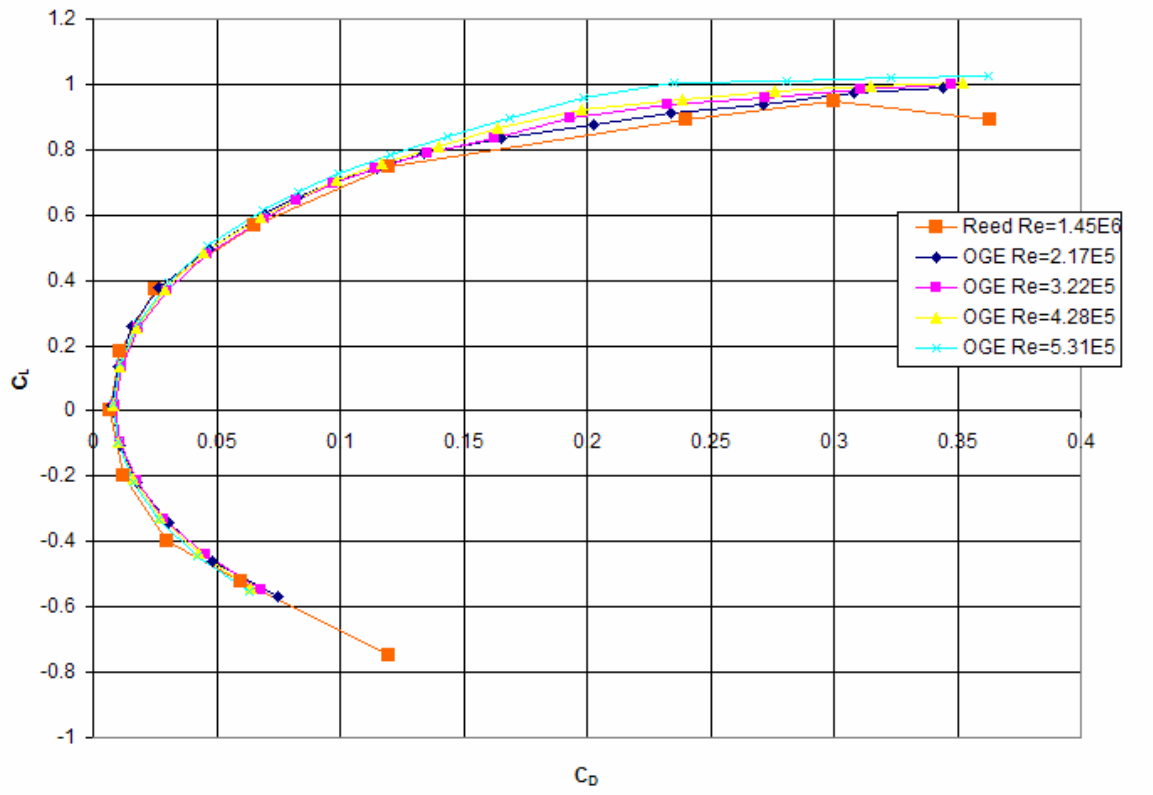

Figure 30: Chevron UCAV Aerodynamic Comparison - C_L vs. C_D

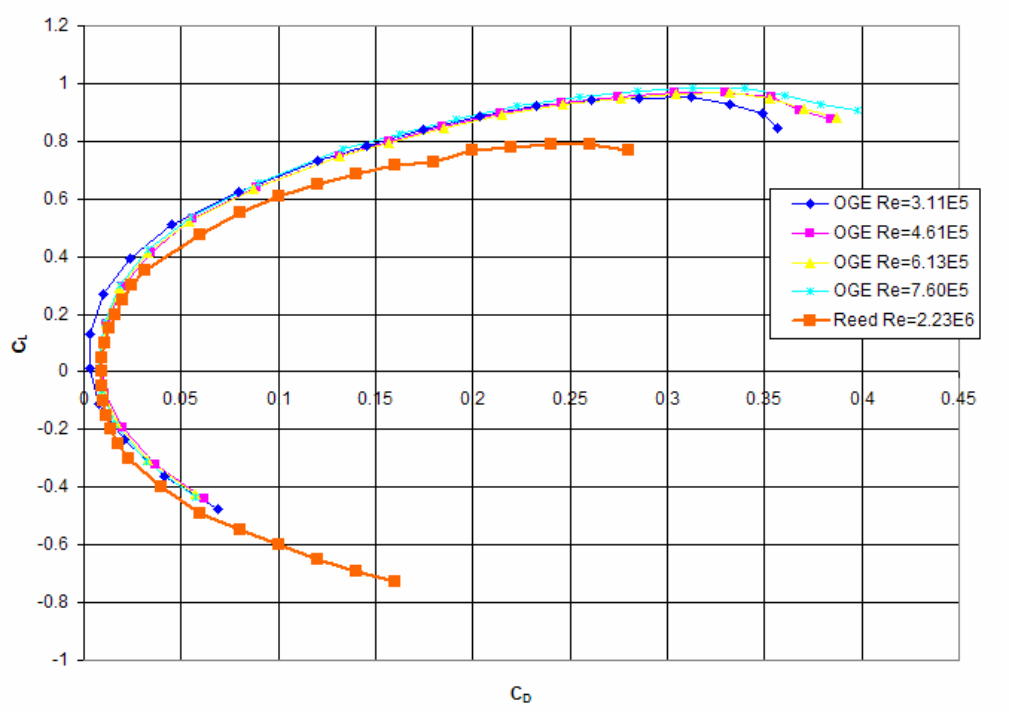

Figure 31: Lambda UCAV Aerodynamic Comparison - C_L vs. C_D

Section 2.3 – In Ground Effect Runs

The following plots illustrate the effects of the decreasing height above ground with respect to lift and drag. As mentioned in section 3.1, the height above ground was measured from the interface between the sting mechanism and the 100 lb. balance. This reference, which is located at the back edge of each model's mounting hole, was 2.5 in aft of Chevron model's CG and 4.75 in aft of Lambda model's CG.

Section 2.3.1 – Lift Coefficient Variation

The OGE data for the following plots are represented by h/b = 0.93. Figures 34 and 35 below and Figures 59 and 63 in the Appendix B show the Chevron model's

variation in lift at seven different angles of attack at -4, -2, 0, 2, 4, 6, and 8 degrees as a function of h/b for 40, 60, 80, and 100 mph. Similarly, the Figures 36 and 37 below and Figures 71 and 75 in the Appendix B show variation in lift as a function of h/b for the Lambda model.

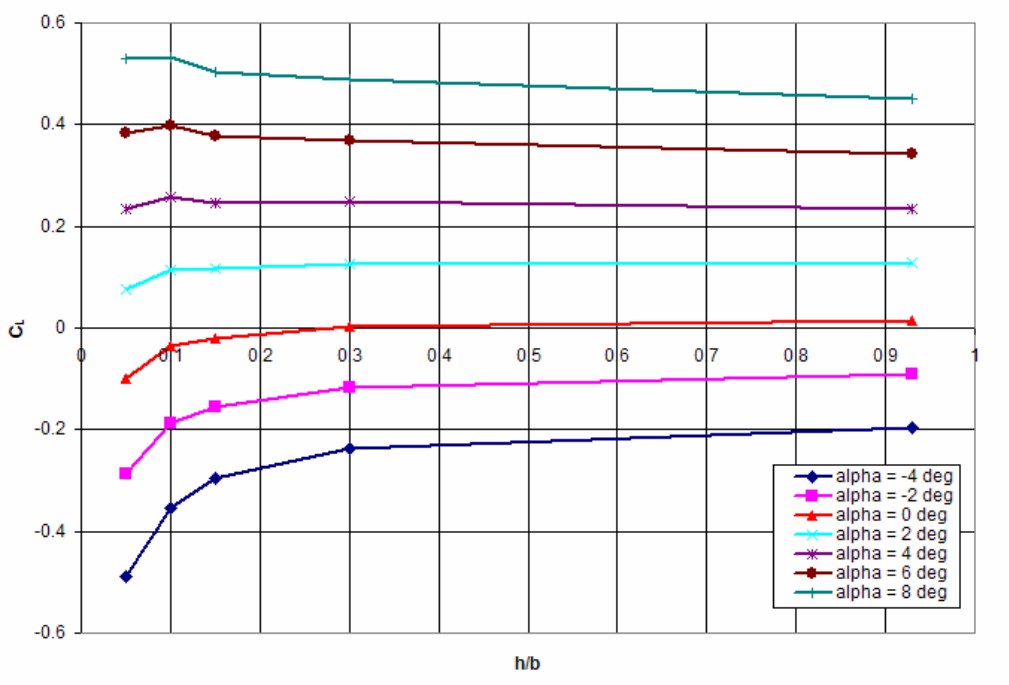

Figure 32: Chevron UCAV Ground Effect - C_L vs. (h/b) 40 mph

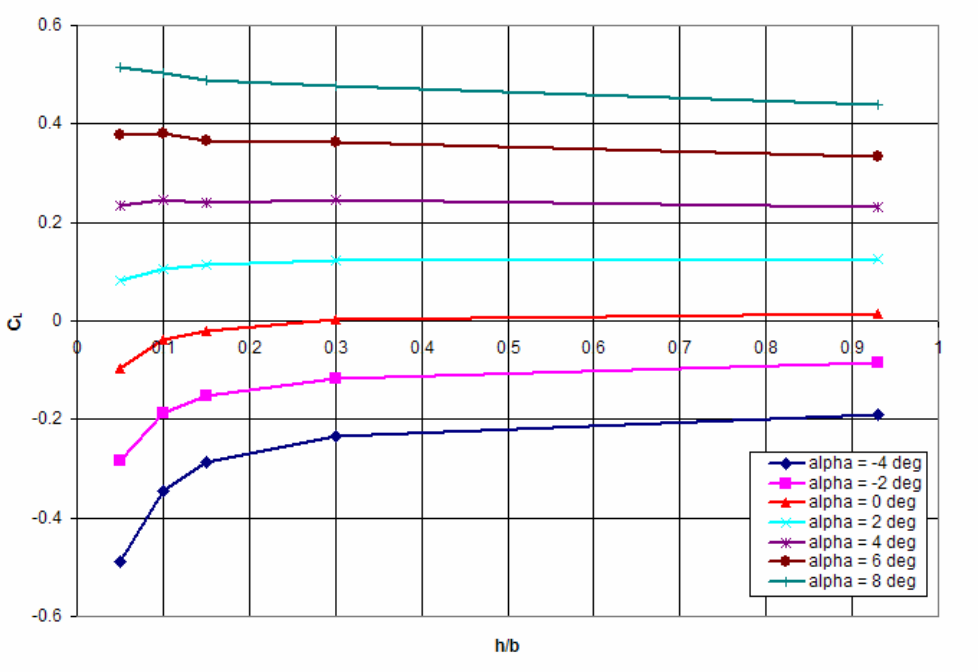

Figure 33: Chevron UCAV Ground Effect - C_L vs. (h/b) 60 mph

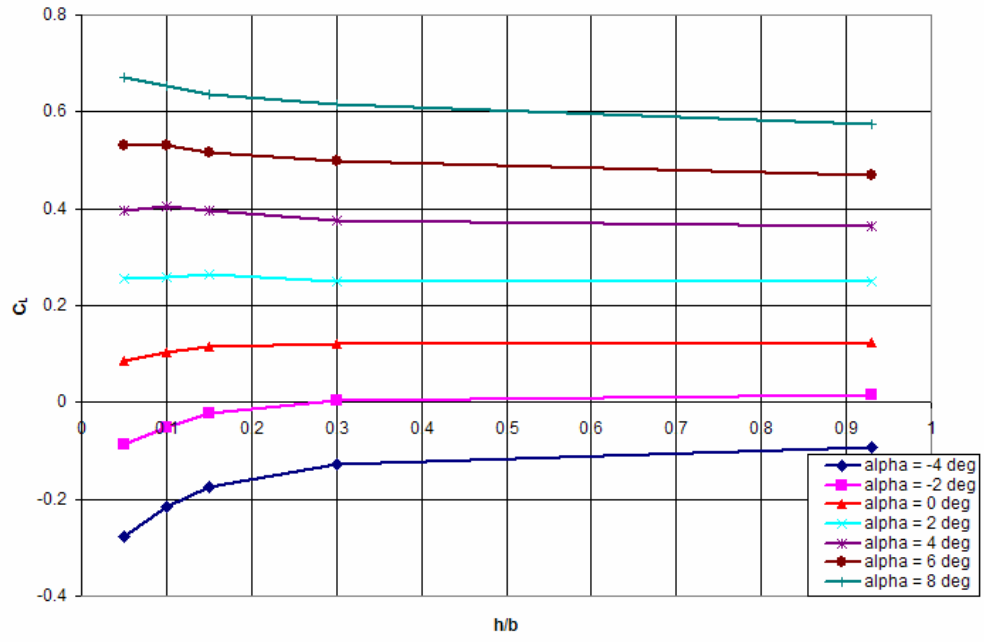

Figure 34: Lambda UCAV Ground Effect - C_L vs. (h/b) 40 mph

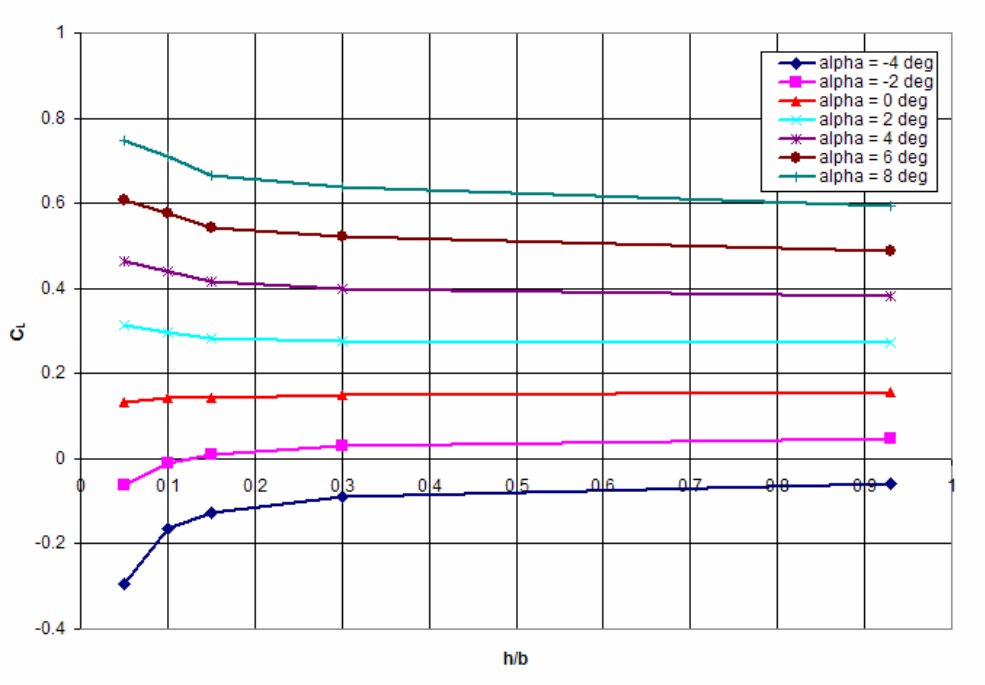

Figure 35: Lambda UCAV Ground Effect - C_L vs. (h/b) 60 mph

The overall trend in C_L as height above ground decreases is consistent with Figures 32 through 35, 57, 61, 69, and 73. At 6 and 8 deg angle of attack (AOA) C_L increases steadily below h/b of 0.3 for the Chevron model from 40 to 100 mph. For the Lambda model, the C_L increases steadily for AOAs at 4, 6, and 8 degrees AOA from 40 to 100 mph as well. This increase is typical and expected for most aircraft flying in ground effect (1). Also, for AOA of 8 degrees, the Chevron model had an average rate of change in C_L increases per h/b of 0.17 for both 40 mph and 60 mph, 0.20 for 80 mph, and 0.19 for 100 mph. At 8 deg AOA the Lambda model's average rate of change in C_L increases per h/b was 0.23 for 40 mph, 0.48 for 60 mph, 0.35 for 80 mph, and 0.38 for 100 mph. For the Chevron model, at 2 deg AOA and below C_L clearly drops, but at AOA

of 4 deg C_L does not vary much for change in h/b. For the Lambda model, at 0 deg AOA and below C_L clearly drops, but at AOA of 2 deg C_L does not vary much for change in h/b. The reason for this increase in C_L trend in ground effect region may be due to the leading-edge vortices not only becoming stronger but also staying more outboard by reducing streamwise velocity due to ground-induced backwash (13).

The behavior of the lift coefficient as height above ground decreases suggests that the influence of the ground on the Chevron wing planform can also be explained using a 2-D theoretical prediction presented by Jones (1). The Chevron model's wing section, the NACA 0015, was inserted into the vortex panal code described in reference 1. Figure 38 shows the section lift coefficient as a function of height above ground for 40 mph.

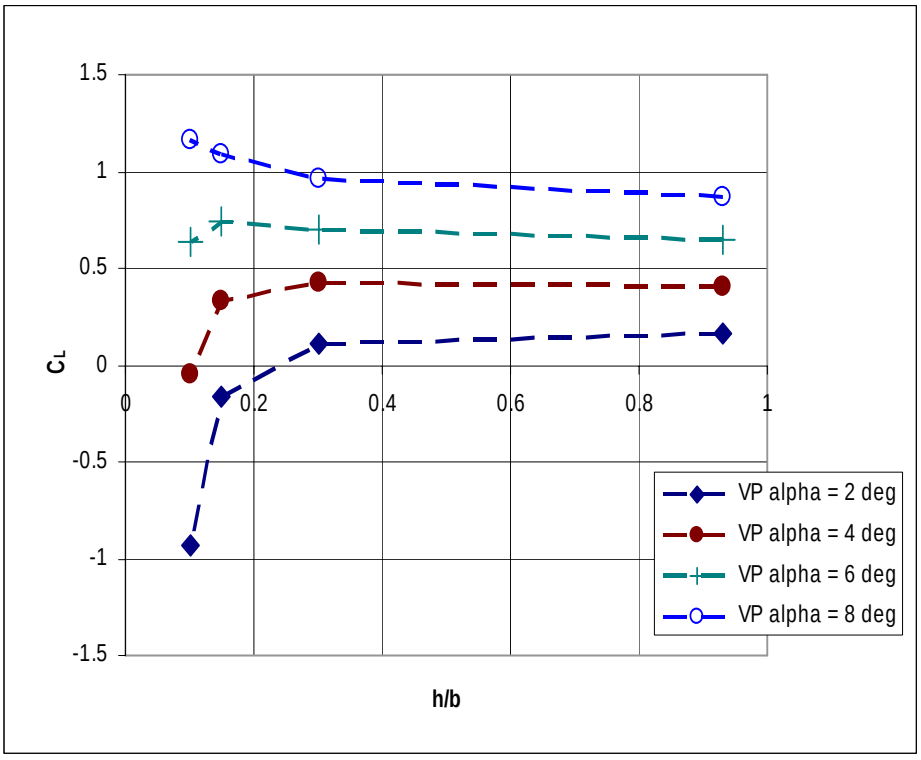

Figure 36: Chevron UCAV Ground Effect - 2-D Vortex Panel Prediction - C_L vs. (h/b) 40 mph (1)

Although, the trends of the C_L curves are similar, the values of lift coefficient in Figure 36 do not match up to those in Figure 34. The reason for this difference in C_L values is because section lift coefficient of 2-D airfoil with infinite wing span is generally higher compared to a wing of finite span (24). With the increase in lift with decrease in height above ground, the airfoil is behaving like a standard airfoil at AOA of 8 deg. This implies the flow is traveling faster across the top surface compared to the lower surface producing a positive pressure differential (1). Jones (1) also presented a pressure coefficient, C_P, contour plot as illustrated Figure 37, which was calculated with a vortex panel code.

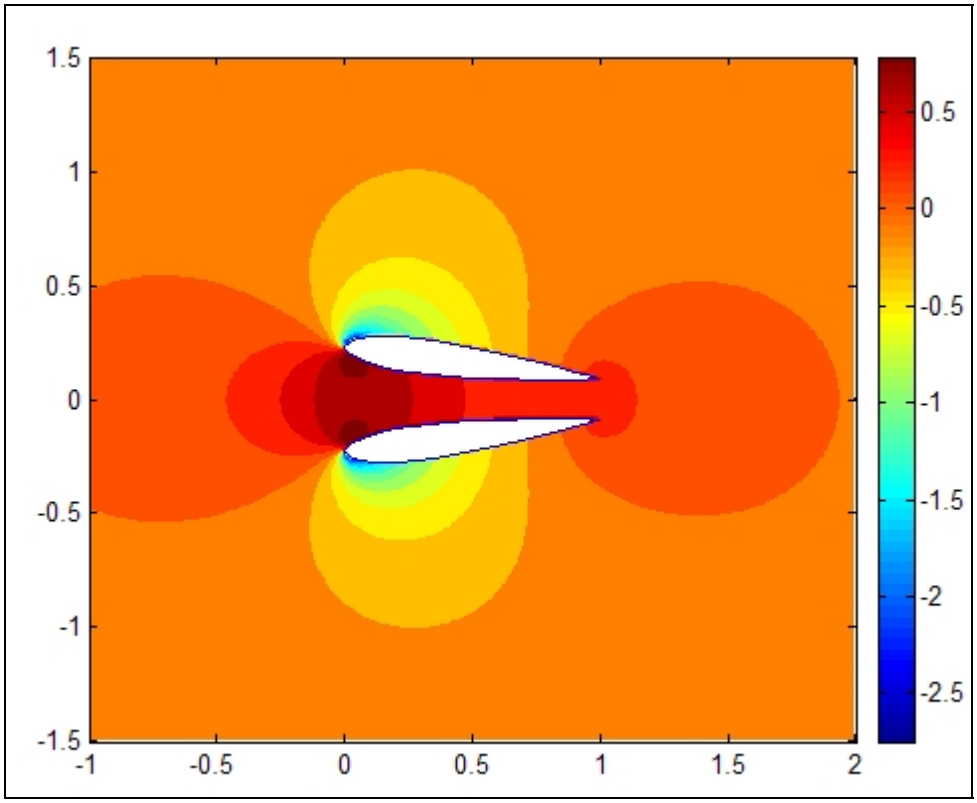

Figure 37: Contour Plot of C_P Around an Airfoil in Reflection AOA=8 deg, h/b=0.15 (1)

Figure 37 illustrates that the 2-D vortex panel code predicted the C_P distribution similar to the thin-airfoil theory. For a symmetric airfoil, the thin airfoil theory states that section lift coefficient is directly proportional to circulation and AOA. But, the vortex panel code calculated the opposite distribution at lower angles of attack as shown in Figure 38.

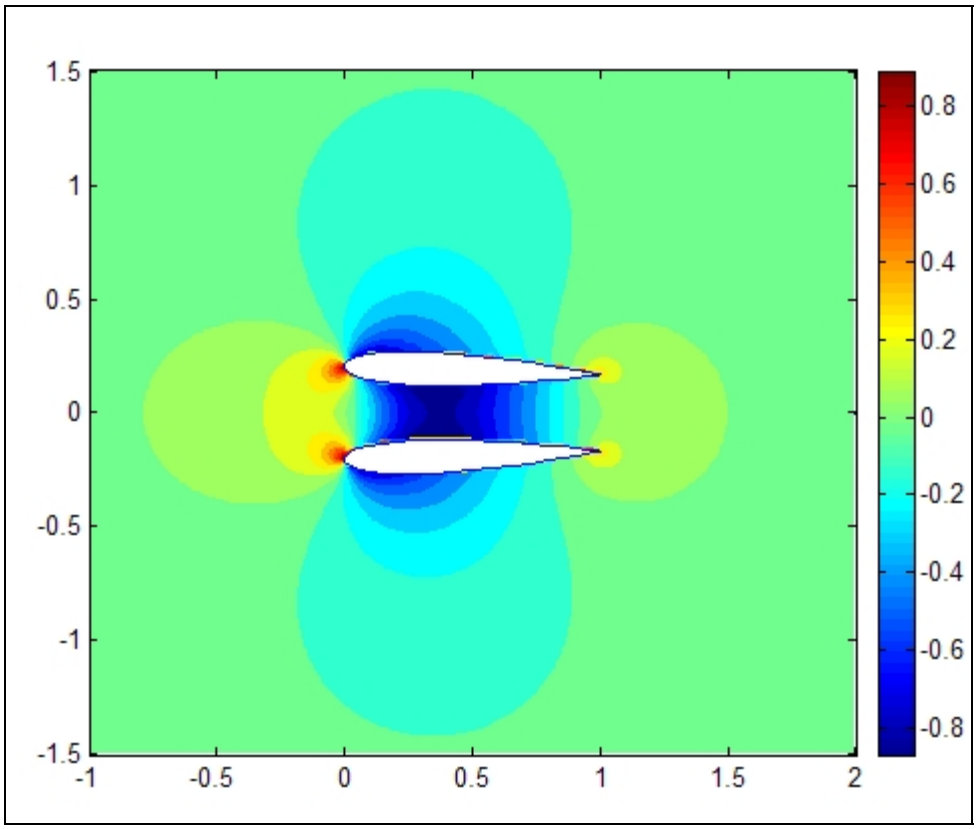

Figure 38: Contour Plot of CP Around an Airfoil in Reflection AOA=2 deg, h/b=0.15 (1)

Jones also stated that at the same height above ground as in Figure 37, Figure 38 show a negative pressure coefficient beneath the airfoil for 2 deg AOA. This C_P distribution suggests that airflow was traveling faster across the lower surface of the

airfoil compared to the upper surface producing negative circulation and negative lift. The 8 deg AOA C_P distribution was due to the airfoil producing lift. The C_P distribution in Figure 40 suggests that the thickness of the airfoil was the reason for the negative lift (1).

In cooperation with this study, Lt Westfall (28) studied the ground effects of the Lambda UCAV model via CFD modeling for his class project. He used the Lambda UCAV Solid Works model that was created in this study and converted it to an IGES file. The IGES file was then used in Gridgen to build a grid that was used in Fluent solver program. Due to time constraint an inviscid model was used and full caparison of the CFD results was not made with the experimental results.

The resulting grids for the Lambda model consisted of the connectors along the top and bottom of the body with 150 grid points each. The trailing edge had 120 grid points on it. The face on the tail had 40 grid points on the top, 11 on the bottom, and 10 up the side. The nose face had 8 grid points up the center and 10 on each of the top and bottom connectors creating semi-circle. This resulted in unstructured meshes of 2,688 cells and 2,483 cells on the top and bottom surfaces, The leading edge was two 50x19 structured meshes. All connectors used equal spacing due to time constraint (28).

The resulting grids for the wind tunnel consisted of 20 grid points on the long connectors along the length of the tunnel, 10 grid points on each of the longer connetors creating the intake and outflow faces of the tunnel, 4 grid points on corners of the outflow, and 5 grid points on the corners of the intake face. This resulted in 4,276 cells in the plane of symmetry, 235 cells on the intake face, 183 cells on the outflow face, and 667

cells on the rest of the wind tunnel. Overall, a block of 306,112 tetrahedrons were created. Figure 39 illustrates the Lambda UCAV model and wind tunnel in Gridgen (28).

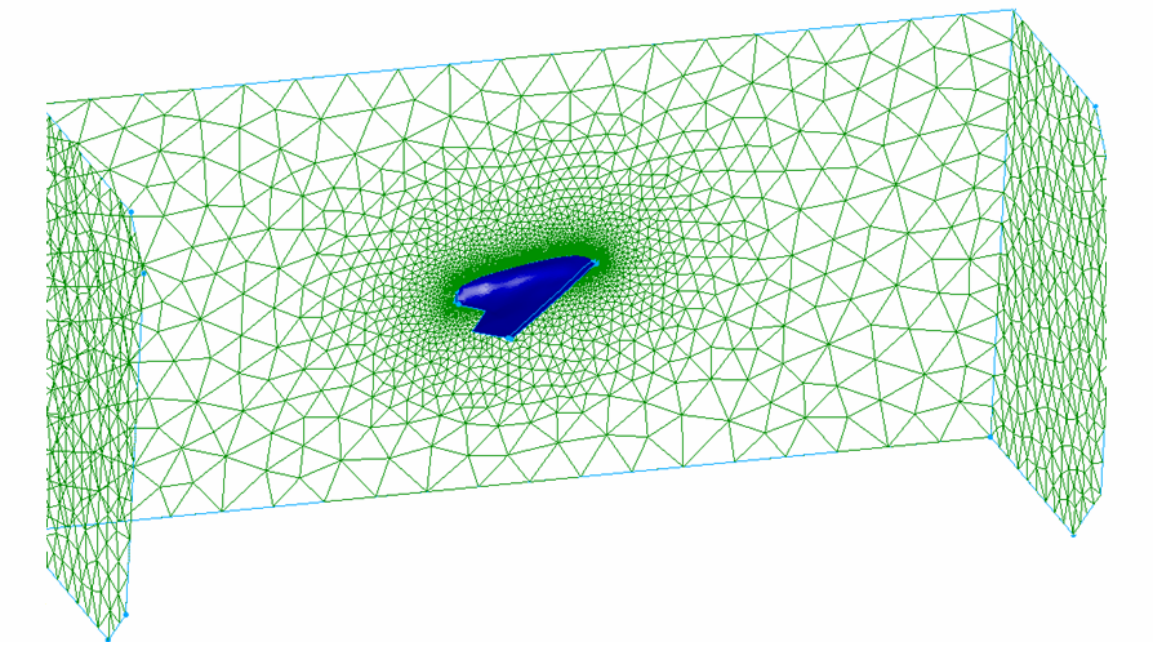

Figure 39: Lambda UCAV model and windtunnel in Gridgen at 8 degrees AOA (28)

The FLUENT solver's resuting OGE C_L is 0.01263 for 8 deg AOA and inlet velocity of 100 mph. Figure 40 illustrates the static pressure contours on the surface of the wing. Due to OGE condition, the pressure distribution does not vary much over the upper surface. In contrast, the pressure distribution varies more on the the lower surface with higher static pressures compared to the upper surface creating lift as illustrated in Figure 41.

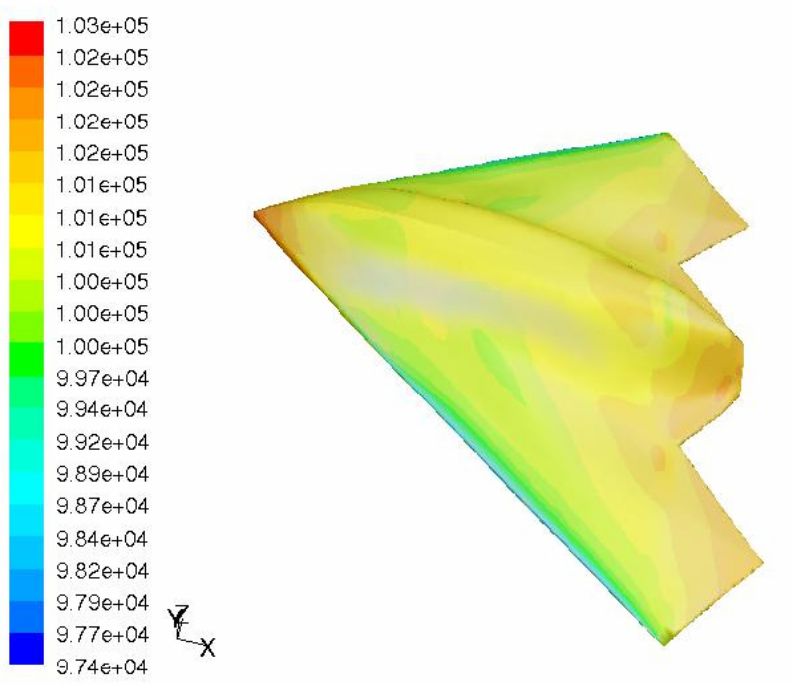

Figure 40: Lambda UCAV model's upper surface contours of static pressure in pascal for OGE at 8 degrees AOA (28)

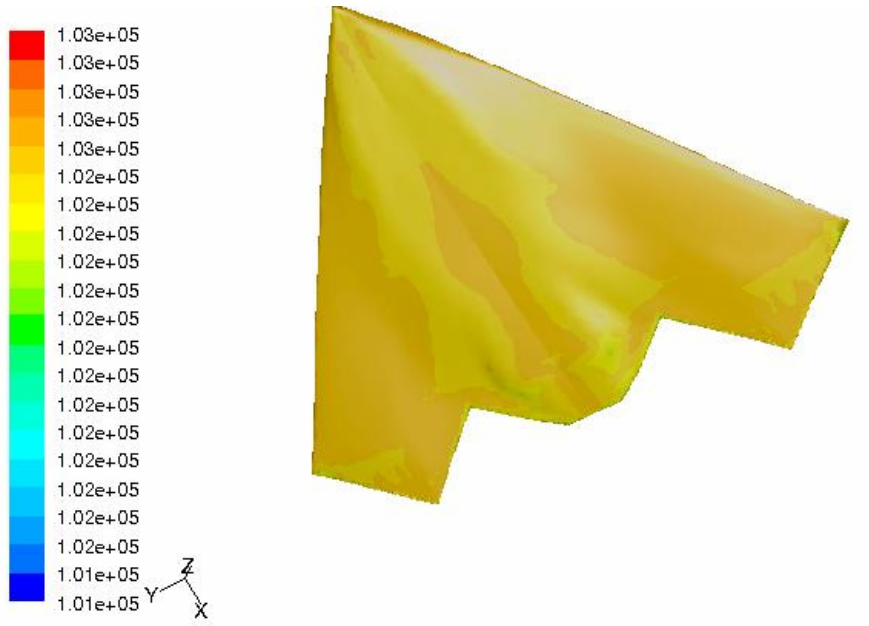

Figure 41: Lambda UCAV model's lower surface contours of static pressure in pascal for OGE at 8 degrees AOA (28)

Figure 42 illustrates the IGE conditions at h/b = 0.3. The resuting Lambda model's C_L for 8 deg AOA is 0.01402. This is an 11% increase is lift from OGE to IGE at h/b = 0.3. The percent change in C_L due to ground effect for Lambda UCAV model predicted by Equation [2] in Chapter 2 was 11.3% while the actual AFIT LSWT experimental C_L increase was 8.5% from OGE to IGE at h/b = 0.3. This difference of 2.5% in C_L may be due to the combination of the inviscid CFD modeling.

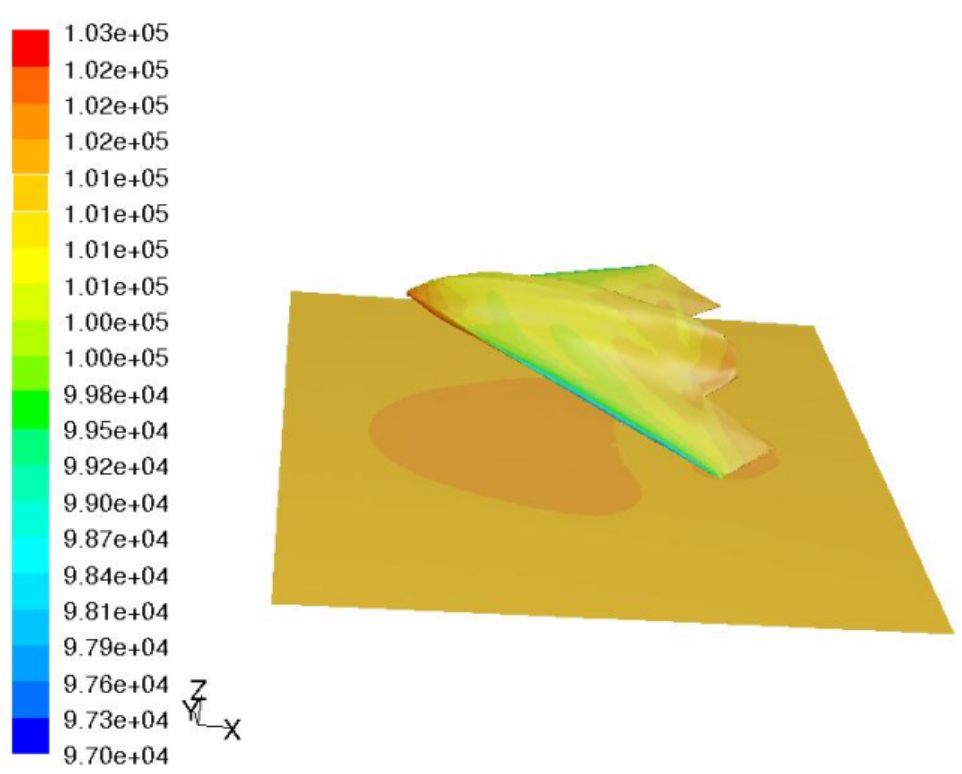

Figure 42: Lambda UCAV model's contours of static pressure in pascal for IGE (h/b = 0.3) (28)

Figure 42 also illustrates the increased pressure on the ground and the bottom surface due to the ground effect resulting in increase in C_L. For IGE, ground effect is due to the interaction of the lambda UCAV's wingtip vortices with the ground. The increase

in C_L results from the reduction of the wing's downwash due to weakened wing tip vortices.

In addition, percent increase in lift coefficient is a valuable reason for studying the ground effect. The magnitude of the increase in lift can be used to classify certain types of aircraft configurations. Figure 3 shows that aircraft with aspect ratios close to 3 can expect a change in lift coefficient around 10% when at a height above ground of h/b = 0.3 (18). As for the OGE data (h/b = 0.93), it was measured at a different Re due to the velocity measurement correction and ground plane blockage, the data from this study can not be directly compared to Figure 3. The Chevron UCAV model showed a 8.8% increase in C_L at 40 mph, 8.7% increase at 60 mph, 8.9% increase at 80 mph, and 14% increase at 100 mph at an AOA of 8 deg from OGE to h/b=0.3. The Lambda UCAV model showed similar increases in C_L with 6.9% increase at 40 mph, 7.6% increase at 60 mph, 9.9% increase at 80 mph, and 8.5% increase at 100 mph all at an AOA of 8 deg from OGE to h/b=0.3 . The percent increases in C_L experimental results are similar to the predicted values from Equation (3), 10.9% increase for Chevron model and 11.3% increase for Lambda model.

Section 2.3.2 – Drag Coefficient Variation

In contrast to lift coefficient, the drag coefficient generally increased for all AOA measured except for at h/b = 0.05 at AOAs greater than or equal to 0 degrees. Figures 43 and 44 bellow and Figures 58 and 62 in the Appendix B illustrate the ground effect influence on C_D of the Chevron UCAV model and Figures 45 and 46 below and Figures 70 and 74 in the Appendix B illustrate the ground effect influence on C_D of the Lambda UCAV model.

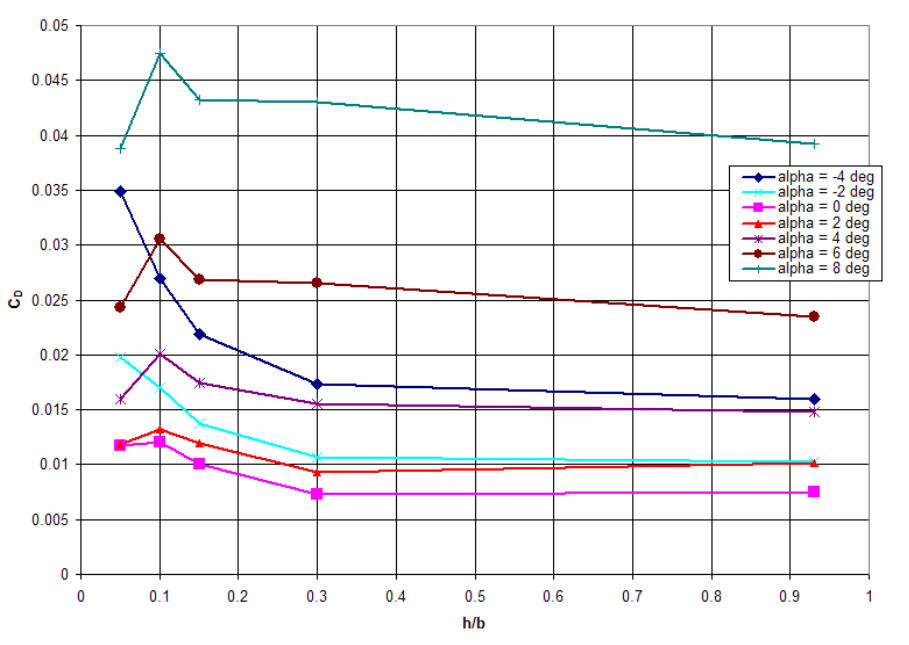

Figure 43: Chevron UCAV Ground Effect - C_D vs. (h/b) 40 mph

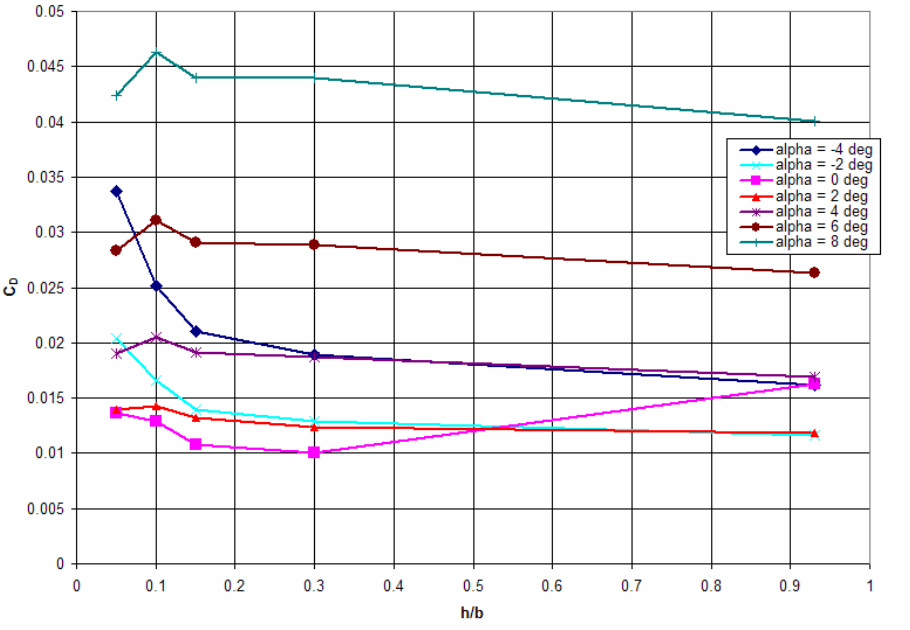

Figure 44: Chevron UCAV Ground Effect - C_D vs. (h/b) 60 mph

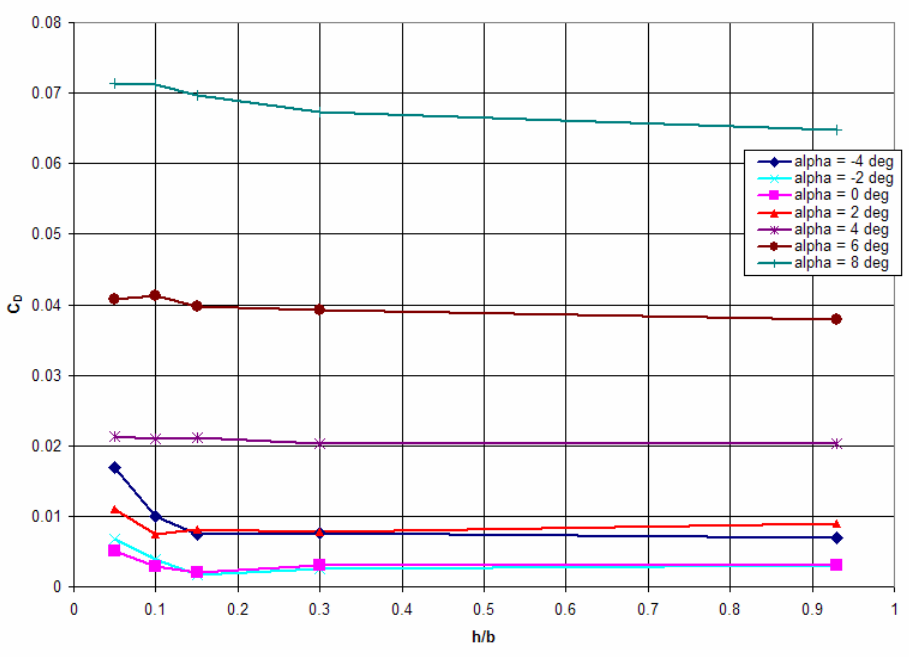

Figure 45: Lambda UCAV Ground Effect - C_D vs. (h/b) 40 mph

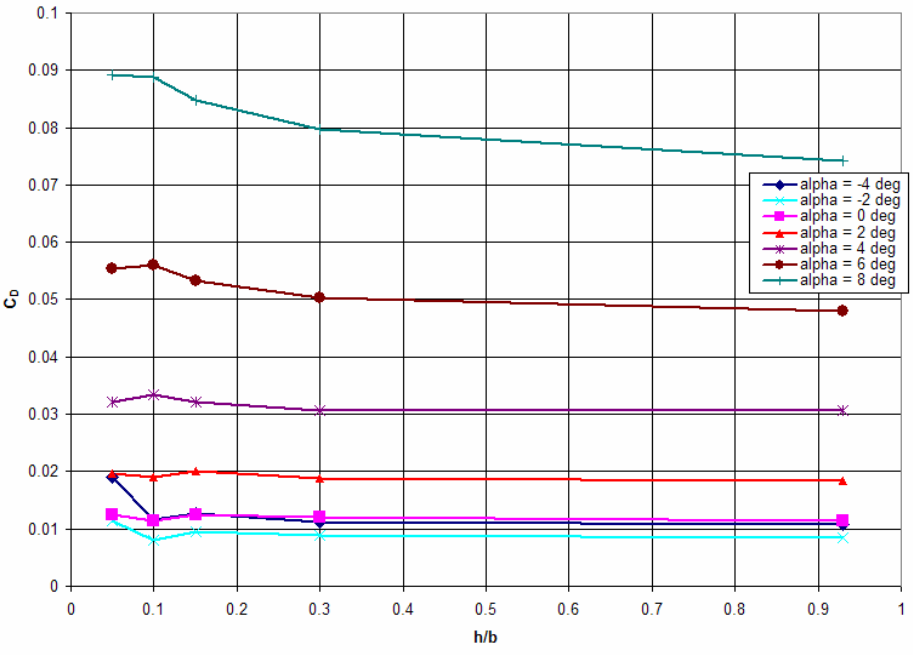

Figure 46: Lambda UCAV Ground Effect - C_D vs. (h/b) 60 mph

For the Chevron UCAV model, the C_D at AOA greater than 0 degress steadily increased as height above ground decreased. For the AOA of 6 and 8 deg, this result was expected after noticing the behavior of the lift. At h/b = 0.05, C_D dropped slightly at an AOA from 2 deg to 8 deg. The C_D increase may be from the C_L^2 effects of the induced drag which is stronger from increase in lift initially. As h/b decreases the McComick's induced drag factor effects gets stronger and decreases the total drag. This trend is consistent with Lee's study illustrated in Figure 4. The slight decrease in C_D from h/b=0.10 to h/b=0.05 may also be from the C_L=1.0 and h/b=0.05 condition which is on the borderline between the conventional ground board adequate and the moving belt ground plane required regions. The C_L=1.0 and h/b=0.05 condition may be further investigated in the future studies with a moving ground plane to verify the increase in lift and decrese in drag trend.

The percent increases in C_D of the Chevron UCAV model were 9.6% at 40 mph, 9.8% at 60 mph, 10.7% at 80 mph, and 9.0% at 100 mph at 8 deg AOA and from OGE to h/b-0.3. The percent increases in C_D of the Lambda UCAV model were 3.9% at 40 mph, 7.5% at 60 mph, 9.8% at 80 mph, and 8.0% at 100 mph at 8 deg AOA and from OGE to h/b-0.3. These percent increases in C_D are comparable to those decribed by Curry (5), and Curry and Owens (14) who found that the Tu-144 and F-16 XL aircraft experienced an increase in drag on the order of 5-15%. This illustrates that other aircraft of similar aspect ratio and wing sweep can experience an increase in C_D while in the ground effect region (1).

Section 2.3.3 – Lift-to-Drag Ratio Variation

In an effort to understand the complexities of the ground effect better for the Chevron and Lambda UCAV models, lift-to-drag ratios (L/D) were calculated. Usually, L/D directly corresponds to aircraft efficiency, and is typically used to illustrate the improved, or in this study's case, unimproved efficiency of the ground effect region (1). Figures 47 and 48 below and Figures 60 and 64 in the Appendix B illustrate the negative trend of L/D for the Chevron UCAV for 40, 60, 80, and 100 mph respectively. Figures 48 and 49 below and Figures 72 and 76 in the Appendix B illustrate the negative trend of L/D for the Lambda UCAV while in the ground effect region for 40, 60, 80, and 100 mph respectively.

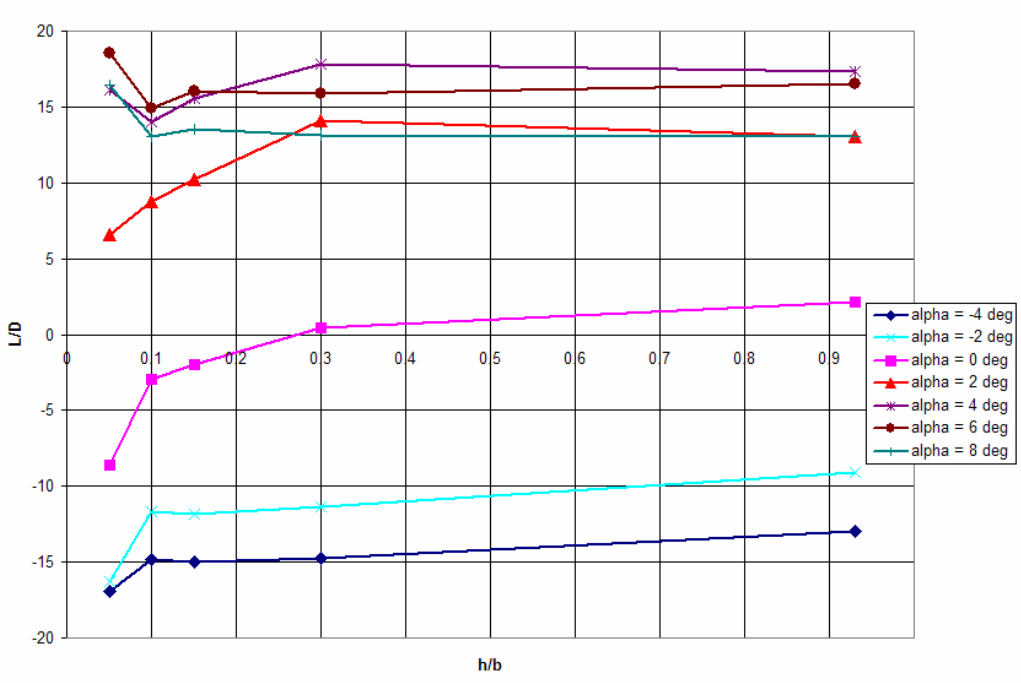

Figure 47: Chevron UCAV L/D vs. (h/b) 40 mph

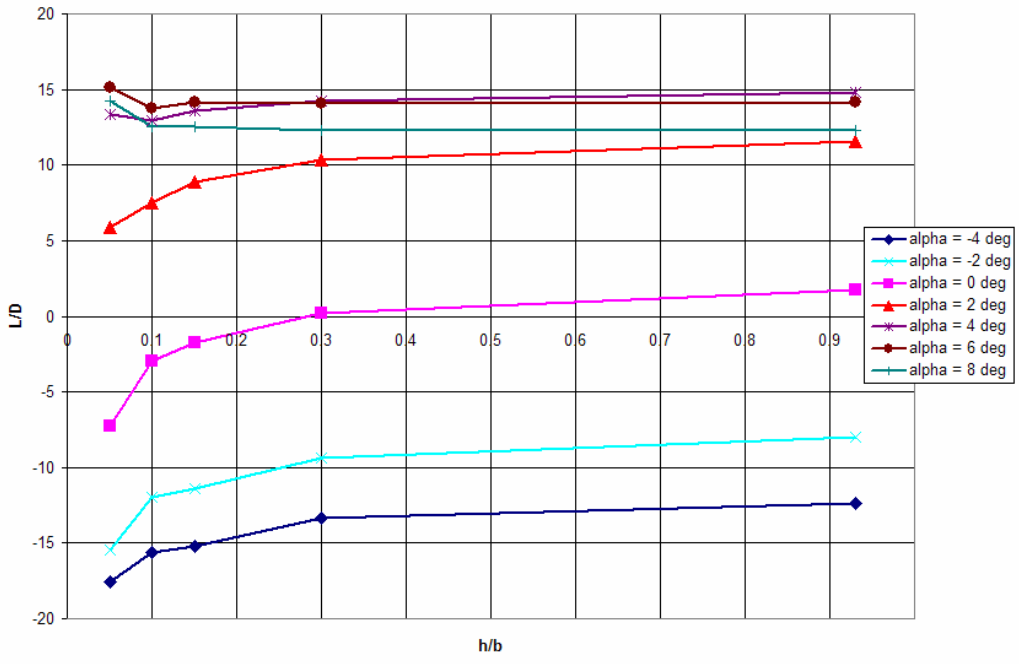

Figure 48: Chevron UCAV L/D vs. (h/b) 60 mph

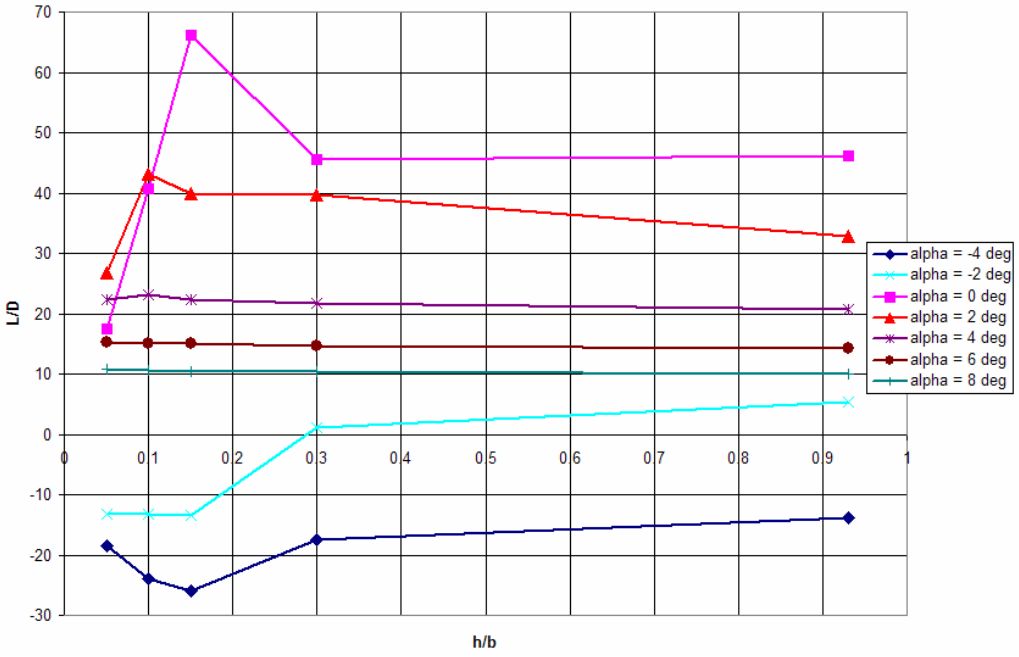

Figure 49: Lambda UCAV L/D vs. (h/b) 40 mph

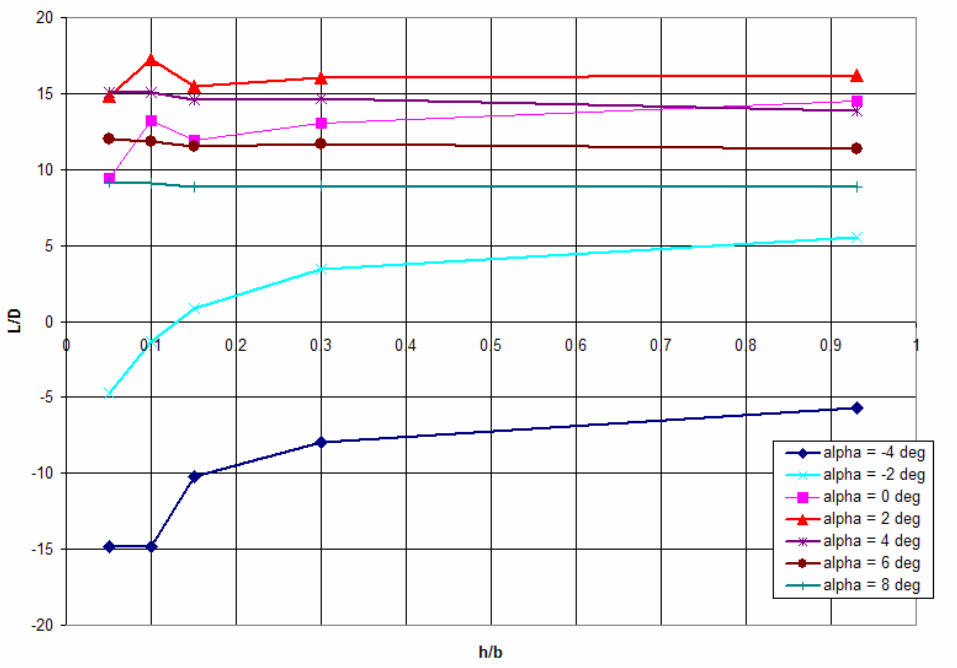

Figure 50: Lambda UCAV L/D vs. (h/b) 60 mph

For the Chevron UCAV, the only positive slope was at an AOA of 4, 6 deg for h/b=0.10 to h/b=0.05 at 40 mph, where it had the maximum value of L/D, as shown in Figure 51. As for the Lambda UCAV, the positive slopes were at AOA from 0 deg to 8 deg as height above ground decreased, while having the maximum value of L/D at AOA of 0 deg as illustrated in Figure 52. In addition, the Chevron UCAV model experienced a reduction in drag for AOAs of 4, 6, and 8 deg from h/b = 0.10 to h/b = 0.05. The Lambda UCAV model experienced a reduction in drag for AOAs of 4 and 8 deg from h/b = 0.10 to h/b = 0.05.

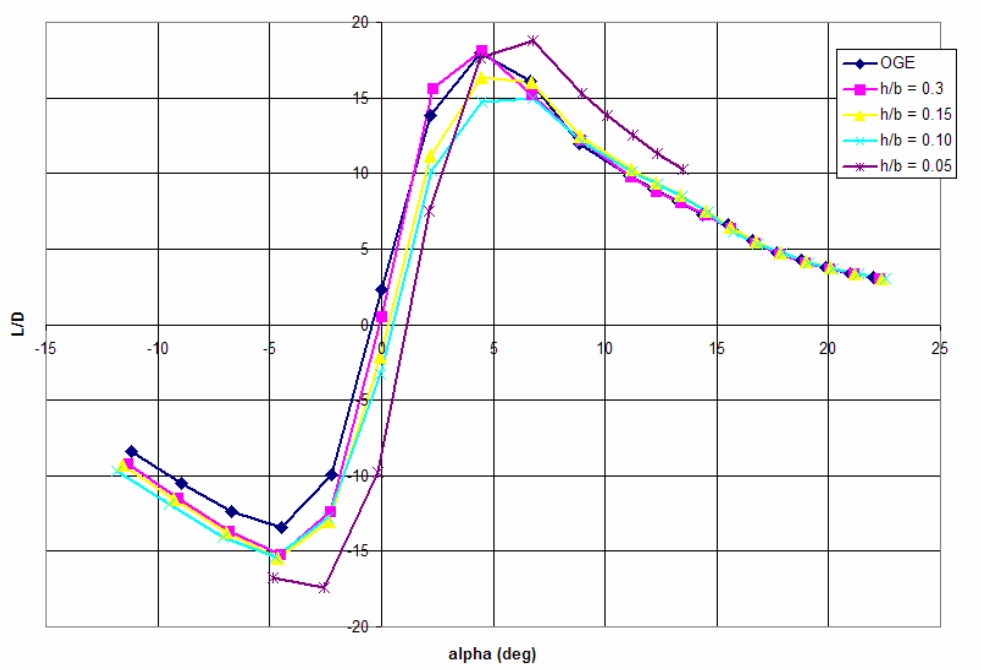

Figure 51: Chevron UCAV Ground Effect - L/D vs. alpha, 40 mph

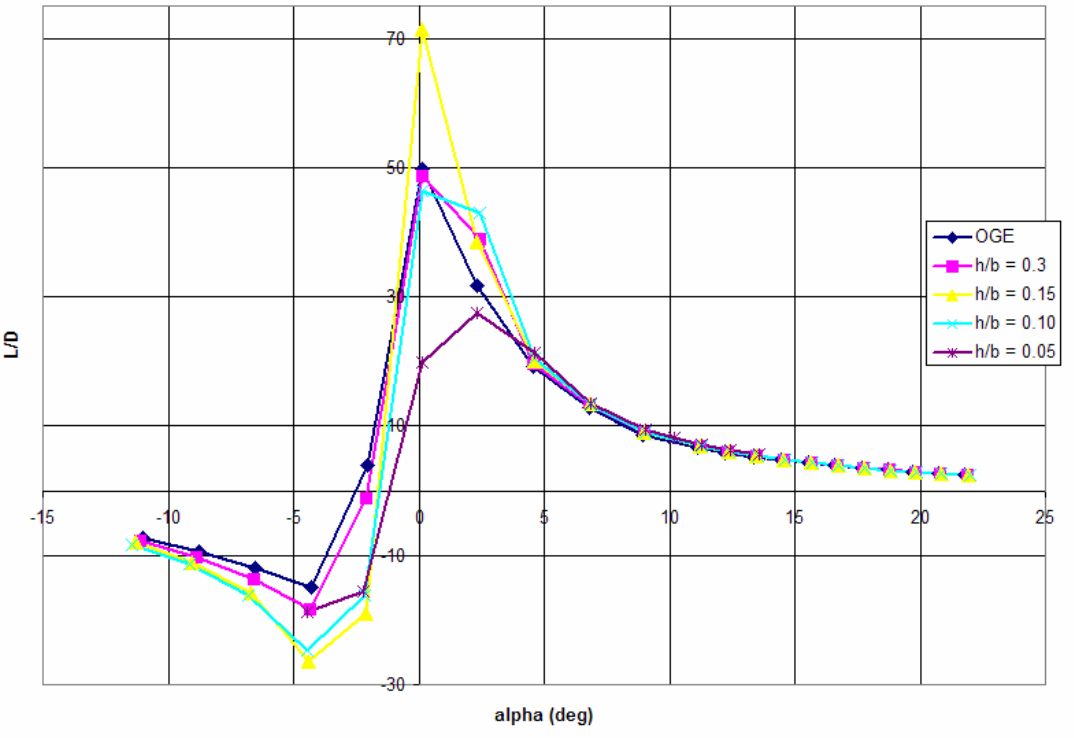

Figure 52: Lambda UCAV Ground Effect - L/D vs. alpha, 40 mph

The Chevron UCAV L/D results in Figure 51 show the maximum L/D range from 15.0 (h/b=0.10) to 18.8 (h/b=0.05) for 40 mph. The L/D maximum ranges for 60, 80, and 100 mph were from 13.8 (h/b=0.10) to 15.4 (h/b=0.05), from 15.1 (h/b=0.10) to 16.0 (OGE) and from 15.2 (h/b=0.10) to 16.4 (OGE), respectively. The highest L/D maximums were at the OGE condition for 80 and 100 mph as opposed to h/b=0.05 condition for 40, and 60 mph.

The Lambda UCAV L/D results showed an anomaly of high L/D maximum at 40 mph as compared to 60, 80, and 100 mph. Figure 52 shows L/D for Lambda UCAV model at 40 mph with maximum L/D range from 27.4 (h/b=0.05) to 71.4 (h/b=0.15). The maximum L/D values at 40 mph were due to extremely low drag compared to lift. As opposed 40 mph, 60, 80, and 100 mph L/D maximums were in much lower range. The L/D maximum ranges were from 15.0 (h/b=0.05) to 17.7 (h/b=0.10) for 60 mph, from 17.0 (h/b=0.30) to 19.6 (h/b=0.10) for 80 mph, and from 17.8 (h/b=0.30) to 19.4 (h/b=0.10) for 100 mph.

Section 3 – Test Section Flow Visualization

To ensure the air flow over the ground plane was uniform, a flow visualization experiment was conducted similar to reference 1. Small tufts were attached the ground plane surfaces covering the leading edge, side edges, across the circular gap, and uniformly across the remainder of the surface (1). The flow visualization results of this study were identical to those in ENS Jones'study in that the flow was straight and uniform beneath the model which confirmed that no obvious irregularities existed where the balance gathered data.

Section 4 – Results and Analysis Summary

The main objective of this study was to identify the ground effect region for the Chevron and Lambda UCAV planforms with respect to forces and moments and aerodynamic coefficients. Models of the Chevron and Lambda UCAVs have been tested in static ground effect. From these test data, the ground effect regions for both models were characterized by an increase in lift and drag, but for lift-to-drag ratio the Chevron UCAV model decreased in ground effect and the Lambda UCAV mocel increased in ground effect.

The C_L increased in ground effect with decrease in height above ground for both the Chevron and the Lambda UCAV models. The Chevron UCAV model results showed the C_L increased with decreasing height above ground and the C_L also increased with increase in velocity for AOAs of 6 and 8 deg. The percent increase in C_L was 8.8% at 40 mph and 14% at 100 mph for 8 deg AOA from OGE to h/b=0.3. But for 4 deg AOA, the C_L does not change much with decrease in height above ground. The percent increase in C_L was 6.2% at 40 mph, 7.4% at 80 mph, and 4.3% at 100 mph for 4 deg AOA. For 2 deg AOA, the C_L decreased with decreasing height above ground and the C_L also decreased further with increase in velocity. At 2 deg AOA, the C_L decrease was -1.6% at 40 mph, and -21.4% at 100 mph. This trend was consistent with Jones' analysis of the C_P contour plot of the 2-D airfoils in reflection for the Chevron UCAV. The negative C_P beneath airfoil in Figure 40 suggested that the flow was traveling faster due to the Ventri effect (1). This higher velocity caused lift to decrease. The trends from a 2-D vortex panel program agreed with the experimental results (1).

The Lambda UCAV model C_L variation results also showed the C_L increased with decrease in height above ground and the C_L also increased and then decreased with increase in velocity for AOAs 2, 4, 6, and 8 deg. For 8 deg AOA from OGE to h/b=0.3, the percent increase in C_L was 6.9% at 40 mph, 9.9% at 80 mph, and 8.5% at 100 mph. At 6 deg AOA the percent increase in C_L was 5.9% at 40 mph, 9.1% at 80 mph, and 7.9% at 100 mph.

Also for the Lambda UCAV model, the percent change in C_L due to ground effect from Equation (3) in Chapter 2 was 11.3%, while the actual AFIT LSWT experimental C_L increase was 8.5% and CFD study's C_L increase was 11% from OGE to IGE at h/b = 0.3. This difference of 2.5% in C_L may be due to the combination of the invicid CFD modeling and studies at different point of reference of quarter chord for the CFD modeling and 2.125 aft of its CG.

In addition, the C_D also increased for both UCAV models while in ground effect with a decrease height above ground. The Chevron UCAV model results showed the C_D increased with decreasing height above ground, and the C_D also increased and then decreased with an increase in velocity for AOAs of 4, 6, and 8 deg. At 8 deg AOA from OGE to h/b=0.3, the percent increase in C_D was 9.6% at 40 mph, 10.7% at 80 mph, and 9% at 100 mph.

Similarly, the lambda UCAV model C_D variation results showed the C_D increased with decreasing height above ground and the C_D increased and then decreased with increase in velocity for AOAs of 4, 6, and 8 deg. At 8 deg AOA from OGE to h/b=0.3, the C_D percent increase was 3.9% at 40 mph, 9.8% at 80 mph, and 8% at 100 mph.

Also, for both Chevron and Lambda UCAV models, the C_D variation with height above ground for AOAs of 2, 4, 6, and 8 deg showed that the drag from OGE to h/b=0.10 increased and drag then decreased from h/b=0.10 to h/b=0.05. Similar trend of increase in C_D with decrease in h/b was noted in Lee's F106 ground effect study illustrated in Figure 4. The slight decrease in C_D at h/b=0.05 was probably from the flight condition of C_{Lmax}=1.0 and h/b=0.05 that was on the borderline between the conventional ground-board-adequate and the moving-belt-ground-plane-required regions.

The L/D for the Chevron UCAV model decreased in ground effect with decrease in height above ground. The L/D variation for the Chevron UCAV model results from OGE to h/b=0.10 showed the L/D decreased with decreasing height above ground and the L/D decreased further with increase in velocity from 40 to 100 mph for AOAs from -7 to 8 deg. From h/b=0.10 to h/b=0.05, the L/D increased for 4, 6, and 8 deg AOA. The overall trend from Figure 51 is that L/D increased for low AOAs and reached maximum at 5 deg AOA. For AOAs greater than 7 deg, L/D decreased upto highest AOA of 22 deg.

The Lambda UCAV model L/D increased with decreasing height above ground. The Lambda L/D variation results showed the L/D increased with decrease in height above ground and the L/D decreased with increase in velocity for AOAs of 4, 6, and 8 deg. But for 2 deg AOA, L/D increased 21% at 40 mph and decreased for 60, 80, and 100 mph. The overall trend from Figure 52 is that L/D increased AOA from -2 deg to 1 deg and reached maximum at 1 deg AOA. For AOAs greater than 3 deg, L/D decreased upto highest AOA of 22 deg.

The moment coefficient, $C_{m,}$ data were taken and reduced but was not analyzied dut to time constraint. All C_m data charts and tables are included in the Appendix B and Appendix C respectively.

As for this study's OGE data comparison with Reed's, the OGE results still compared to a reasonable degree of accuracy, even though not all test conditions could be matched with Reed's study. Re differences were the likely reason for the slight variation for both UCAV models. As Re increases the total drag increases due to stronger influence of increase in skin friction and form drag over decrease in induced drag. The variation for the Lambda UCAV may be from the 3-D modeling process from its proof model vs. the original Lambda UCAV.

In addition, the ground plane used in this study had no major installation or testing issues. The airflow traveled across the ground plane with uniform flow, but blockage corrections for wind tunnel speed were necessary.

Finally, the existing aerodynamic database for moderately swept, low aspect ratio, tailless, blended wing body UAVs was expanded. This was accomplished for full range of angles of attack at low speeds for both Chevron and Lambda UCAVs. All data from this study are in the appendix to include additional ground effect plots in Appendix B, and data tables in the Appendix C.

V. Conclusions & Recommendations

Section 1 – Conclusions

Two UCAV models (Chevron and Lambda) were tested in static ground effect. The ground effect regions for both models were characterized by an increase in lift and drag, but for lift-to-drag ratio the Chevron UCAV model decreased in ground effect and the Lambda UCAV model increased in ground effect.

The C_L increased in ground effect with decrease in height above ground for both the Chevron and the Lambda UCAV models. The C_L for the Chevron UCAV model increased with decreasing height above ground and the C_L also increased with increases in velocity for AOAs of 6 and 8 deg, but for 4 deg AOA, the C_L does not change much with decrease in height above ground. The C_L decreased for 2 deg AOA and below as height above ground decreased. This trend was consistent with a prior 2-D vortex panel code analysis. The C_L for the Lambda UCAV model increased with a decrease in height above ground even for the two lower AOAs, 2 and 4 deg. The Lambda UCAV model also compared well with the theoretical and computational (CFD) C_L calculations and was within 2.5% in increase in C_L.

In addition, the C_D increased for both UCAV models in ground effect with decrase in height above ground. The Chevron and Lambda UCAV models' results showed the C_D increased with decrease in height above ground and the C_D also increased with increases in velocity for AOAs of 4, 6 and 8 deg. In addition, for both of the Chevron and Lambda UCAV model, the C_D trend with height above ground for AOA equal to 2, 4, 6 and 8 deg showed that the drag from OGE to h/b=0.10 increased and , the

C_D then decreased from h/b=0.10 to h/b=0.05. The C_D increase may be from the C_L^2 effects of the induced drag which is stronger from increase in lift initially. As h/b decreases the McComick's induced drag factor effects gets stronger and decreases the total drag. The slight decrease in C_D from h/b=0.10 to h/b=0.05 may also be from the C_L=1.0 and h/b=0.05 condition which is on the borderline between the conventional ground board adequate and the moving belt ground plane required regions. The C_L=1.0 and h/b=0.05 condition may be further investigated in the future studies with a moving ground plane to verify the increase in lift and decrese in drag trend.

The L/D variation for the Chevron UCAV model decreased with decreasing height above ground and the L/D decreased further with increase in velocity from 60 to 100 mph for AOAs of 2, 4, 6, and 8 deg. And, the Lambda UCAV model L/D increased with decreasing height above ground and the L/D decreased with increase in velocity for AOAs of 4, 6, and 8 deg.

The moment coefficient, $C_{m,}$ data were taken and reduced but was not analyzied dut to time constraint. All C_m data charts and tables are included in the Appendix B and Appendix C respectively.

The OGE results compared to a reasonable degree of accuracy to Reed's full scale, even though not all test conditions could be matched. Re differences were the likely reason for the slight variation for both UCAV models. As Re increases the total drag increases due to stronger influence of increase in skin friction and form drag over decrease in induced drag. The variation for the Lambda UCAV may be from the 3-D modeling process from its proof model vs. the original Lambda UCAV.

In addition, the ground plane used in this study had no major installation or testing issues. The airflow traveled across the ground plane with uniform flow, but blockage corrections for wind tunnel speed were necessary.

Finally, the existing aerodynamic database for moderately swept, low aspect ratio, tailless, blended wing body UAVs was expanded. This was accomplished for full range of angles of attack at low speeds for both Chevron and Lambda UCAVs.

Section 2 - Recommendations

This study should significantly add to the tailless, blended wing body configurations database for the Chevron and Lambda UCAV planforms. Based on the findings of this study, the following are recommendations for further experiments and analysis:

- use a moving ground plane or set up a boundary layer removal system, such as blowing or sucking air along the top surface of the ground plane , to better simulate an actual aircraft flying over the ground;
- the control and stability study in ground effect using flaps similart to Reed's study
- analyze the effects of sideslip and lateral stability of the chevron UCAV in ground effect;
-study a dynamic ground effect experiment for the Chevron and Lambda UCAVs and compare with static ground plane
- do a CFD study including viscous effects to compare with this study's ground effect results

- measure the wake and/or vortices shed by the UCAV at all ground plane heights in order to analyze ground effects

Appendix A: Data Reduction Sample Calculation

The following is a sample calculation for the MATLAB© data reduction program used for this experiment for the following test condition:

$U_\infty = 40$ mph

$\frac{h}{b} = 0.15$

$\alpha = 2.17$ deg

Test room conditions and model specifics:

$T = 531.0$ °R

$P = 14.186$ psia

$R = 1716 \ \frac{\text{ft-lb}_f}{\text{slug-R}}$

$\mu = 0.372 \text{x} 10^{-6} \ \frac{\text{slug}}{\text{ft-sec}}$

$c_r = 0.6183$ ft

$S = 0.607 \text{ ft}^2$

$b = 1.333$ ft

$AR = \frac{b^2}{S} = 2.93$

$\gamma = 1.4$

$\rho = \frac{P}{R * T} = 0.0022 \frac{slugs}{ft^3}$

$q_\infty = \frac{1}{2} * \rho * U_\infty^2 = 3.858 \frac{lb_f}{ft^2}$

$a = \sqrt{\gamma * R * T} = 1129.4 \frac{ft}{\text{sec}}$

Blockage / Velocity Corrections:

ε = blockage correction term

sb = solid blockage

gp = ground plane

tc = transducer correction

K_1 = body shape factor = 1.04

$\tau_1 = f(\text{test section shape \&} \frac{2b}{B}) = 0.86$

$Wing\ volume = Body\ volume = 0.03668\ \text{ft}^3$

C = tunnel cross section area = 9.4722 ft^2

$$\varepsilon_{sb,wing} = \frac{K_1 * \tau_1 * Wing\ volume}{C^{3/2}} = 0.001125$$

$\varepsilon_{gp} = 1.016$ (calculated from hot-wire results)

$\varepsilon_{tc} = 0.983$ (calculated from hot-wire results)

$$\varepsilon_{total} = \varepsilon_{sb} + (\varepsilon_{gp} * \varepsilon_{tc} - 1) = 3.039x10^{-5}$$

Note: solid blockage correction equations taken from Barlow, et al. (27)

Calculating the flight parameters with corrections applied:

$$U_{\infty,corr} = U_{\infty} * (1 + \varepsilon_{total}) = 58.6684 \frac{ft}{\text{sec}} = 40.0012 \text{ mph}$$

$$q_{\infty,corr} = q_{\infty} * (1 + \varepsilon_{total})^2 = 3.8583 \frac{lb_f}{ft^2}$$

$$M = \frac{U_{\infty,corr}}{a} = 0.0519$$

$$\text{Re} = \frac{\rho * U_{\infty,corr} * c_r}{\mu} = 2.19x10^5$$

The raw data from the control computer contained the following measurements: [N_1, N_2, S_1, S_2, A_1, ℓ]. These force and moment measurements were subtracted from the tare effects and corrected for the balance interactions. Refer to DeLuca (26) or Rivera (29) see a complete procedure of data reduction program. The remainder of the sample

calculation will carry on after the balance and tare effects were removed from the inputted data.

The corrected data was originally in the UCAV's body axis frame. The following equations converted the drag, side, and lift forces $\begin{bmatrix} D & S^* & L \end{bmatrix}$; and roll, pitch, and yaw moments $\begin{bmatrix} \ell & m & n \end{bmatrix}$ into the wind axis frame:

$$\begin{bmatrix} D \\ S^* \\ L \end{bmatrix}_{wind} = \begin{bmatrix} A^*\cos\theta^*\cos\psi + Y^*\sin\psi + N^*\sin\theta^*\cos\psi \\ -A^*\sin\psi^*\cos\theta + Y^*\cos\psi - N^*\sin\theta^*\sin\psi \\ -A^*\sin\theta + N^*\cos\theta \end{bmatrix}$$

$$\begin{bmatrix} \ell \\ m \\ n \end{bmatrix}_{wind,bc} = \begin{bmatrix} \ell^*\cos\theta^*\cos\psi - m^*\sin\psi + n^*\sin\theta^*\cos\psi \\ \ell^*\sin\psi^*\cos\theta + m^*\cos\psi + n^*\sin\theta^*\sin\psi \\ -\ell^*\sin\theta + n^*\cos\theta \end{bmatrix}_{body,bc}$$

where:

$A = A_1 corrected = 0.01561$ lb_f
$Y = S_1 corrected = 0.00285$ lb_f
$N = N_1 corrected = 0.49611$ lb_f
$l = lcorrected = -0.02482$ lb_f-in
$m = N_2 corrected = -0.21113$ lb_f-in
$n = S_2 corrected = -0.01180$ lb_f-in
θ = pitch angle (AOA) = 0.0379 rad = 2.174 deg
ψ = yaw angle = 0 deg

Carrying out the above force equations for drag and lift: (side force was treated as negligible and not used in the analysis)

D = 0.03442 lb_f
L = 0.49516

Non-dimensionalizing the lift and pitching moment yields:

$$C_{L_w} = \frac{L}{q_{\infty,corr} * S} = 0.21143$$

The value for lift coefficient agree to those in Table 16 to 38%. The 38% error in C_L may be attributed to the several reasons discussed in Chapter V, and also its small value which ampifies any variance to high percentage error.

The drag coefficient was corrected for test section geometry and flow field interference as such:

$$\delta = \frac{b}{Tunnel\ span\,(B)} = 0.3636$$

$$\Delta C_{D_w} = \frac{\delta * S}{C}(C_{L_w})^2 = 0.00104$$

The final drag coefficient is as follows:

$$C_{D_u} = \frac{D}{q_{\infty,corr} * S}$$

$$C_{D,corr} = C_{D_w} + \Delta C_{D_w} = 0.01574$$

The corrected drag coefficient disagrees with the value in Table 16 by 23%. The 23% error in C_D may also be attributed to the several reasons discussed in Chapter V, and its small value which ampifies any variance to high percentage error.

Appendix B: Additional Ground Effect Plots

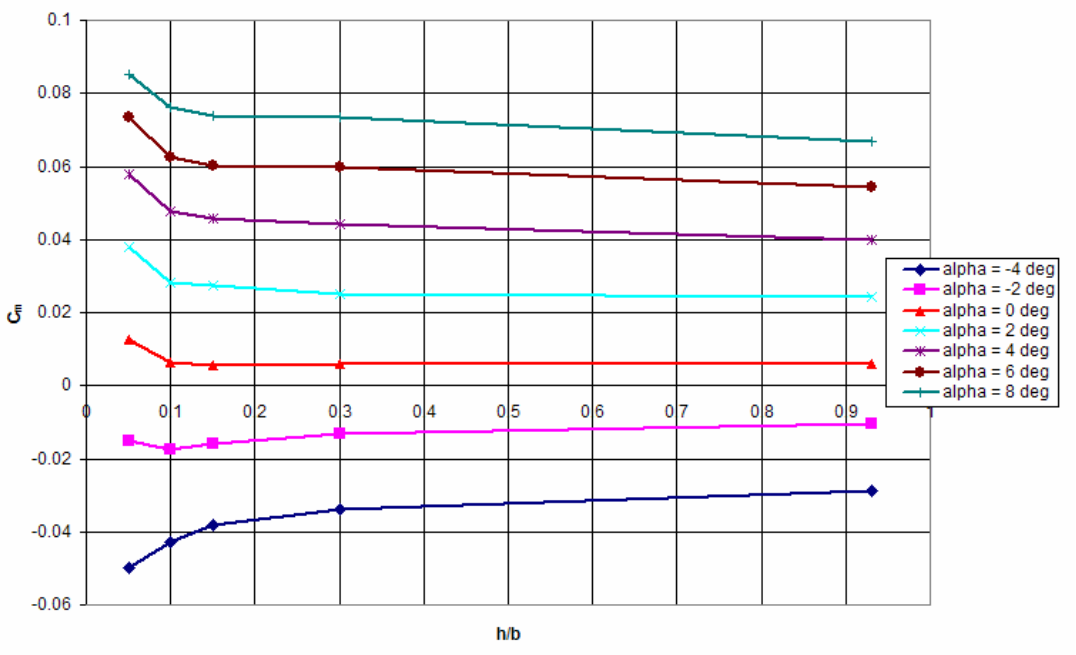

Figure 53: Chevron UCAV C_m vs. (h/b) 40 mph

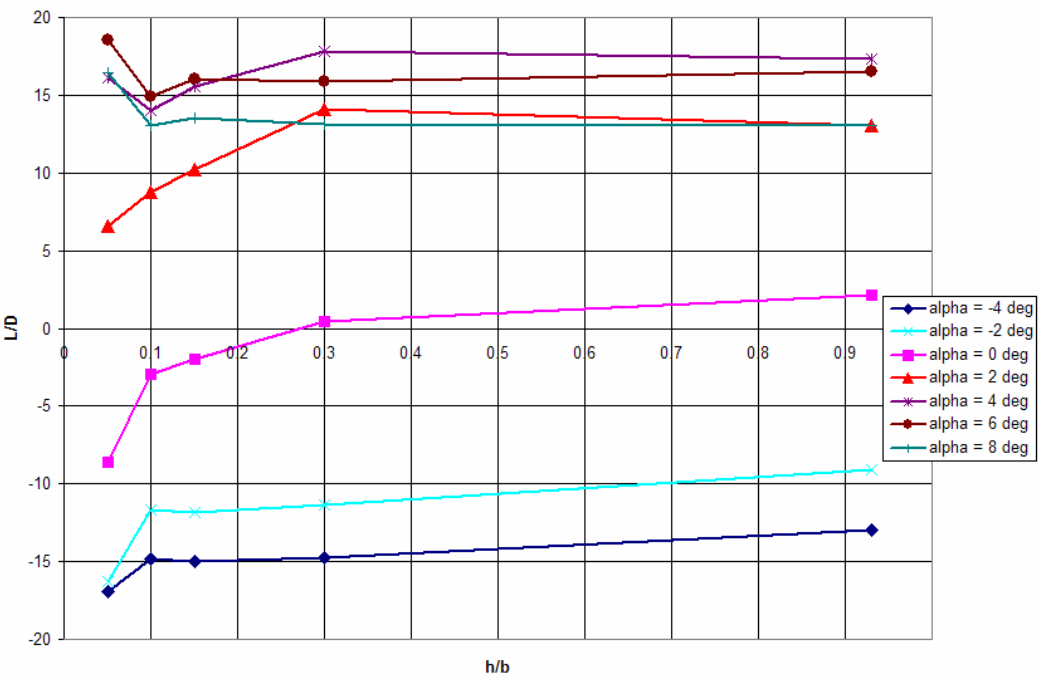

Figure 54: Chevron UCAV L/D vs. (h/b) 40 mph

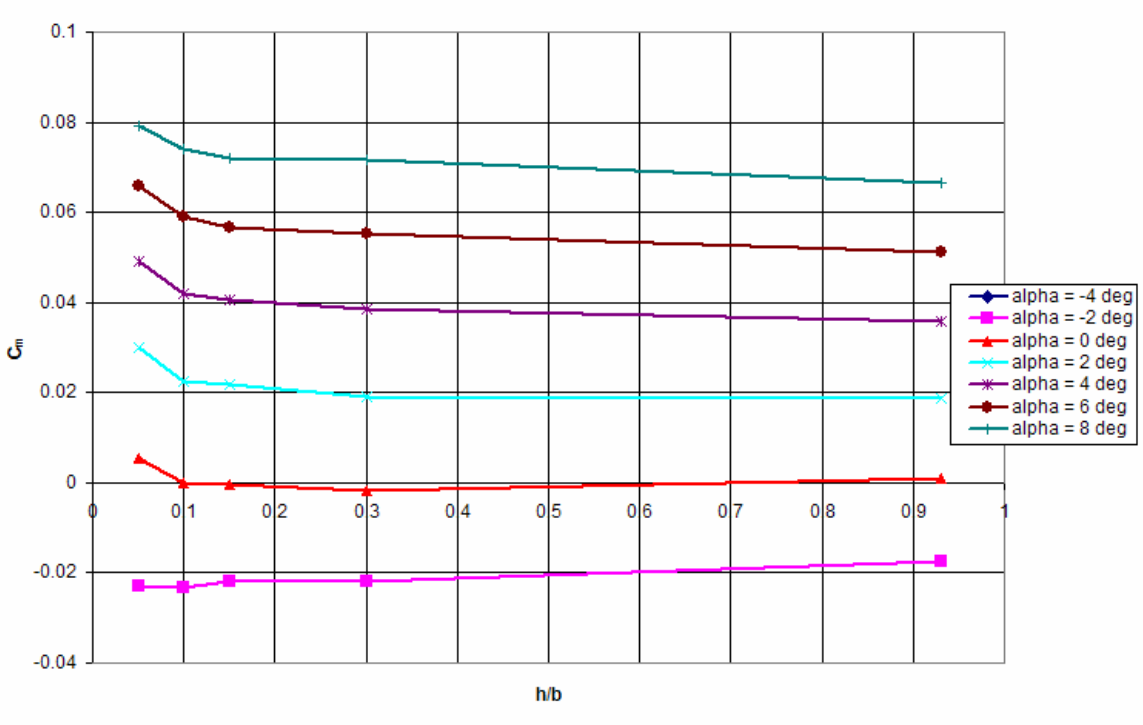

Figure 55: Chevron UCAV C_m vs. (h/b) 60 mph

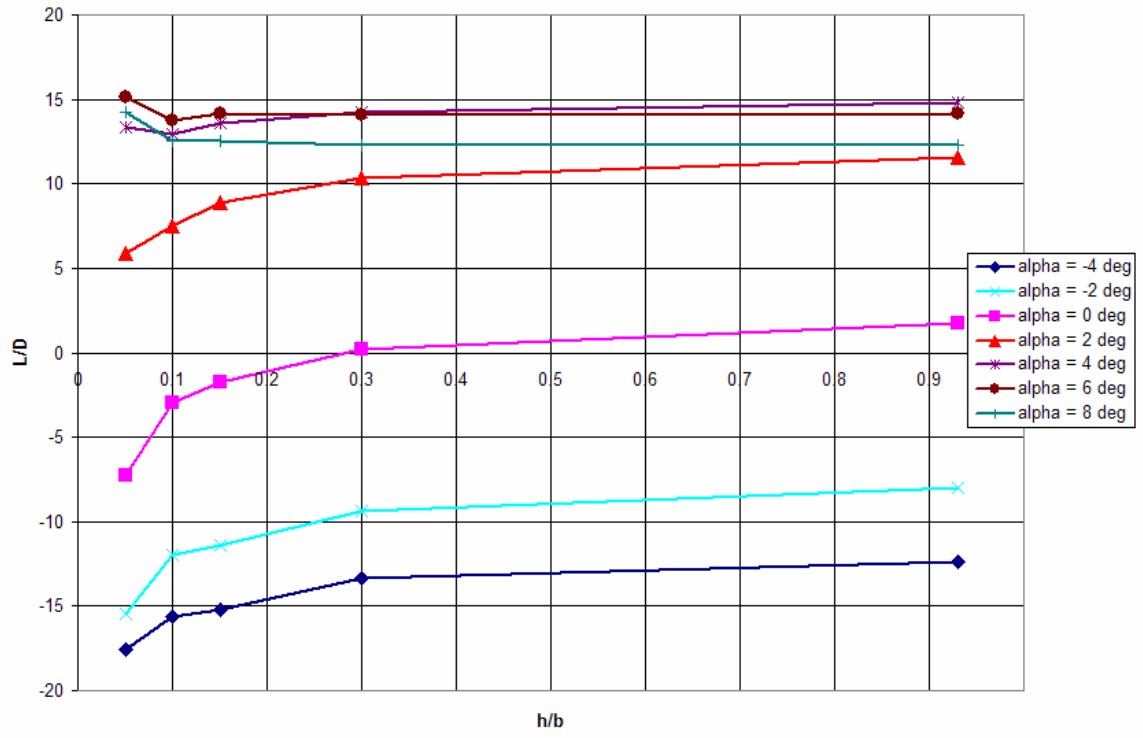

Figure 56: Chevron UCAV L/D vs. (h/b) 60 mph

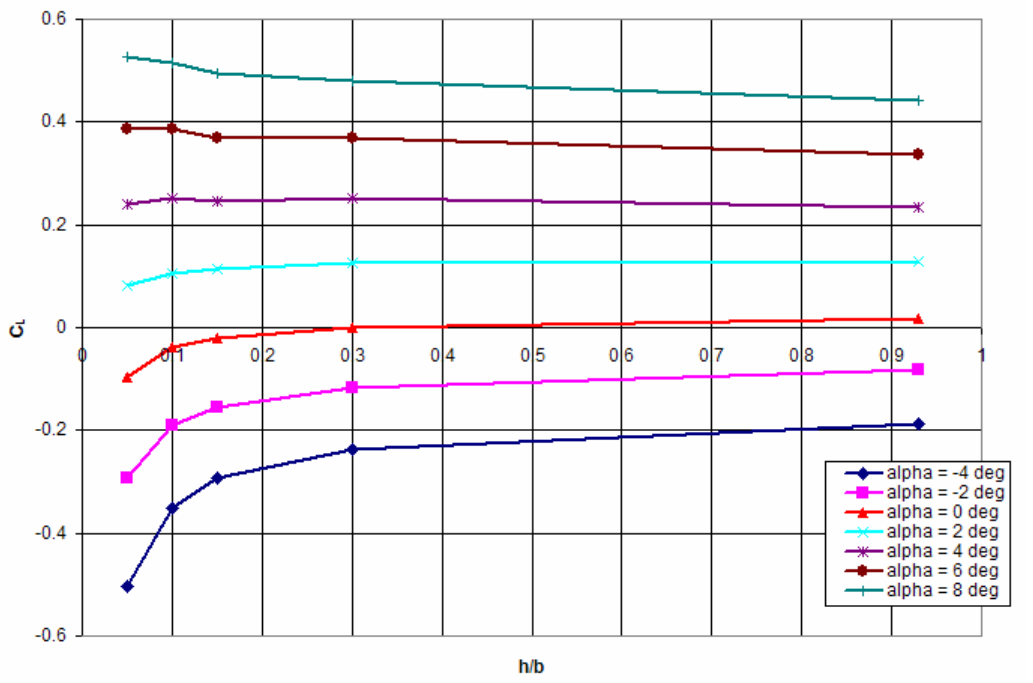

Figure 57: Chevron UCAV C_L vs. (h/b) 80 mph

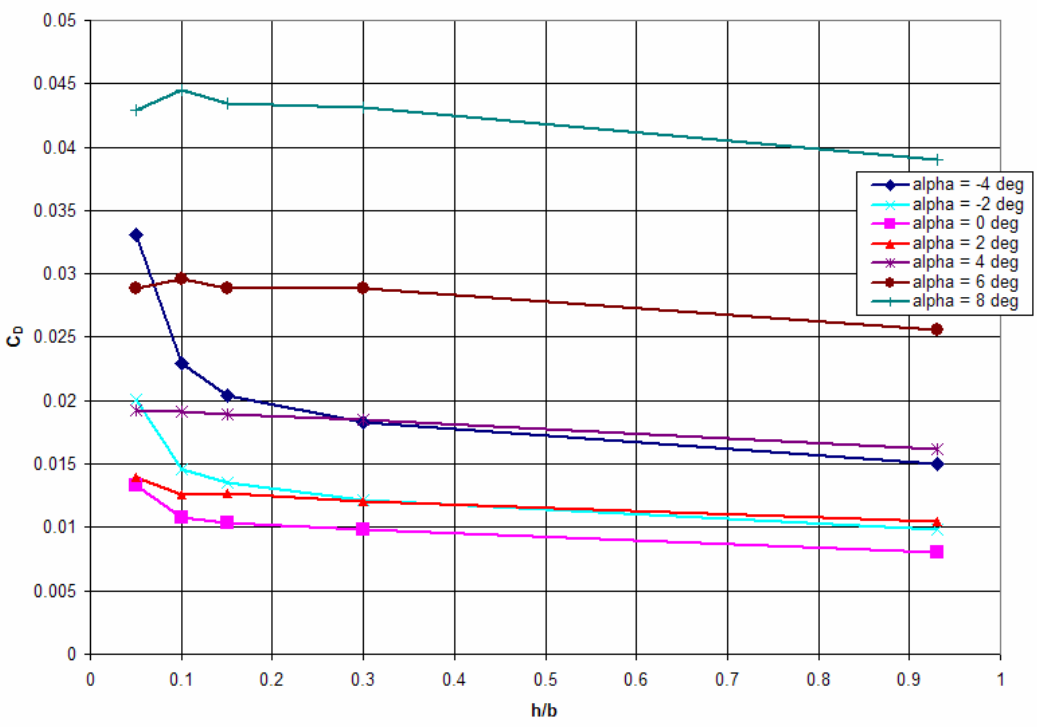

Figure 58: Chevron UCAV C_D vs. (h/b) 80 mph

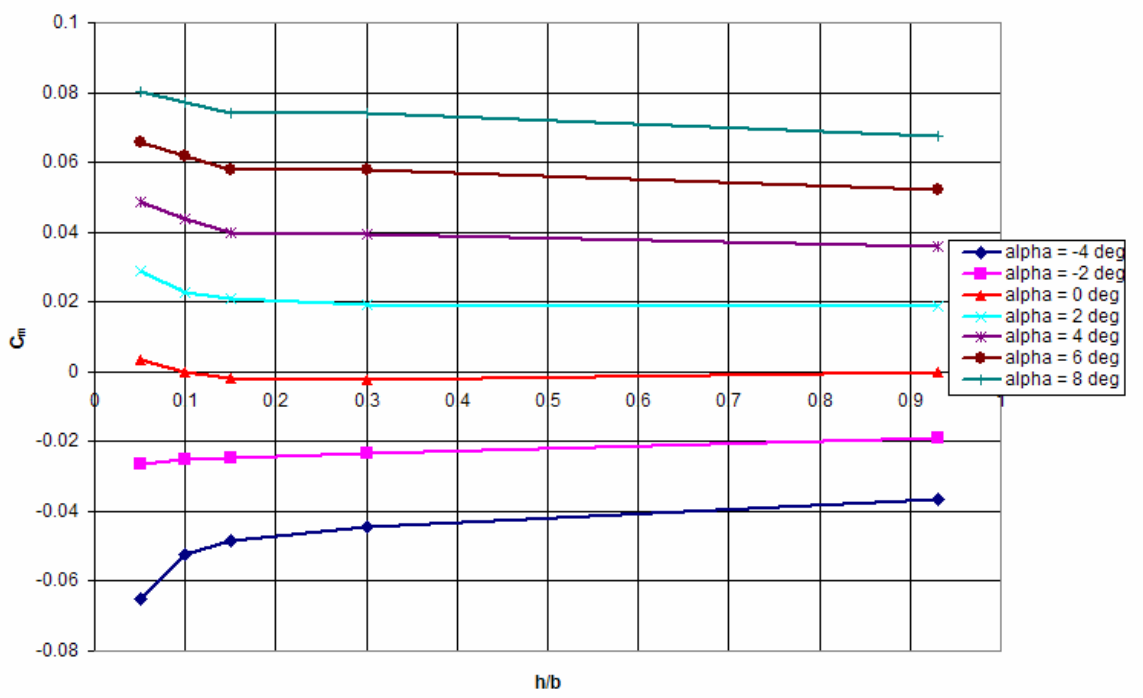

Figure 59: Chevron UCAV C_m vs. (h/b) 80 mph

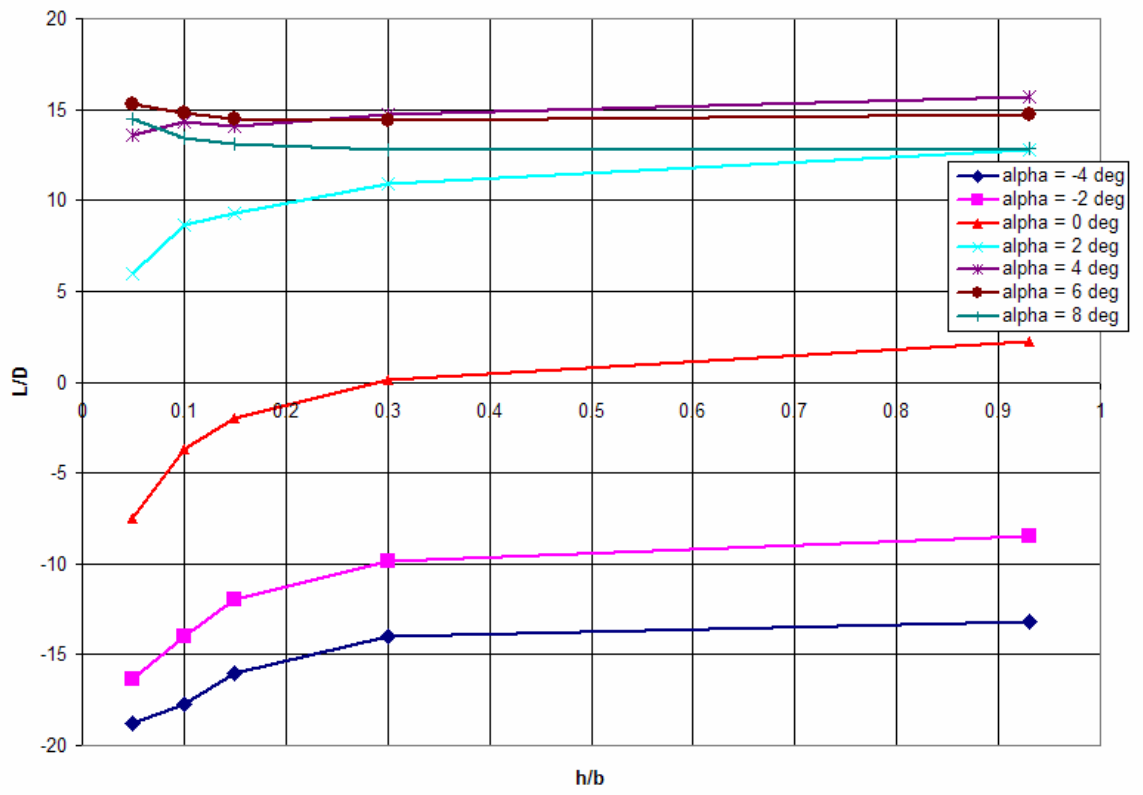

Figure 60: Chevron UCAV L/D vs. (h/b) 80 mph

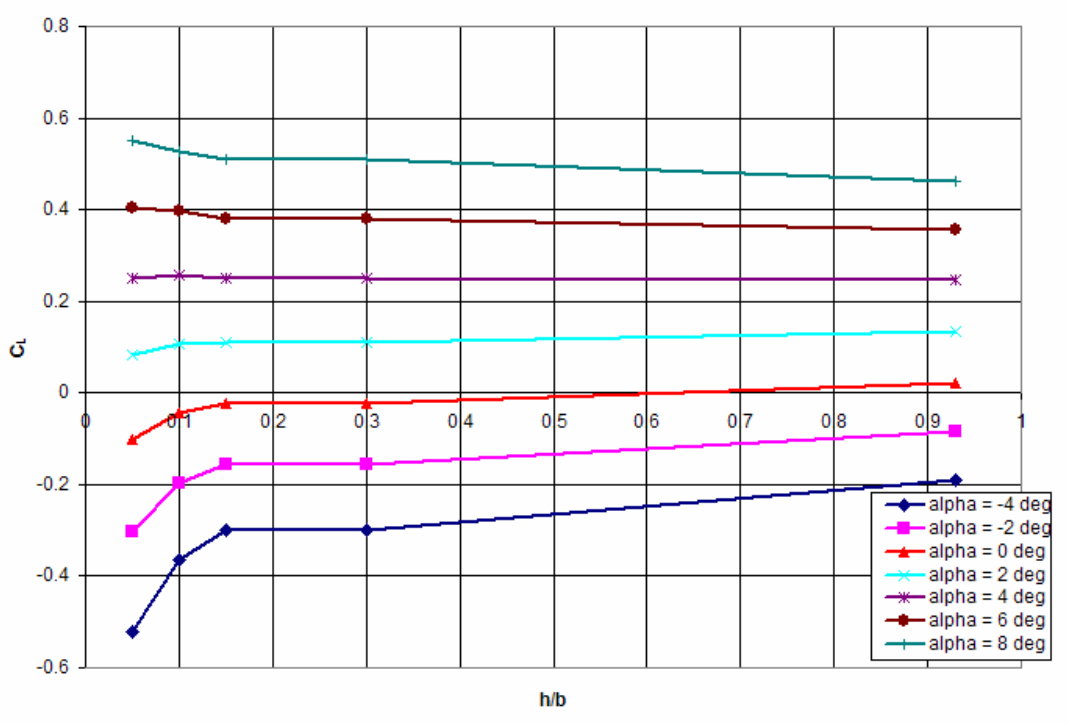

Figure 61: Chevron UCAV C_L vs. (h/b) 100 mph

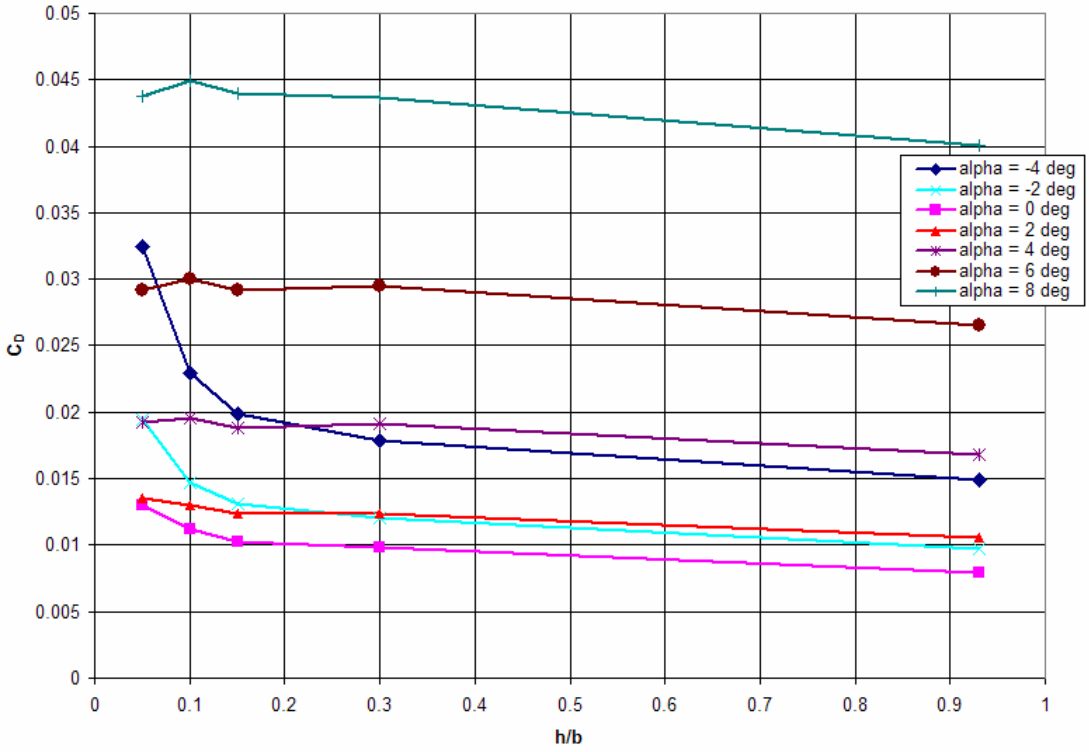

Figure 62: Chevron UCAV C_D vs. (h/b) 100 mph

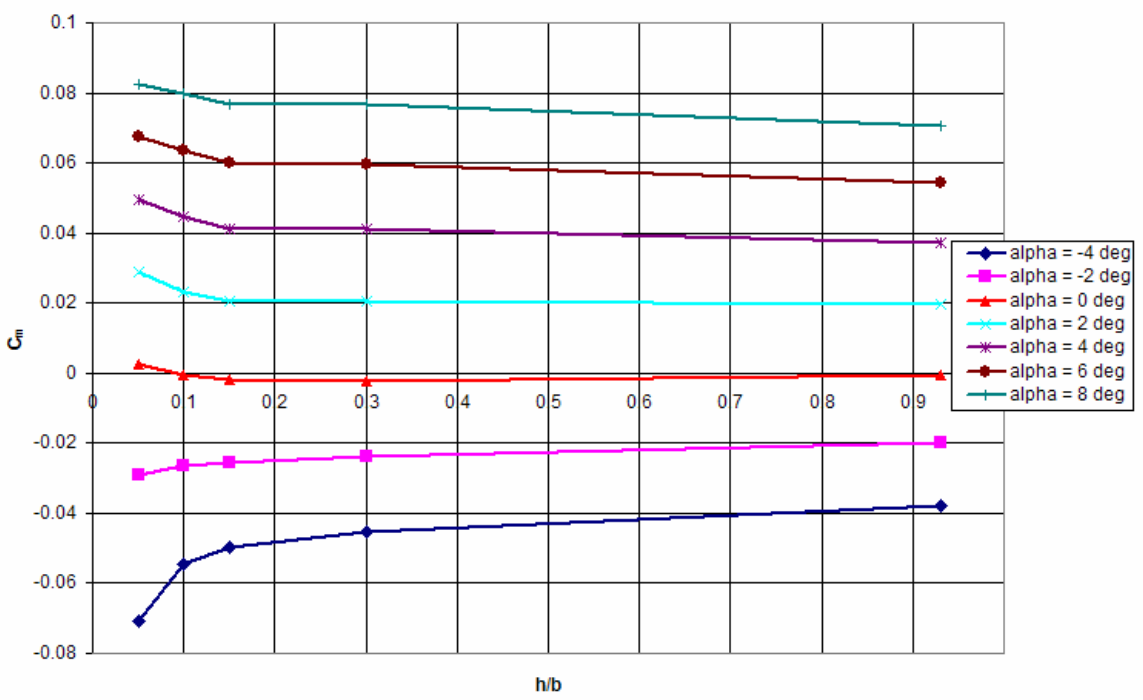

Figure 63: Chevron UCAV C_m vs. (h/b) 100 mph

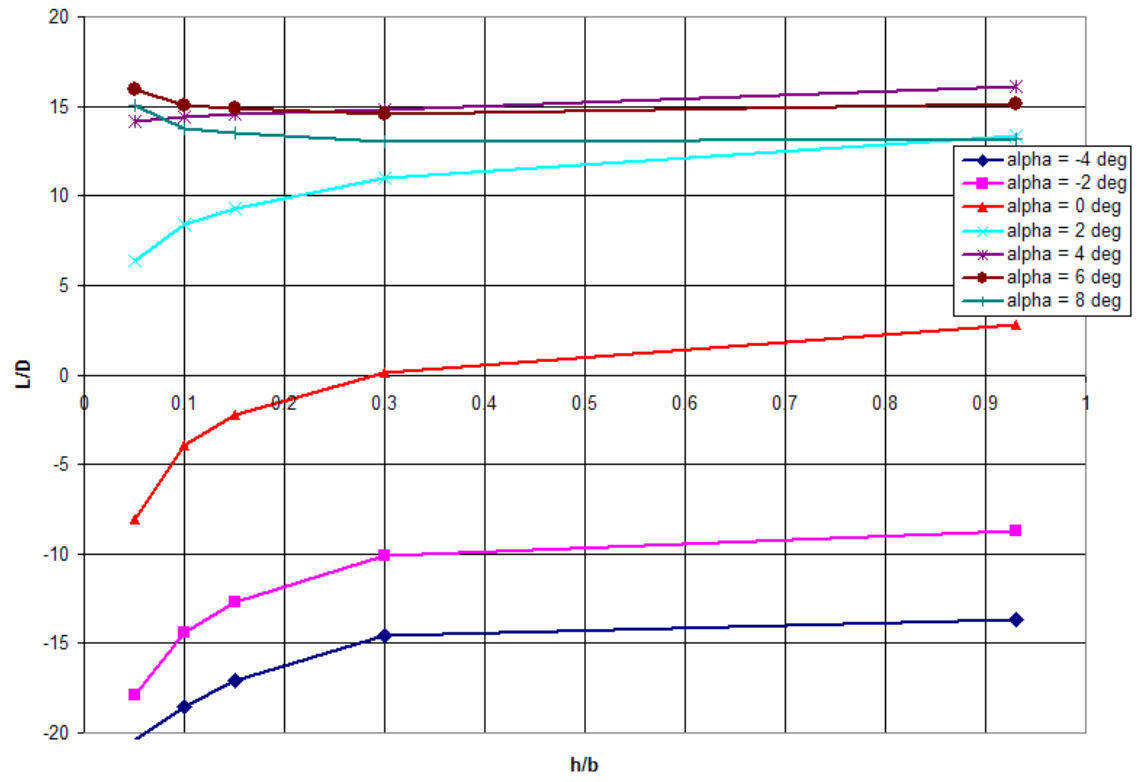

Figure 64: Chevron UCAV L/D vs. (h/b) 100 mph

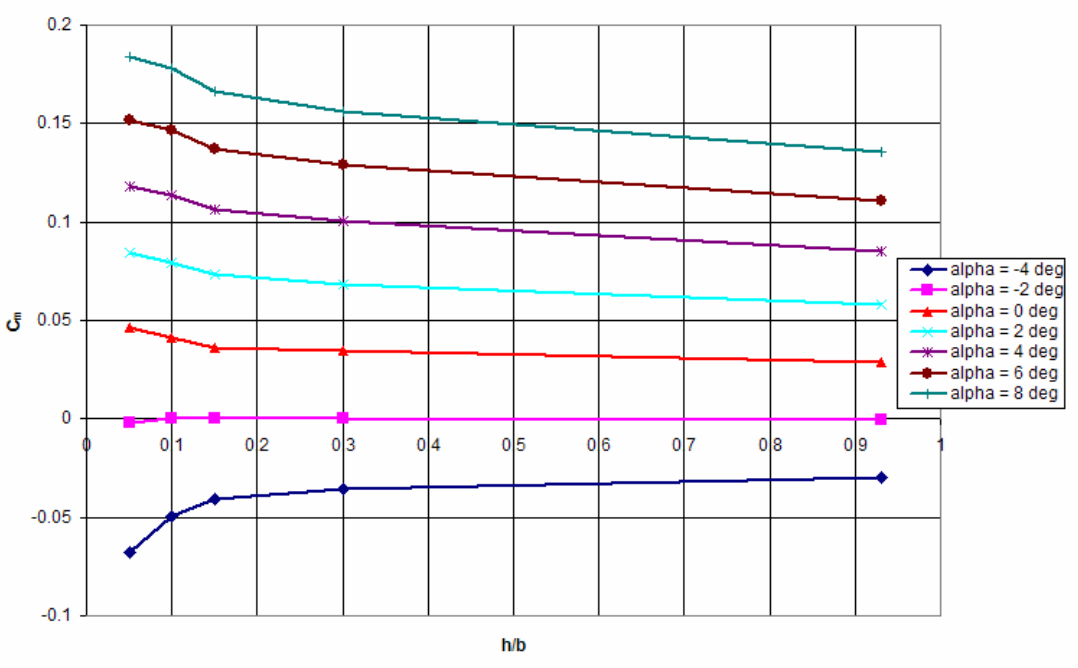

Figure 65: Lambda UCAV C_m vs. (h/b) 40 mph

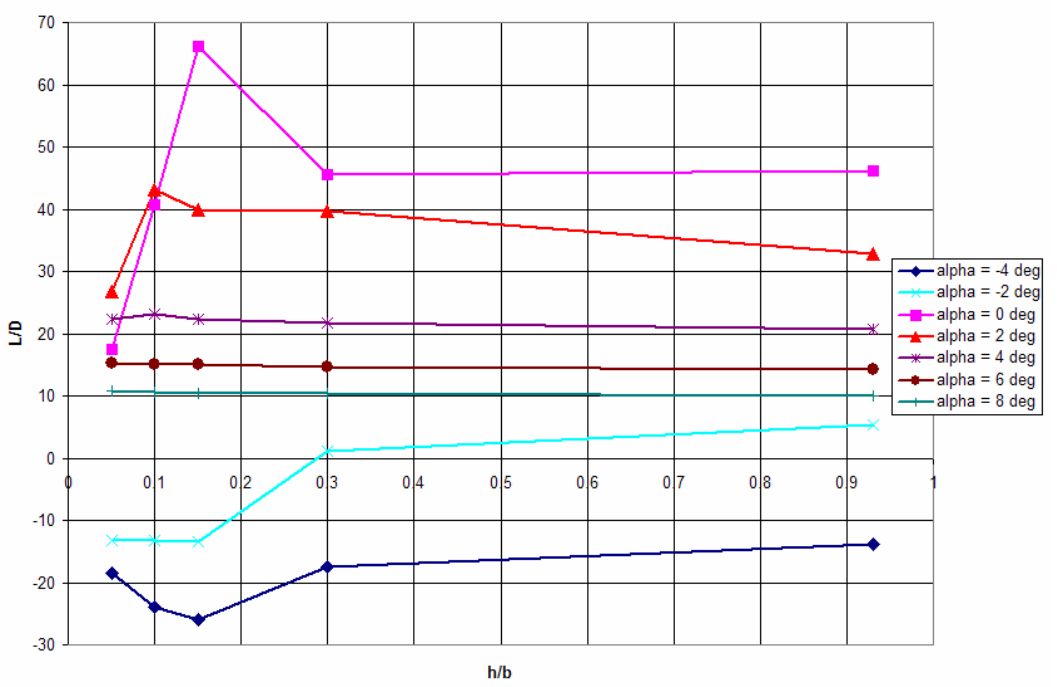

Figure 66: Lambda UCAV L/D vs. (h/b) 40 mph

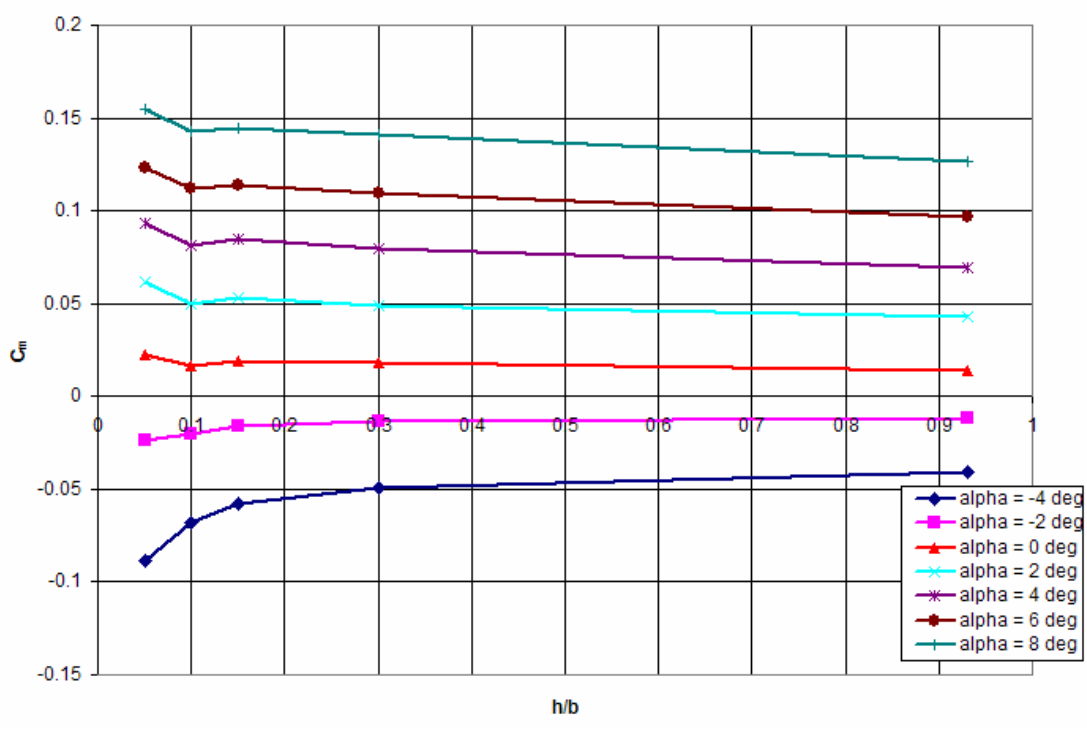

Figure 67: Lambda UCAV C_m vs. (h/b) 60 mph

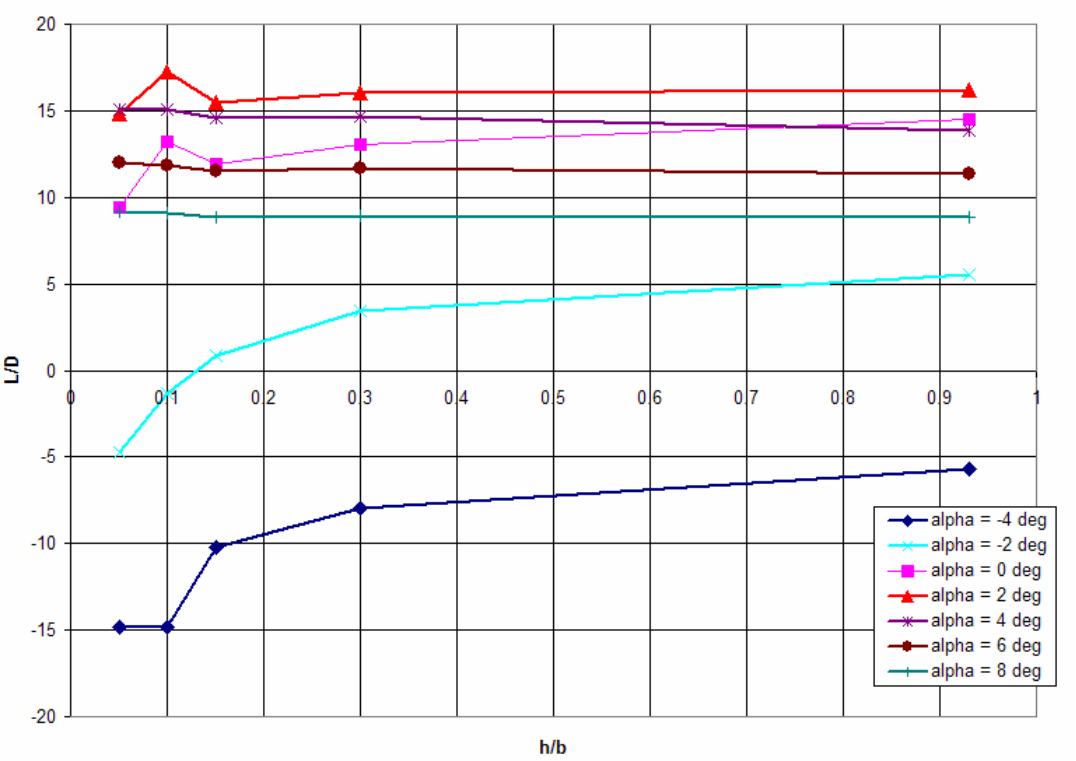

Figure 68: Lambda UCAV L/D vs. (h/b) 60 mph

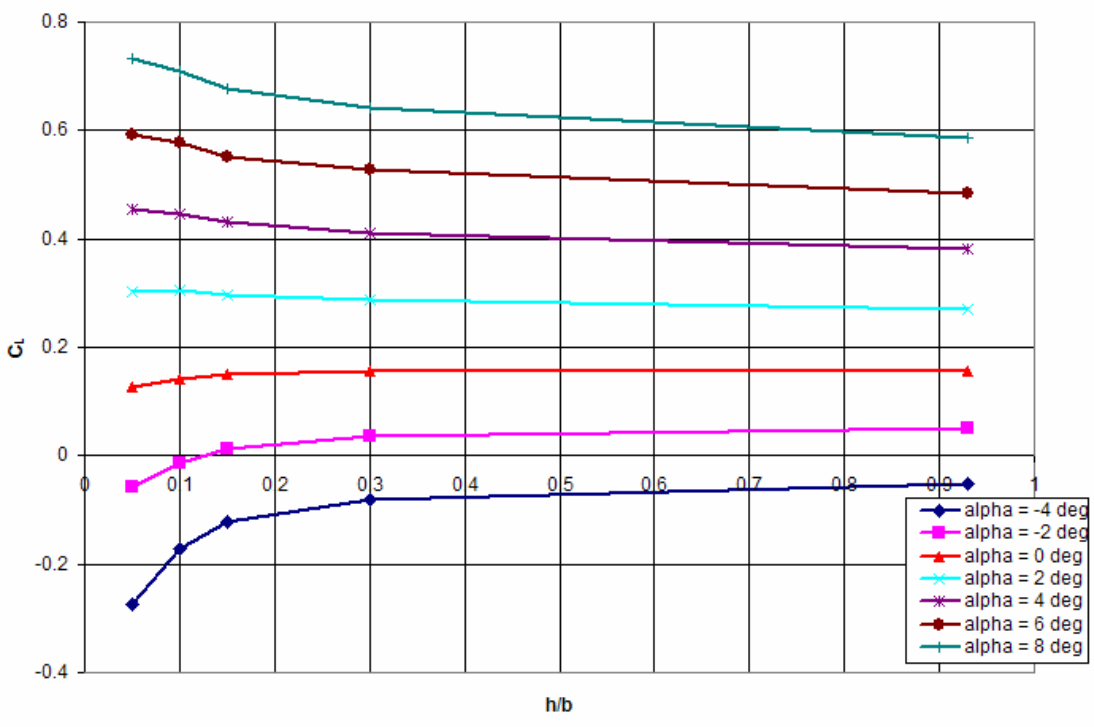

Figure 69: Lambda UCAV C_L vs. (h/b) 80 mph

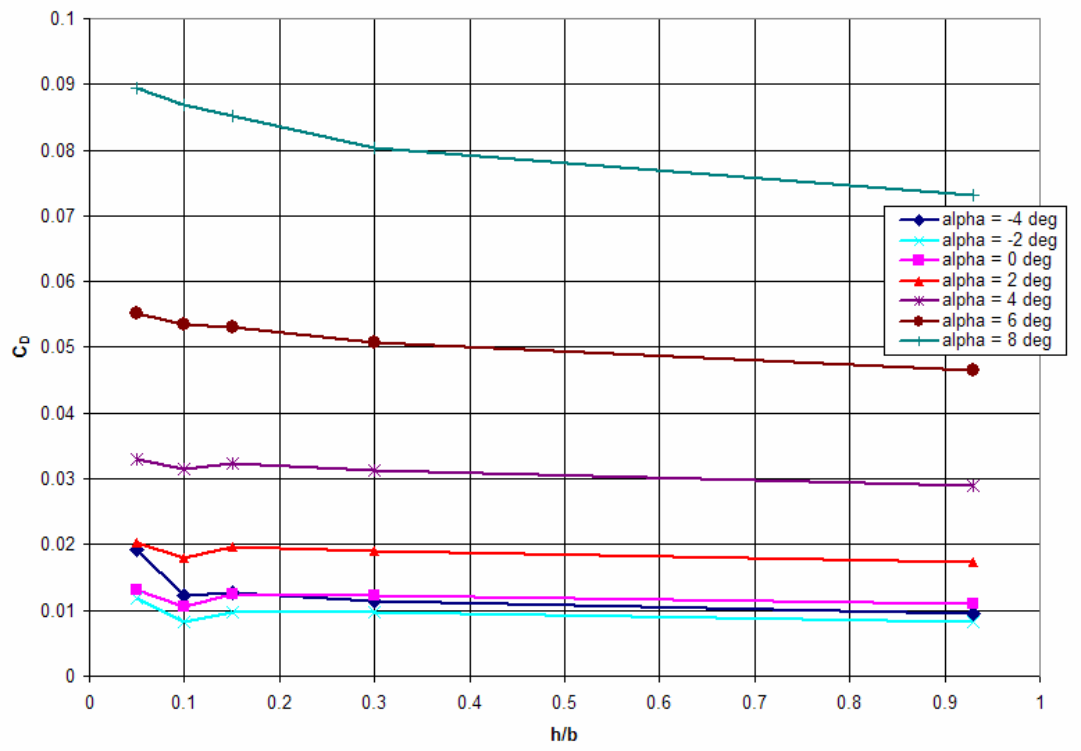

Figure 70: Lambda UCAV C_D vs. (h/b) 80 mph

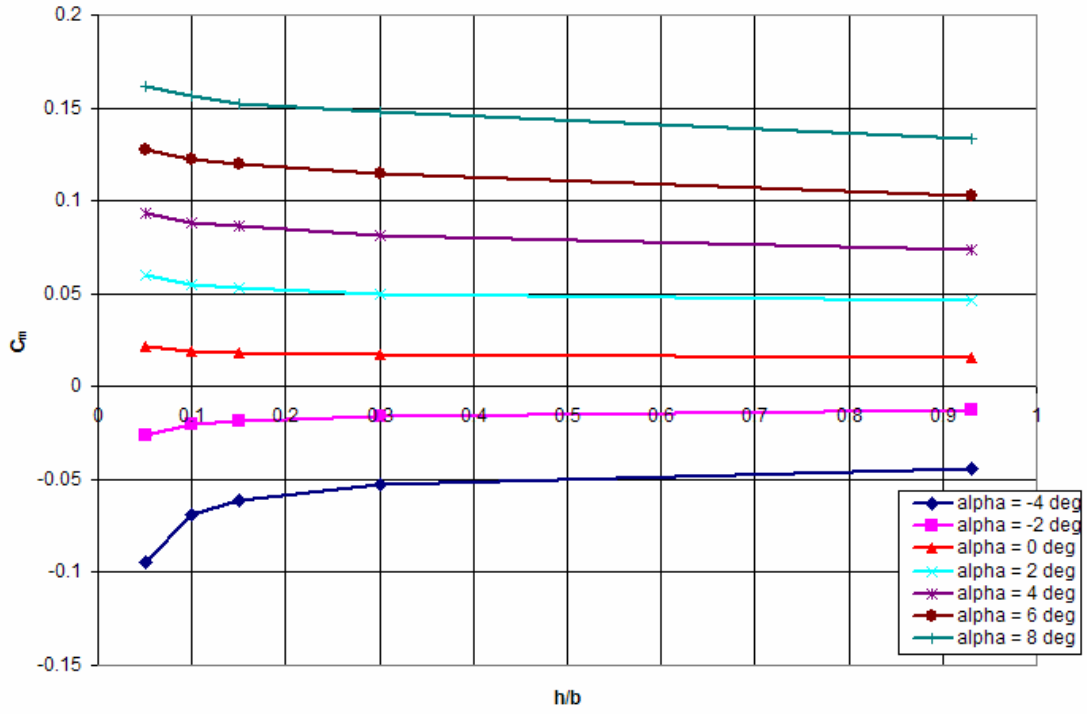

Figure71: Lambda UCAV C_m vs. (h/b) 80 mph

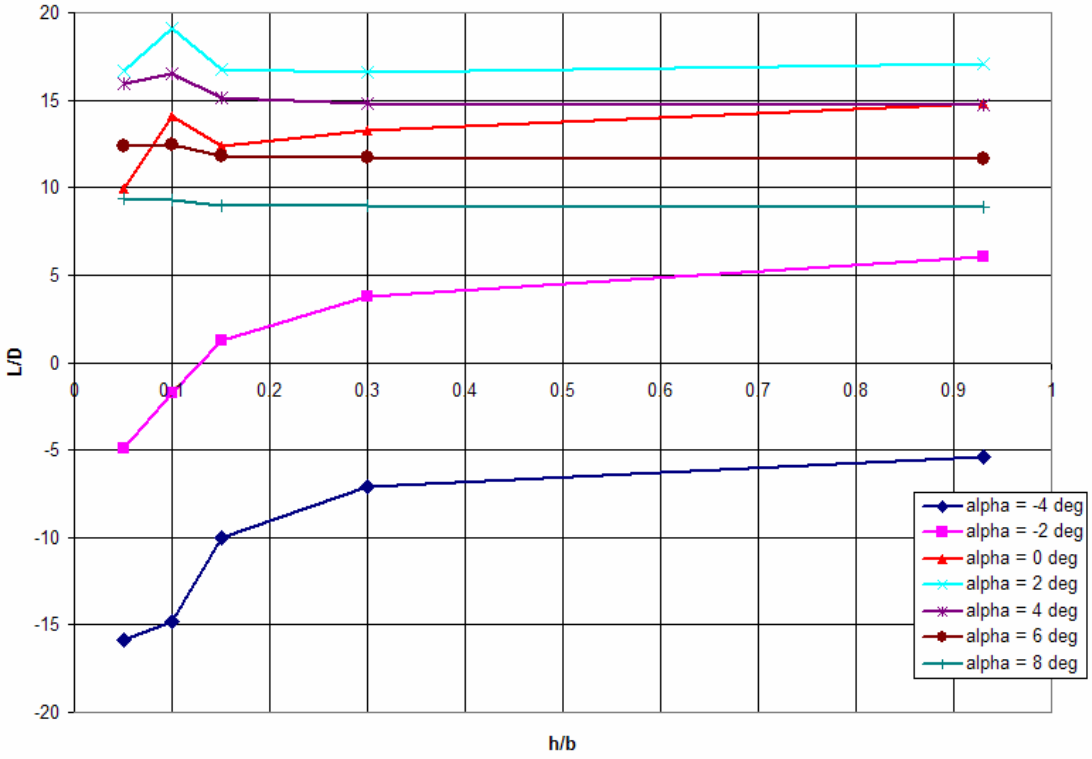

Figure 72: Lambda UCAV L/D vs. (h/b) 80 mph

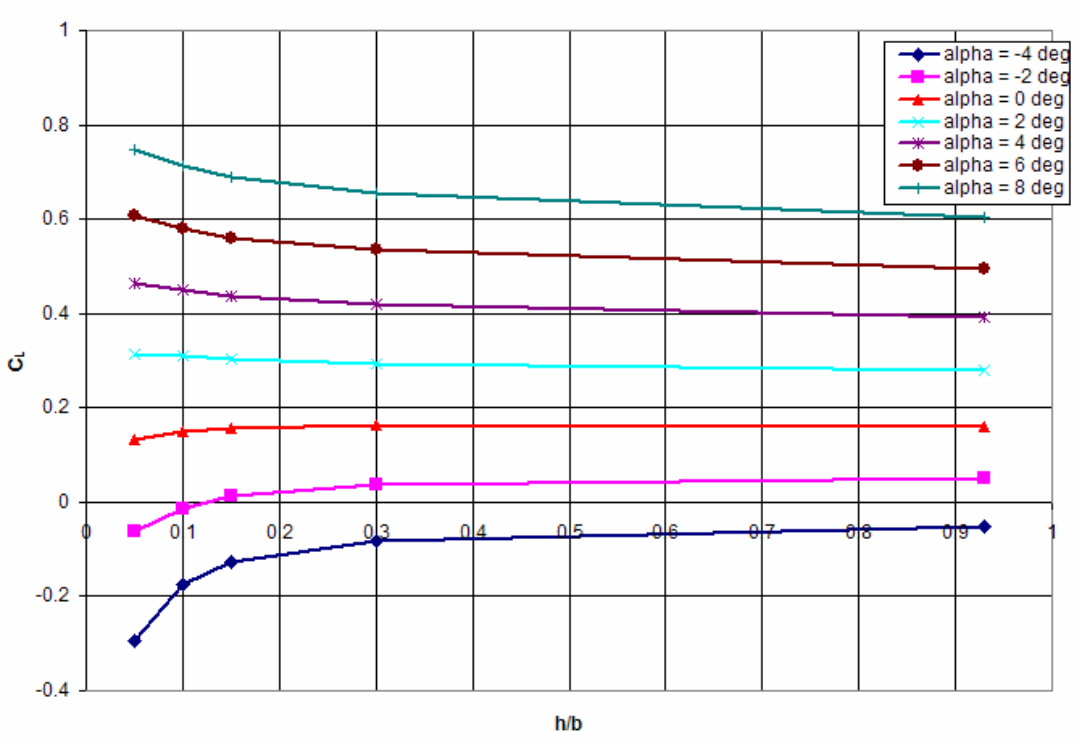

Figure73: Lambda UCAV C_L vs. (h/b) 100 mph

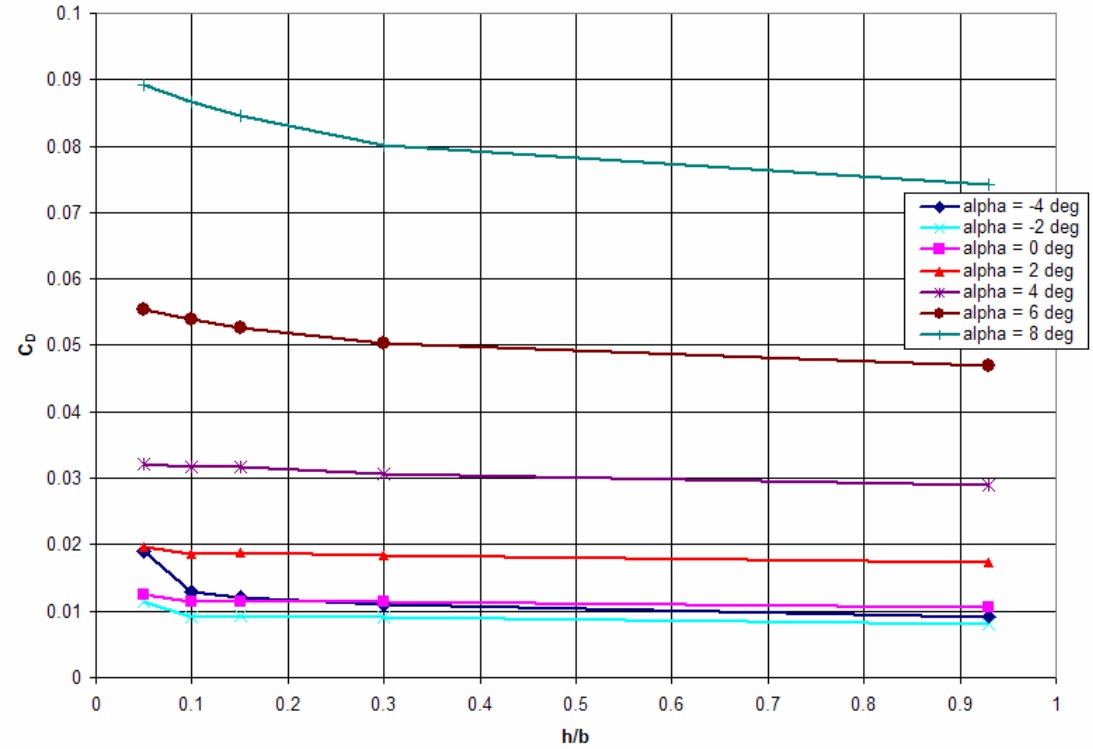

Figure 74: Lambda UCAV C_D vs. (h/b) 100 mph

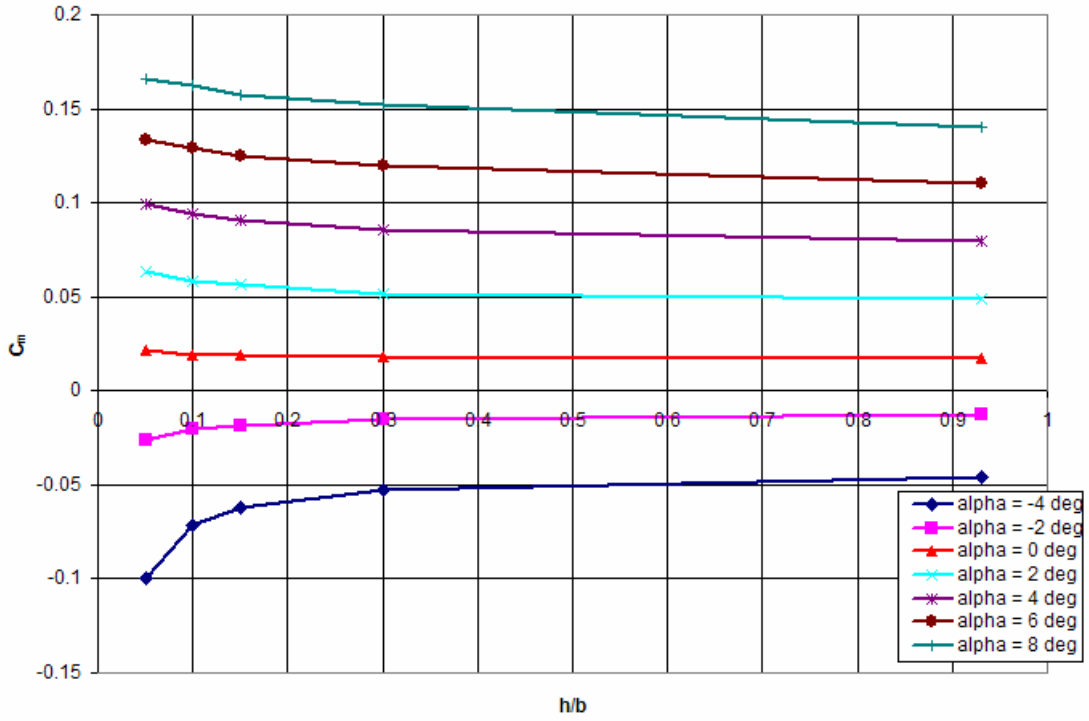

Figure 75: Lambda UCAV C_m vs. (h/b) 100 mph

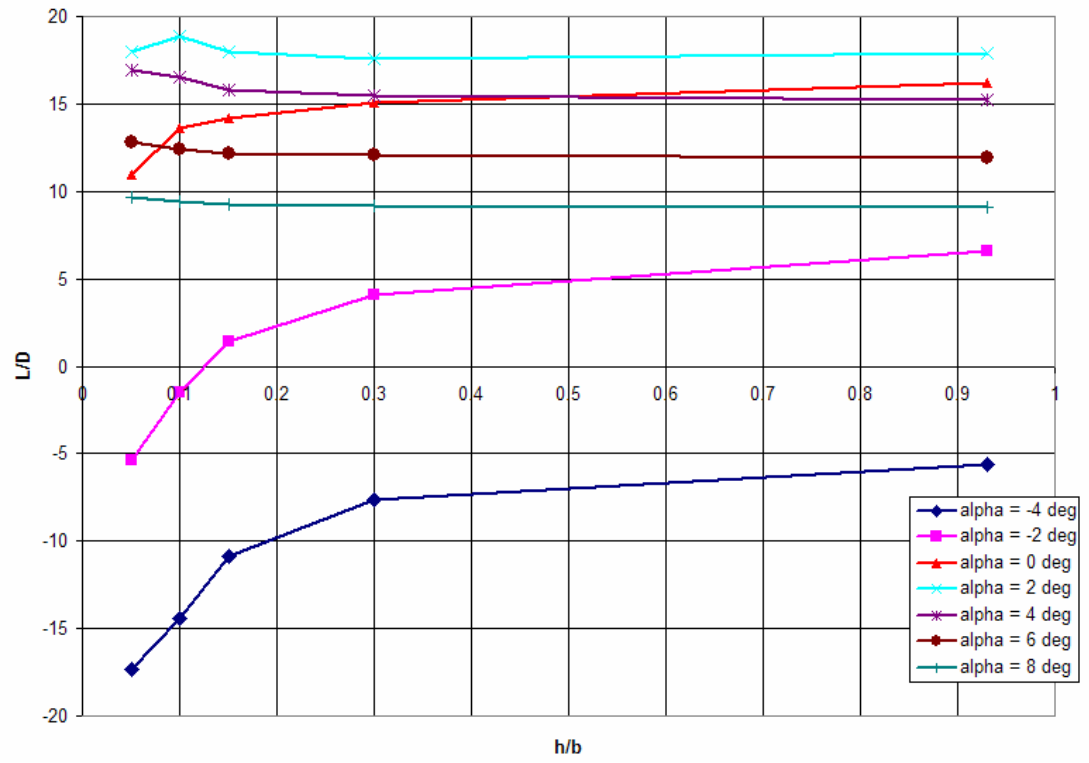

Figure 76: Lambda UCAV L/D vs. (h/b) 100 mph

Appendix C: Data Tables

The following tables were outputted from the data reduction program and used in various plots.

Table 14: Chevron UCAV U=40mph, h/b=0.93 (OGE)

Mach No.	Re No.	q_c	Uoo	alpha_c	C_L	C_D_c	Cm_cg_c_w
0.0514998	217312.71	3.8017814	39.6533880	-11.1928268	-0.5676953	0.0748160	-0.0846766
0.0515192	217394.85	3.8046557	39.6683748	-8.9600716	-0.4585087	0.0483980	-0.0680599
0.0515187	217392.72	3.8045813	39.6679871	-6.7163633	-0.3411170	0.0303092	-0.0512825
0.0515149	217376.54	3.8040150	39.6650345	-4.4672853	-0.2197028	0.0174384	-0.0332541
0.0515027	217325.00	3.8022113	39.6556298	-2.2245804	-0.1030628	0.0105903	-0.0124918
0.0515089	217351.15	3.8031262	39.6604005	0.0228410	0.0171104	0.0074918	0.0063111
0.0515129	217368.15	3.8037213	39.6635035	2.1838560	0.1377283	0.0104248	0.0258048
0.0515463	217509.05	3.8086540	39.6892133	4.4305810	0.2573798	0.0158897	0.0434831
0.0516126	217788.87	3.8184597	39.7402720	6.6773555	0.3770684	0.0266804	0.0592541
0.0516893	218112.49	3.8298164	39.7993247	8.8361792	0.4960448	0.0471379	0.0717791
0.0517359	218309.07	3.8367227	39.8351937	11.0643268	0.6017797	0.0695273	0.0833712
0.0517640	218427.61	3.8408906	39.8568245	12.1781564	0.6548389	0.0829299	0.0886691
0.0517443	218344.54	3.8379699	39.8416676	13.2845858	0.7016053	0.0978040	0.0952925
0.0517259	218266.87	3.8352398	39.8274950	14.3831160	0.7432035	0.1148762	0.1019224
0.0517212	218246.92	3.8345385	39.8238534	15.4854662	0.7869142	0.1340484	0.1062561
0.0516982	218150.25	3.8311424	39.8062142	16.5904251	0.8333282	0.1654320	0.1026435
0.0516773	218061.91	3.8280403	39.7900950	17.6902865	0.8751745	0.2029050	0.0953715
0.0516523	217956.19	3.8243294	39.7708044	18.7808890	0.9108340	0.2343442	0.0923835
0.0516255	217843.46	3.8203745	39.7502344	19.8641013	0.9402083	0.2715127	0.0892054
0.0515977	217725.88	3.8162514	39.7287786	20.9503104	0.9725767	0.3080418	0.0892183
0.0515402	217483.52	3.8077600	39.6845547	22.0183948	0.9906185	0.3440449	0.0859392

Table 15: Chevron UCAV U=40mph, h/b=0.3

Mach No.	Re No.	q_c	Uoo	alpha_c	C_L	C_D_c	Cm_cg_c_w
0.0499807	210902.67	3.5808080	38.4837375	-11.3369812	-0.6756827	0.0837442	-0.0994213
0.0498702	210436.35	3.5649906	38.3986469	-9.0845693	-0.5517711	0.0552236	-0.0801018
0.0498773	210466.54	3.5660135	38.4041555	-6.8073291	-0.4092603	0.0338902	-0.0608326
0.0499361	210714.39	3.5744172	38.4493807	-4.5314619	-0.2677781	0.0192928	-0.0395702
0.0499712	210862.73	3.5794519	38.4764497	-2.2648892	-0.1332585	0.0111680	-0.0154896
0.0500350	211131.89	3.5885959	38.5255639	0.0047673	0.0035712	0.0072367	0.0058571
0.0501033	211419.89	3.5983927	38.5781154	2.2769433	0.1422883	0.0096029	0.0276487
0.0501576	211649.32	3.6062069	38.6199804	4.4570098	0.2771779	0.0170536	0.0488022
0.0501672	211689.78	3.6075856	38.6273618	6.7251728	0.4128888	0.0310438	0.0647975
0.0501095	211446.46	3.5992971	38.5829629	8.8995936	0.5435490	0.0513955	0.0795979
0.0499653	210837.74	3.5786033	38.4718886	11.1461208	0.6630524	0.0781359	0.0933392
0.0498746	210455.07	3.5656248	38.4020622	12.2689864	0.7228805	0.0942825	0.0999662
0.0498525	210361.72	3.5624626	38.3850298	13.3750594	0.7693800	0.1089302	0.1080905
0.0497955	210121.35	3.5543257	38.3411678	14.4830747	0.8180836	0.1285613	0.1139357
0.0497581	209963.42	3.5489847	38.3123501	15.5974600	0.8708098	0.1546294	0.1159115
0.0497309	209848.76	3.5451097	38.2914286	16.7094227	0.9224705	0.1912146	0.1098364
0.0496626	209560.28	3.5353694	38.2387889	17.8168786	0.9700059	0.2300269	0.1033343
0.0496670	209579.24	3.5360091	38.2422483	18.9253306	1.0190366	0.2709190	0.0985462
0.0497024	209728.62	3.5410517	38.2695066	20.0097827	1.0493397	0.3101126	0.0975649
0.0496551	209528.88	3.5343102	38.2330600	21.1016606	1.0859546	0.3538632	0.0932037
0.0495815	209218.24	3.5238383	38.1763771	22.2676558	1.1121698	0.3970143	0.0893101

Table 16: Chevron UCAV U=40 mph, h/b=0.15

Mach No.	Re No.	q_c	Uoo	alpha_c	C_L	C_D_c	Cm_cg_c_w
0.0500594	211234.84	3.5920963	38.5443488	-11.5543334	-0.8385033	0.1068978	-0.1303941
0.0500214	211074.58	3.5866477	38.5151051	-9.2621400	-0.6847910	0.0699857	-0.0997260
0.0499945	210961.13	3.5827933	38.4944044	-6.9426739	-0.5106484	0.0431443	-0.0718723
0.0499992	210980.86	3.5834635	38.4980045	-4.6286904	-0.3406129	0.0247273	-0.0452366
0.0500301	211111.29	3.5878957	38.5218053	-2.3227138	-0.1765755	0.0143063	-0.0194052
0.0500542	211212.82	3.5913474	38.5403309	-0.0290695	-0.0217762	0.0100180	0.0052400
0.0501074	211437.44	3.5989902	38.5813182	2.1737247	0.1301388	0.0120916	0.0291397
0.0501633	211673.10	3.6070173	38.6243196	4.4559959	0.2764183	0.0187253	0.0498950
0.0501723	211711.41	3.6083228	38.6313087	6.7411205	0.4248353	0.0307677	0.0653938
0.0501519	211625.36	3.6053904	38.6156082	8.9219891	0.5603257	0.0523958	0.0800906
0.0500721	211288.36	3.5939169	38.5541154	11.1665001	0.6783187	0.0765547	0.0945378
0.0499844	210918.54	3.5813468	38.4866327	12.2860232	0.7356430	0.0913106	0.1019221
0.0499404	210732.59	3.5750350	38.4527031	13.4027488	0.7901223	0.1071291	0.1089672
0.0498963	210546.81	3.5687340	38.4188021	14.5104969	0.8386258	0.1284791	0.1136398
0.0498782	210470.08	3.5661335	38.4048016	13.4123104	0.7972851	0.1096090	0.1099345
0.0498839	210494.19	3.5669507	38.4092017	14.5200619	0.8457910	0.1299071	0.1133239
0.0498762	210461.86	3.5658549	38.4033016	15.6396724	0.9024316	0.1594442	0.1121428
0.0498357	210290.87	3.5600631	38.3721006	16.7640581	0.9633983	0.1977963	0.1050585
0.0498058	210164.87	3.5557981	38.3491090	17.8784873	1.0161575	0.2369905	0.0987645
0.0497692	210010.27	3.5505687	38.3208990	18.9888268	1.0666022	0.2809482	0.0947951
0.0496826	209644.72	3.5382191	38.2541969	20.0989470	1.1161335	0.3265493	0.0912487
0.0495770	209199.16	3.5231954	38.1728944	21.2003638	1.1598941	0.3756729	0.0858609

Table 17: Chevron UCAV U=40 mph, h/b=0.10

Mach No.	Re No.	q_c	Uoo	alpha_c	C_L	C_D_c	Cm_cg_c_w
0.0499807	210902.81	3.5808127	38.4837630	−11.8189955	−1.0367642	0.1315526	−0.1771957
0.0498677	210426.14	3.5646448	38.3967847	−9.4754333	−0.8445710	0.0876741	−0.1291158
0.0498595	210391.40	3.5634677	38.3904444	−7.0904434	−0.6213439	0.0531275	−0.0879382
0.0498764	210462.84	3.5658884	38.4034816	−4.7293192	−0.4159949	0.0310279	−0.0520317
0.0499063	210588.70	3.5701545	38.4264471	−2.3752431	−0.2159256	0.0179621	−0.0218341
0.0499533	210787.16	3.5768865	38.4626595	−0.0527583	−0.0395217	0.0119740	0.0056694
0.0500000	210984.29	3.5835801	38.4986309	2.2642262	0.1327618	0.0134232	0.0309324
0.0500277	211100.93	3.5875434	38.5199138	4.4788128	0.2935107	0.0218990	0.0521026
0.0500486	211189.48	3.5905536	38.5360710	6.7768904	0.4516309	0.0349667	0.0679293
0.0500139	211042.92	3.5855718	38.5093281	8.9675702	0.5944710	0.0573978	0.0828603
0.0500143	211044.75	3.5856341	38.5096623	11.2144090	0.7142077	0.0826013	0.0968856
0.0500133	211040.47	3.5854888	38.5088823	12.3312535	0.7695253	0.0967711	0.1047638
0.0499926	210953.09	3.5825201	38.4929368	13.4518611	0.8269128	0.1135762	0.1098950
0.0499941	210959.13	3.5827255	38.4940400	14.5732154	0.8856088	0.1375831	0.1122148
0.0499830	210912.42	3.5811389	38.4855157	15.6965086	0.9450081	0.1759775	0.1053528
0.0499450	210751.93	3.5756912	38.4562321	16.8285911	1.0117406	0.2134289	0.0993672
0.0498758	210460.10	3.5657952	38.4029802	17.9590089	1.0764770	0.2556356	0.0934519
0.0497577	209961.61	3.5489237	38.3120206	19.0803033	1.1351281	0.3048383	0.0897332
0.0496903	209677.47	3.5393246	38.2601727	20.2000801	1.1918932	0.3534166	0.0839511
0.0496084	209331.77	3.5276636	38.1970927	21.3205444	1.2499225	0.4078293	0.0764400
0.0495279	208991.97	3.5162202	38.1350885	22.5199888	1.3011948	0.4642601	0.0677557

Table 18: Chevron UCAV U=40 mph, h/b=0.05

Mach No.	Re No.	q_c	Uoo	alpha_c	C_L	C_D_c	Cm_cg_c_w
0.0502853	212188.08	3.6245897	38.7182886	−4.8595571	−0.5787298	0.0423446	−0.0656909
0.0502319	211962.69	3.6168934	38.6771603	−2.5393255	−0.3388413	0.0221096	−0.0224719
0.0502923	212217.44	3.6255927	38.7236457	−0.1483693	−0.1111448	0.0116996	0.0105386
0.0503333	212390.75	3.6315168	38.7552691	2.1163412	0.0871523	0.0118136	0.0393131
0.0503245	212353.39	3.6302395	38.7484528	4.4454411	0.2685116	0.0168864	0.0621498
0.0503358	212401.28	3.6318770	38.7571911	6.7629742	0.4412061	0.0279963	0.0787378
0.0503249	212355.23	3.6303023	38.7487880	8.9725398	0.5981938	0.0473715	0.0899371
0.0502609	212084.92	3.6210661	38.6994644	10.1027797	0.6635460	0.0582829	0.0967644
0.0502234	211926.89	3.6156718	38.6706284	11.2259146	0.7228267	0.0699571	0.1037189
0.0502686	212117.62	3.6221829	38.7054315	12.3508333	0.7841928	0.0837668	0.1105861
0.0502851	212187.43	3.6245675	38.7181702	13.4682652	0.8392013	0.0979207	0.1151153

Table 19: Chevron UCAV U=60 mph, h/b=0.93 (OGE)

Mach No.	Re No.	q_c	Uoo	alpha_c	C_L	C_D_c	Cm_cg_c_w
0.0765345	322951.52	8.3963693	58.9294643	-11.1674529	-0.5486874	0.0682957	-0.0959663
0.0765439	322991.18	8.3984315	58.9367008	-8.9324428	-0.4378116	0.0453118	-0.0791451
0.0765376	322964.54	8.3970464	58.9318405	-6.7013619	-0.3298793	0.0286264	-0.0594529
0.0765062	322832.19	8.3901656	58.9076901	-4.4594610	-0.2138416	0.0175101	-0.0394628
0.0764544	322613.24	8.3787888	58.8677382	-2.2155281	-0.0962816	0.0111465	-0.0194271
0.0764523	322604.66	8.3783430	58.8661721	0.0218202	0.0163457	0.0088361	0.0010754
0.0764741	322696.40	8.3831092	58.8829132	2.1815103	0.1359711	0.0114808	0.0205365
0.0765584	323052.14	8.4016024	58.9478255	4.4249768	0.2531816	0.0181873	0.0391711
0.0766806	323567.70	8.4284398	59.0418998	6.6676620	0.3698069	0.0297422	0.0564476
0.0767853	324009.50	8.4514721	59.1225163	8.8138828	0.4793423	0.0463403	0.0726099
0.0768440	324257.28	8.4644030	59.1677281	11.0487553	0.5901150	0.0690628	0.0849215
0.0768492	324279.45	8.4655605	59.1717735	12.1647054	0.6447626	0.0825411	0.0902152
0.0768835	324423.96	8.4731074	59.1981429	13.2785404	0.6970767	0.0972661	0.0947043
0.0768674	324356.30	8.4695738	59.1857977	14.3829104	0.7430495	0.1140541	0.1002819
0.0768308	324201.81	8.4615077	59.1576078	15.4877710	0.7886408	0.1356019	0.1015959
0.0767705	323947.17	8.4482209	59.1111432	16.5087322	0.8373038	0.1622501	0.0981243
0.0767019	323657.91	8.4331400	59.0583601	17.7171252	0.8952796	0.1934972	0.0960764
0.0766314	323360.12	8.4176288	59.0040217	18.8175601	0.9383047	0.2323766	0.0928977
0.0766044	323246.29	8.4117038	58.9832519	19.8917958	0.9609546	0.2719708	0.0886160
0.0765894	323183.01	8.4084106	58.9717049	20.9639573	0.9827997	0.3106706	0.0861132
0.0765217	322897.49	8.3935599	58.9196048	22.0281900	0.9979562	0.3478341	0.0843613

Table 20: Chevron UCAV U=60 mph, h/b=0.3

Mach No.	Re No.	q_c	Uoo	alpha_c	C_L	C_D_c	Cm_cg_c_w
0.0756898	319386.98	8.2120443	58.2790375	-11.3143479	-0.6587279	0.0798578	-0.1140169
0.0755847	318943.74	8.1892673	58.1981595	-9.0530499	-0.5281596	0.0533939	-0.0953227
0.0756550	319240.17	8.2044966	58.2522491	-6.7969366	-0.4014752	0.0339210	-0.0710165
0.0756612	319266.54	8.2058522	58.2570614	-4.5284436	-0.2655171	0.0205984	-0.0482705
0.0756929	319400.20	8.2127241	58.2814495	-2.2637839	-0.1324305	0.0132366	-0.0245257
0.0757669	319712.26	8.2287799	58.3383916	0.0025549	0.0019139	0.0100004	-0.0018513
0.0758424	320030.88	8.2451896	58.3965313	2.2751981	0.1409810	0.0127107	0.0218142
0.0759300	320400.82	8.2642625	58.4640343	4.4504401	0.2722564	0.0202340	0.0429559
0.0759385	320436.62	8.2661095	58.4705669	6.7139975	0.4045173	0.0328303	0.0608949
0.0758564	320090.25	8.2482490	58.4073644	8.8735848	0.5240656	0.0515549	0.0788012
0.0757905	319811.90	8.2339100	58.3565739	8.9596235	0.5233455	0.0517320	0.0787436
0.0756476	319209.03	8.2028958	58.2465657	11.1276507	0.6492163	0.0767185	0.0910096
0.0754906	318546.36	8.1688734	58.1256482	12.2549881	0.7123942	0.0919548	0.0968825
0.0754029	318176.31	8.1499053	58.0581254	13.3721512	0.7672014	0.1075905	0.1028109
0.0753685	318031.37	8.1424818	58.0316775	14.4856856	0.8200394	0.1268951	0.1085603
0.0753547	317972.84	8.1394848	58.0209968	15.5978705	0.8711174	0.1525600	0.1070770
0.0753512	317958.34	8.1387425	58.0183511	16.7176836	0.9286588	0.1850123	0.1014671
0.0752522	317540.55	8.1173683	57.9421162	17.8450066	0.9910768	0.2218030	0.0981190
0.0752070	317349.91	8.1076246	57.9073304	18.9498967	1.0374393	0.2665528	0.0945941
0.0751696	317192.03	8.0995596	57.8785219	20.0303395	1.0647390	0.3095969	0.0914923
0.0751090	316936.42	8.0865106	57.8318795	21.1231703	1.1020677	0.3542434	0.0890823
0.0750819	316822.08	8.0806773	57.8110169	22.2747804	1.1175069	0.4015950	0.0835452

Table 21: Chevron UCAV U=60 mph, h/b=0.15

Mach No.	Re No.	q_c	Uoo	alpha_c	C_L	C_D_c	Cm_cg_c_w
0.0762369	321695.55	8.3311889	58.7002863	-11.5279700	-0.8187542	0.0966008	-0.1392629
0.0761393	321283.81	8.3098763	58.6251556	-9.2237241	-0.6560133	0.0639120	-0.1106136
0.0761597	321369.92	8.3143312	58.6408677	-6.9242512	-0.4968478	0.0395202	-0.0797945
0.0762303	321667.61	8.3297416	58.6951873	-4.6147591	-0.3301769	0.0234058	-0.0529968
0.0762617	321800.40	8.3366203	58.7194175	-2.3173968	-0.1725924	0.0144396	-0.0253798
0.0763039	321978.36	8.3458434	58.7518901	-0.0279077	-0.0209059	0.0107714	-0.0008252
0.0763504	322174.52	8.3560156	58.7876838	2.1683044	0.1260784	0.0134612	0.0236288
0.0763435	322145.49	8.3545101	58.7823876	4.4461906	0.2690731	0.0205027	0.0445487
0.0762897	321918.49	8.3427402	58.7409666	6.7229980	0.4112596	0.0330308	0.0621639
0.0762179	321615.64	8.3270501	58.6857037	8.8979127	0.5422899	0.0516085	0.0790518
0.0761387	321281.39	8.3097512	58.6247142	11.1552298	0.6698760	0.0767528	0.0902053
0.0761112	321165.29	8.3037466	58.6035292	12.2760675	0.7281850	0.0908567	0.0962826
0.0760973	321106.52	8.3007076	58.5928044	13.3964058	0.7853708	0.1073740	0.1014149
0.0760400	320864.98	8.2882248	58.5487312	14.5164082	0.8430540	0.1277599	0.1051313
0.0759795	320609.59	8.2750357	58.5021284	15.6385821	0.9016148	0.1547111	0.1018162
0.0759695	320567.20	8.2728477	58.4943937	16.7713554	0.9688649	0.1877488	0.0964656
0.0759472	320473.05	8.2679890	58.4772140	17.8960497	1.0293137	0.2304373	0.0921234
0.0758436	320036.04	8.2454554	58.3974725	18.9967771	1.0725579	0.2753778	0.0862461
0.0757017	319437.10	8.2146218	58.2881824	20.1015803	1.1181061	0.3213172	0.0844073
0.0755775	318913.22	8.1876998	58.1925894	21.1895479	1.1517917	0.3709429	0.0793091
0.0754462	318359.10	8.1592721	58.0914794	22.2844699	1.1899379	0.4211253	0.0727175

Table22: Chevron UCAV U=60 mph, h/b=0.10

Mach No.	Re No.	q_c	Uoo	alpha_c	C_L	C_D_c	Cm_cg_c_w
0.0765231	322903.25	8.3938594	58.9206561	-11.7962282	-1.0197090	0.1200846	-0.1892534
0.0764376	322542.48	8.3751135	58.8548256	-9.4369083	-0.8157116	0.0789879	-0.1399832
0.0764469	322581.59	8.3771448	58.8619628	-7.0710560	-0.6068207	0.0484356	-0.0951740
0.0765069	322834.86	8.3903043	58.9081771	-4.7121252	-0.4031147	0.0285424	-0.0595070
0.0765525	323027.33	8.4003118	58.9432978	-2.3751456	-0.2158526	0.0173631	-0.0277427
0.0765757	323125.18	8.4054015	58.9611518	-0.0557386	-0.0417543	0.0128470	-0.0005807
0.0765712	323106.35	8.4044220	58.9577162	2.2497497	0.1219173	0.0144354	0.0253133
0.0765670	323088.73	8.4035057	58.9545023	4.4601479	0.2795287	0.0221662	0.0465068
0.0765596	323057.39	8.4018755	58.9487836	6.7463503	0.4287531	0.0354172	0.0649625
0.0765439	322991.25	8.3984355	58.9367147	9.0139025	0.5640064	0.0551109	0.0814374
0.0765272	322920.50	8.3947562	58.9238035	11.1878156	0.6942864	0.0797285	0.0920318
0.0764950	322784.63	8.3876937	58.8990118	12.3084517	0.7524443	0.0941575	0.0984667
0.0764631	322650.16	8.3807067	58.8744750	13.4349303	0.8142298	0.1122053	0.1030073
0.0764661	322662.73	8.3813598	58.8767691	14.5570655	0.8735108	0.1347098	0.1028755
0.0764183	322461.03	8.3708843	58.8399639	15.6898009	0.9399833	0.1620836	0.0986508
0.0763785	322293.22	8.3621739	58.8093428	16.8233163	1.0077892	0.1993945	0.0920757
0.0763087	321998.59	8.3468921	58.7555812	17.9484483	1.0685660	0.2462257	0.0861963
0.0762334	321681.00	8.3304351	58.6976305	19.0600541	1.1199592	0.2917487	0.0819133
0.0761133	321174.28	8.3042112	58.6051686	20.1706965	1.1698817	0.3419070	0.0778514
0.0759988	320691.06	8.2792422	58.5169957	21.2804476	1.2198856	0.3960667	0.0703846
0.0758816	320196.27	8.2537139	58.4267100	22.4704852	1.2641112	0.4509846	0.0626786

Table 23: Chevron UCAV U=60 mph, h/b=0.05

Mach No.	Re No.	q_c	Uoo	alpha_c	C_L	C_D_c	Cm_cg_c_w
0.0770335	325056.88	8.5061998	59.3136320	−4.8610876	−0.5798764	0.0403803	−0.0759718
0.0769794	324828.78	8.4942662	59.2720110	−2.5326434	−0.3338357	0.0223705	−0.0305832
0.0769491	324700.69	8.4875687	59.2486391	−0.1473048	−0.1103474	0.0136030	0.0036178
0.0769919	324881.69	8.4970335	59.2816649	2.1224169	0.0917037	0.0139395	0.0314673
0.0770184	324993.43	8.5028798	59.3020554	4.4458651	0.2688292	0.0202481	0.0534545
0.0770197	324998.92	8.5031670	59.3030573	6.7471545	0.4293555	0.0322132	0.0718015
0.0770335	325056.88	8.5061998	59.3136320	8.9477866	0.5796509	0.0501742	0.0846547
0.0770047	324935.54	8.4998507	59.2914918	10.0819129	0.6479144	0.0608653	0.0901017
0.0769592	324743.43	8.4898031	59.2564373	11.2071197	0.7087473	0.0724868	0.0963210
0.0769636	324762.05	8.4907765	59.2598344	12.3347146	0.7721181	0.0866408	0.0998421
0.0769362	324646.48	8.4847345	59.2387461	13.4666586	0.8379978	0.1035590	0.1023715

Table 24: Chevron UCAV U=80 mph, h/b=0.93 (OGE)

Mach No.	Re No.	q_c	Uoo	alpha_c	C_L	C_D_c	Cm_cg_c_w
0.1028205	433869.99	15.1543075	79.1689300	−11.1582576	−0.5417991	0.0639043	−0.0983614
0.1027688	433651.70	15.1390624	79.1290985	−8.9294805	−0.4355925	0.0429658	−0.0799881
0.1027945	433760.18	15.1466376	79.1488930	−6.6946653	−0.3248628	0.0268967	−0.0611477
0.1027729	433669.25	15.1402877	79.1323006	−4.4551922	−0.2106437	0.0162998	−0.0405904
0.1027369	433517.17	15.1296704	79.1045495	−2.2111182	−0.0929781	0.0100622	−0.0207713
0.1027238	433461.86	15.1258105	79.0944582	0.0257767	0.0193096	0.0080207	0.0000848
0.1028163	433852.47	15.1530834	79.1657324	2.1849240	0.1385283	0.0106829	0.0205923
0.1029250	434311.17	15.1851420	79.2494317	4.4291560	0.2563123	0.0175112	0.0396458
0.1030807	434967.94	15.2311030	79.3692736	6.6704697	0.3719102	0.0289972	0.0576352
0.1031902	435429.92	15.2634745	79.4535727	8.8209157	0.4846107	0.0451983	0.0738679
0.1032992	435890.09	15.2957529	79.5375404	11.0554815	0.5951537	0.0683344	0.0875975
0.1032867	435837.33	15.2920502	79.5279129	13.2943682	0.7089334	0.0984617	0.0960844
0.1031651	435324.10	15.2560565	79.4342634	14.4010075	0.7566062	0.1170059	0.0995198
0.1030847	434984.83	15.2322865	79.3723571	15.5165748	0.8102180	0.1399422	0.0989994
0.1030199	434711.51	15.2131498	79.3224828	16.6336060	0.8656754	0.1637487	0.0965180
0.1029782	434535.49	15.2008328	79.2903653	17.7541361	0.9230049	0.1977038	0.0933400
0.1029335	434346.72	15.1876282	79.2559190	18.8400333	0.9551396	0.2388797	0.0907261
0.1029109	434251.53	15.1809723	79.2385503	19.9136960	0.9773602	0.2760624	0.0869579
0.1028242	433885.68	15.1554034	79.1717925	20.9779056	0.9932485	0.3148166	0.0856278
0.1027266	433473.83	15.1266455	79.0966414	22.0370399	1.0045858	0.3526565	0.0827238

Table25: Chevron UCAV U=80 mph, h/b=0.3

Mach No.	Re No.	q_c	Uoo	alpha_c	C_L	C_D_c	Cm_cg_c_w
0.0994464	419632.28	14.1760305	76.5709521	-11.3200042	-0.6629651	0.0767372	-0.1189964
0.0993893	419391.29	14.1597531	76.5269789	-9.0579223	-0.5318096	0.0513215	-0.0974429
0.0994229	419533.39	14.1693504	76.5529090	-6.7976137	-0.4019824	0.0322861	-0.0740135
0.0994380	419597.11	14.1736543	76.5645343	-4.5329361	-0.2688825	0.0201148	-0.0498963
0.0994662	419715.76	14.1816717	76.5861860	-2.2633643	-0.1321162	0.0124685	-0.0261072
0.0994909	419819.97	14.1887149	76.6052014	0.0013893	0.0010407	0.0097991	-0.0024700
0.0995873	420226.99	14.2162399	76.6794695	2.2798723	0.1444825	0.0123793	0.0224818
0.0996396	420447.60	14.2311708	76.7197260	4.4600507	0.2794558	0.0202011	0.0440089
0.0996065	420307.98	14.2217209	76.6942497	6.7206478	0.4094991	0.0328629	0.0641276
0.0994890	419812.13	14.1881846	76.6037698	8.9757763	0.5354458	0.0510332	0.0815044
0.0993150	419078.07	14.1386106	76.4698246	11.1419699	0.6599429	0.0765206	0.0952432
0.0991827	418519.59	14.1009529	76.3679193	12.2763680	0.7284101	0.0924467	0.1005908
0.0991092	418209.45	14.0800616	76.3113269	13.3966173	0.7855292	0.1098758	0.1052578
0.0990400	417917.54	14.0604129	76.2580621	14.5137483	0.8410614	0.1308137	0.1076644
0.0989622	417589.16	14.0383255	76.1981420	15.6359585	0.8996494	0.1571126	0.1050972
0.0988402	417074.39	14.0037359	76.1042102	16.7663173	0.9650908	0.1859469	0.1009594
0.0987758	416802.61	13.9854915	76.0546188	17.8949866	1.0285173	0.2293062	0.0982298
0.0987250	416588.39	13.9711190	76.0155292	18.9894362	1.0670587	0.2734829	0.0937203
0.0987005	416485.01	13.9641856	75.9966650	20.0766125	1.0994025	0.3175038	0.0916690
0.0987302	416610.24	13.9725845	76.0195160	21.1472002	1.1200687	0.3597526	0.0892076
0.0986919	416448.68	13.9617498	75.9900367	22.2920907	1.1304742	0.4046040	0.0843675

Table26: Chevron UCAV U=80 mph, h/b=0.15

Mach No.	Re No.	q_c	Uoo	alpha_c	C_L	C_D_c	Cm_cg_c_w
0.1000583	422214.40	14.3510262	77.0421168	-11.5529722	-0.8374836	0.0954740	-0.1443596
0.0999472	421745.66	14.3191786	76.9565839	-9.2373467	-0.6662180	0.0617742	-0.1165902
0.0999736	421856.94	14.3267361	76.9768894	-6.9359149	-0.5055852	0.0384586	-0.0842109
0.1000102	422011.63	14.3372449	77.0051160	-4.6236259	-0.3368190	0.0227276	-0.0558508
0.1000174	422041.91	14.3393023	77.0106409	-2.3214583	-0.1756350	0.0140608	-0.0281259
0.1001222	422484.09	14.3693654	77.0913272	-0.0303885	-0.0227643	0.0103650	-0.0020693
0.1001509	422605.21	14.3776052	77.1134270	2.1692446	0.1267828	0.0129070	0.0228688
0.1001415	422565.63	14.3749127	77.1062063	4.4525505	0.2738373	0.0203629	0.0441794
0.1000927	422359.38	14.3608834	77.0685709	6.7283952	0.4153027	0.0328617	0.0641942
0.0999998	421967.44	14.3342425	76.9970528	8.9098494	0.5512318	0.0511086	0.0811903
0.0998957	421528.37	14.3044278	76.9169354	11.1756549	0.6851767	0.0773513	0.0937826
0.0997659	420980.48	14.2672670	76.8169610	12.3046665	0.7496088	0.0927030	0.0985822
0.0997500	420913.57	14.2627320	76.8047514	13.4332817	0.8129948	0.1109713	0.1025624
0.0997467	420899.54	14.2617811	76.8021914	14.5576966	0.8739835	0.1342082	0.1027086
0.0996728	420587.64	14.2406522	76.7452788	15.6854783	0.9367452	0.1606753	0.0984598
0.0996774	420607.07	14.2419678	76.7488235	16.8189364	1.0045082	0.1907064	0.0933172
0.0996753	420598.43	14.2413831	76.7472481	17.9437021	1.0650105	0.2398888	0.0898777
0.0994899	419815.99	14.1884456	76.6044744	19.0442717	1.1081365	0.2831439	0.0855856
0.0992937	418988.22	14.1325487	76.4534297	20.1472591	1.1523245	0.3311217	0.0845475
0.0991877	418540.88	14.1023870	76.3718026	21.2272994	1.1800717	0.3801916	0.0785098
0.0990739	418060.76	14.0700516	76.2841959	22.3976276	1.2095329	0.4300729	0.0728487

Table 27: Chevron UCAV U=80 mph, h/b=0.10

Mach No.	Re No.	q_c	Uoo	alpha_c	C_L	C_D_c	Cm_cg_c_w
0.1001644	422661.93	14.3814652	77.1237777	-11.8455836	-1.0566816	0.1200437	-0.1991028
0.1000882	422340.75	14.3596167	77.0651718	-9.4690249	-0.8397704	0.0761575	-0.1477262
0.1001843	422746.06	14.3871910	77.1391292	-7.0905433	-0.6214188	0.0458219	-0.1005413
0.1001809	422731.84	14.3862228	77.1365337	-4.7236302	-0.4117332	0.0263843	-0.0624334
0.1001626	422654.49	14.3809586	77.1224195	-2.3807740	-0.2200689	0.0153784	-0.0297534
0.1001756	422709.21	14.3846831	77.1324058	-0.0581450	-0.0435570	0.0107675	-0.0009430
0.1002283	422931.92	14.3998442	77.1730428	2.2517973	0.1234512	0.0127699	0.0257967
0.1002623	423075.39	14.4096156	77.1992223	4.4672839	0.2848743	0.0207776	0.0484380
0.1002856	423173.53	14.4163012	77.2171294	6.7548152	0.4350942	0.0338648	0.0682583
0.1002426	422992.30	14.4039565	77.1840617	9.0340311	0.5790850	0.0534147	0.0846061
0.1002365	422966.42	14.4021934	77.1793377	11.2128459	0.7130368	0.0793285	0.0958216
0.1001681	422677.79	14.3825442	77.1266711	12.3445489	0.7794851	0.0954541	0.1001411
0.1000814	422312.03	14.3576639	77.0599315	13.4772442	0.8459276	0.1139781	0.1031965
0.1000245	422071.99	14.3413467	77.0161305	14.6076192	0.9113810	0.1397689	0.1005534
0.0999466	421743.08	14.3190039	76.9561143	15.7404629	0.9779347	0.1672641	0.0947405
0.0998762	421446.15	14.2988477	76.9019316	16.8838352	1.0531245	0.2020806	0.0910264
0.0998240	421225.61	14.2838869	76.8616901	18.0043817	1.1104662	0.2545388	0.0850391
0.0997648	420975.81	14.2669506	76.8161094	19.1140976	1.1604437	0.2999122	0.0818502
0.0995903	420239.43	14.2170819	76.6817403	20.2222811	1.2085242	0.3518680	0.0776628
0.0993901	419394.67	14.1599817	76.5275965	21.3282761	1.2557144	0.4057167	0.0700244
0.0992308	418722.56	14.1146332	76.4049554	22.5121564	1.2953275	0.4619766	0.0621789

Table28: Chevron UCAV U=80, h/b=0.05

Mach No.	Re No.	q_c	Uoo	alpha_c	C_L	C_D_c	Cm_cg_c_w
0.1014218	427967.89	14.7448123	78.0919653	-4.8881101	-0.6001192	0.0397347	-0.0836255
0.1013384	427615.86	14.7205652	78.0277296	-2.5492397	-0.3462681	0.0221330	-0.0344903
0.1013664	427734.17	14.7287120	78.0493180	-0.1481538	-0.1109834	0.0132480	0.0015010
0.1014302	428003.31	14.7472528	78.0984277	2.1252739	0.0938438	0.0140393	0.0305459
0.1014129	427930.35	14.7422255	78.0851148	4.4560172	0.2764343	0.0204625	0.0527651
0.1013975	427865.60	14.7377647	78.0733002	6.7618990	0.4404008	0.0329906	0.0719667
0.1014611	428133.84	14.7562495	78.1222464	8.9668935	0.5939641	0.0507407	0.0865314
0.1014936	428270.96	14.7657026	78.1472656	10.1058834	0.6658710	0.0621040	0.0920160
0.1014704	428173.02	14.7589501	78.1293947	11.2377883	0.7317214	0.0747851	0.0970715
0.1014932	428269.32	14.7655901	78.1469677	12.3728099	0.8006557	0.0901711	0.0988229
0.1015294	428421.92	14.7761143	78.1748126	13.5109323	0.8711637	0.1081525	0.0995587

Table 29: Chevron UCAV U=100 mph, h/b=0.93 (OGE)

Mach No.	Re No.	q_c	Uoo	alpha_c	C_L	C_D_c	Cm_cg_c_w
0.1263986	533362.27	22.9013689	97.3234396	-11.1749100	-0.5542736	0.0631654	-0.1015948
0.1263595	533197.17	22.8871933	97.2933141	-8.9414862	-0.4445861	0.0419879	-0.0830535
0.1263344	533091.31	22.8781063	97.2739978	-6.7018783	-0.3302661	0.0265944	-0.0636363
0.1263300	533072.86	22.8765225	97.2706305	-4.4625938	-0.2161884	0.0161643	-0.0420474
0.1263290	533068.29	22.8761303	97.2697967	-2.2132749	-0.0945937	0.0099411	-0.0218059
0.1263022	532955.28	22.8664322	97.2491763	0.0319594	0.0239411	0.0079378	-0.0004492
0.1263777	533273.91	22.8937822	97.3073176	2.1955712	0.1465042	0.0108760	0.0215039
0.1265203	533875.85	22.9454945	97.4171543	4.4499950	0.2719230	0.0183105	0.0412667
0.1267224	534728.52	23.0188473	97.5727430	6.6994469	0.3936173	0.0303172	0.0604191
0.1269048	535498.19	23.0851594	97.7131843	8.8517621	0.5077180	0.0464355	0.0775881
0.1269872	535846.07	23.1151637	97.7766637	11.0814746	0.6146254	0.0689809	0.0917557
0.1269729	535785.36	23.1099259	97.7655852	12.1995543	0.6708682	0.0828488	0.0966900
0.1268746	535370.59	23.0741597	97.6899021	13.3210122	0.7288927	0.0994969	0.1002533
0.1267889	535009.19	23.0430177	97.6239564	14.4373610	0.7838390	0.1207051	0.1016791
0.1267577	534877.32	23.0316602	97.5998948	15.5551402	0.8391077	0.1431990	0.1001668
0.1267256	534742.12	23.0200175	97.5752230	16.6763973	0.8977308	0.1686747	0.0964378
0.1266164	534281.30	22.9803597	97.4911378	17.8024975	0.9592329	0.1985432	0.0950149
0.1265328	533928.58	22.9500269	97.4267750	18.9033490	1.0025700	0.2352273	0.0935154
0.1264511	533583.76	22.9203935	97.3638554	19.9561660	1.0091749	0.2812441	0.0884109
0.1263786	533277.91	22.8941251	97.3080464	21.0155460	1.0214453	0.3232145	0.0855202
0.1262582	532769.65	22.8505060	97.2153039	22.1544648	1.0273773	0.3623506	0.0816886

Table 30: Chevron UCAV U=100 mph, h/b=0.3

Mach No.	Re No.	q_c	Uoo	alpha_c	C_L	C_D_c	Cm_cg_c_w
0.1231677	519728.97	21.7455666	94.8357519	-11.3277807	-0.6687905	0.0748803	-0.1215089
0.1229464	518794.86	21.6674698	94.6653026	-9.0640746	-0.5364183	0.0496576	-0.0996731
0.1228699	518472.20	21.6405264	94.6064264	-6.8015519	-0.4049325	0.0313639	-0.0763559
0.1229030	518612.00	21.6521983	94.6319362	-4.5384006	-0.2729760	0.0195976	-0.0508942
0.1230141	519080.61	21.6913446	94.7174430	-2.2652037	-0.1334941	0.0122928	-0.0267603
0.1230949	519421.57	21.7198508	94.7796601	0.0015023	0.0011254	0.0098572	-0.0023500
0.1231913	519828.34	21.7538822	94.8538831	2.2871746	0.1499527	0.0127847	0.0239209
0.1231979	519856.10	21.7562057	94.8589484	4.4746635	0.2904024	0.0209595	0.0457646
0.1231143	519503.49	21.7267024	94.7946081	6.7394785	0.4236054	0.0336365	0.0662672
0.1229246	518702.90	21.6597890	94.6485224	8.9950729	0.5499010	0.0515937	0.0846404
0.1227474	517955.46	21.5974115	94.5121362	11.1558354	0.6703297	0.0762421	0.0987686
0.1225362	517063.99	21.5231314	94.3494682	12.2881937	0.7372689	0.0920533	0.1038710
0.1224117	516538.55	21.4794098	94.2535898	13.4151780	0.7994332	0.1104734	0.1073422
0.1223627	516332.12	21.4622456	94.2159233	14.5352538	0.8571714	0.1335877	0.1072650
0.1223028	516079.10	21.4412160	94.1697535	15.6676545	0.9233932	0.1600621	0.1041529
0.1222448	515834.58	21.4209030	94.1251356	16.8024983	0.9921943	0.1895715	0.0993991
0.1220993	515220.62	21.3699422	94.0131060	17.9344349	1.0580684	0.2262422	0.0996539
0.1219839	514733.71	21.3295696	93.9242583	19.0157928	1.0868027	0.2759538	0.0935466
0.1219775	514706.60	21.3273229	93.9193116	20.0885701	1.1083600	0.3193627	0.0914015
0.1219882	514751.69	21.3310595	93.9275385	21.1539892	1.1251544	0.3644644	0.0866952
0.1219361	514532.02	21.3128576	93.8874555	22.3101528	1.1440047	0.4110563	0.0832617

Table 31: Chevron UCAV U=100 mph, h/b=0.15

Mach No.	Re No.	q_c	Uoo	alpha_c	C_L	C_D_c	Cm_cg_c_w
0.1236551	521785.41	21.9179907	95.2109936	-11.5811540	-0.8585949	0.0951269	-0.1496426
0.1235227	521226.82	21.8710872	95.1090653	-9.2535462	-0.6783533	0.0596866	-0.1205070
0.1236092	521591.75	21.9017240	95.1756560	-6.9457542	-0.5129559	0.0370516	-0.0875628
0.1236858	521915.03	21.9288812	95.2346445	-4.6374288	-0.3471589	0.0223002	-0.0575274
0.1238252	522503.38	21.9783497	95.3420022	-2.3268189	-0.1796506	0.0135523	-0.0293766
0.1238456	522589.33	21.9855812	95.3576859	-0.0339533	-0.0254347	0.0102356	-0.0024217
0.1237865	522340.01	21.9646082	95.3121921	2.2593487	0.1291081	0.0126694	0.0234384
0.1237721	522279.13	21.9594882	95.3010827	4.4657643	0.2837360	0.0204183	0.0459544
0.1237234	522073.62	21.9422102	95.2635832	6.7465810	0.4289259	0.0334013	0.0666521
0.1235811	521473.03	21.8917549	95.1539928	8.9380687	0.5723711	0.0519572	0.0843176
0.1235010	521135.13	21.8633938	95.0923360	11.2099315	0.7108536	0.0796979	0.0966797
0.1235291	521253.86	21.8733564	95.1139992	12.3365596	0.7735002	0.0953506	0.1001925
0.1234751	521026.08	21.8542446	95.0724372	13.4704262	0.8408202	0.1157751	0.1026205
0.1233625	520550.66	21.8143800	94.9856862	14.6052077	0.9095745	0.1417347	0.1001259
0.1232297	519990.36	21.7674451	94.8834476	15.7412239	0.9785048	0.1698239	0.0947052
0.1231100	519485.39	21.7251885	94.7913054	16.8808716	1.0509044	0.2021072	0.0917289
0.1230138	519079.27	21.6912331	94.7171995	17.9923660	1.1014651	0.2514380	0.0880393
0.1228922	518566.25	21.6483778	94.6235869	19.0857070	1.1391761	0.2978788	0.0844331
0.1227067	517783.55	21.5830770	94.4807665	20.1755186	1.1734940	0.3451451	0.0805904
0.1225206	516998.16	21.5176513	94.3374559	21.2689865	1.2113000	0.3932781	0.0758405
0.1224631	516755.69	21.4974724	94.2932116	22.4187658	1.2253677	0.4424838	0.0694536

Table 32: Chevron UCAV U=100 mph, h/b=0.10

Mach No.	Re No.	q_c	Uoo	alpha_c	C_L	C_D_c	Cm_cg_c_w
0.1245020	525358.97	22.2192384	95.8630654	-11.8445610	-1.0927522	0.1234009	-0.2072697
0.1243765	524829.66	22.1744888	95.7664824	-9.4994761	-0.8625817	0.0756144	-0.1552679
0.1244259	525038.05	22.1921010	95.8045065	-7.1204239	-0.6438026	0.0457070	-0.1053639
0.1244576	525171.62	22.2033940	95.8288795	-4.7462139	-0.4286509	0.0264828	-0.0653623
0.1244843	525284.23	22.2129167	95.8494272	-2.3913412	-0.2279849	0.0154589	-0.0315234
0.1245724	525656.19	22.2443866	95.9173000	-0.0643932	-0.0482375	0.0110994	-0.0014163
0.1246190	525852.65	22.2610174	95.9531491	2.2545920	0.1255447	0.0131921	0.0262802
0.1246167	525843.07	22.2602060	95.9514003	4.4789981	0.2936495	0.0212806	0.0497606
0.1246668	526054.51	22.2781110	95.9899818	6.7706354	0.4469452	0.0344605	0.0705910
0.1246248	525877.09	22.2630865	95.9576084	9.0568875	0.5962069	0.0539102	0.0873286
0.1245507	525564.55	22.2366311	95.9005777	11.2376675	0.7316309	0.0806232	0.0980020
0.1244818	525273.86	22.2120403	95.8475364	12.3737946	0.8013933	0.0976199	0.1009090
0.1244101	524971.34	22.1864625	95.7923349	13.5050776	0.8667778	0.1182112	0.1013050
0.1243201	524591.39	22.1543589	95.7230045	14.6429630	0.9378574	0.1450308	0.0969075
0.1242208	524172.53	22.1189944	95.6465738	15.7807276	1.0080974	0.1738563	0.0898650
0.1241424	523841.67	22.0910801	95.5862014	16.9203685	1.0804920	0.2107617	0.0876784
0.1240318	523375.18	22.0517530	95.5010809	18.0344083	1.1329594	0.2626237	0.0830825
0.1238939	522793.09	22.0027285	95.3948651	19.1385708	1.1787769	0.3125825	0.0790550
0.1236899	521932.12	21.9303173	95.2377630	20.2430008	1.2240455	0.3608705	0.0743631
0.1234266	520821.08	21.8370503	95.0350298	21.3401750	1.2646279	0.4150019	0.0658093
0.1231653	519718.76	21.7447120	94.8338884	22.5236248	1.3039186	0.4696325	0.0589202

Table 33: Chevron UCAV U=100 mph, h/b=0.05

Mach No.	Re No.	q_c	Uoo	alpha_c	C_L	C_D_c	Cm_cg_c_w
0.1253413	528900.51	22.5198161	96.5092959	−4.9234573	−0.6265981	0.0394941	−0.0917259
0.1252616	528564.19	22.4911852	96.4479273	−2.5705068	−0.3621996	0.0214537	−0.0382728
0.1252655	528580.79	22.4925978	96.4509559	−0.1565980	−0.1173090	0.0129914	0.0002593
0.1252633	528571.62	22.4918177	96.4492833	2.1288398	0.0965152	0.0135391	0.0307551
0.1252737	528615.50	22.4955520	96.4572897	4.4710410	0.2876888	0.0206107	0.0543727
0.1252934	528698.45	22.5026122	96.4724251	6.7910097	0.4622078	0.0336850	0.0742616
0.1253354	528875.76	22.5177085	96.5047798	9.0055383	0.6229132	0.0520991	0.0890370
0.1253370	528882.37	22.5182715	96.5059862	10.1449782	0.6951573	0.0638130	0.0943066
0.1252928	528695.99	22.5024029	96.4719764	11.2832291	0.7657615	0.0780528	0.0977039
0.1252479	528506.41	22.4862679	96.4373834	12.4255068	0.8401314	0.0944909	0.0982608
0.1252123	528356.56	22.4735189	96.4100409	13.5669272	0.9131099	0.1141758	0.0971078

Table 34: Lambda UCAV U=40mph, h/b=0.93 (OGE)

Mach No.	Re No.	q_c	Uoo	alpha_c	C_L	C_D_c	Cm_cg_c_w
0.0513652	309909.00	3.7761046	39.5469636	−11.0001051	−0.4733480	0.0690946	−0.1503780
0.0513582	309866.85	3.7750773	39.5415841	−8.7798712	−0.3617475	0.0410577	−0.1087208
0.0513629	309895.30	3.7757705	39.5452142	−6.5412149	−0.2347159	0.0207045	−0.0708046
0.0513602	309879.02	3.7753738	39.5431367	−4.3046098	−0.1094024	0.0075540	−0.0342772
0.0513395	309753.92	3.7723262	39.5271731	−2.0724539	0.0121842	0.0030485	−0.0013794
0.0513365	309735.75	3.7718837	39.5248551	0.1572787	0.1317411	0.0030055	0.0313631
0.0514123	310193.47	3.7830400	39.5832644	2.3237458	0.2711786	0.0100575	0.0627813
0.0515045	310749.82	3.7966223	39.6542586	4.5566665	0.3934059	0.0237968	0.0928746
0.0515754	311177.13	3.8070708	39.7087863	6.7857437	0.5124138	0.0454457	0.1205769
0.0516150	311416.18	3.8129225	39.7392921	8.9165791	0.6220053	0.0794823	0.1475805
0.0516165	311425.61	3.8131533	39.7404948	11.1353361	0.7323686	0.1199803	0.1707885
0.0515637	311106.86	3.8053518	39.6998205	12.2381810	0.7824964	0.1453867	0.1807402
0.0515160	310819.22	3.7983184	39.6631151	13.3532901	0.8420594	0.1745713	0.1897379
0.0515229	310860.87	3.7993362	39.6684291	14.4503421	0.8873349	0.2035562	0.1983748
0.0515256	310877.06	3.7997321	39.6704956	15.5341035	0.9206401	0.2327333	0.2039163
0.0515102	310783.75	3.7974514	39.6585885	16.6043352	0.9434502	0.2607282	0.2101175
0.0514704	310543.92	3.7915928	39.6279843	17.6514801	0.9460845	0.2851728	0.2130277
0.0514456	310394.32	3.7879405	39.6088936	18.7060883	0.9558078	0.3124653	0.2142437
0.0514092	310174.41	3.7825750	39.5808316	19.7191998	0.9299347	0.3320897	0.2081842
0.0513856	310032.39	3.7791119	39.5627085	20.7233734	0.8974126	0.3492187	0.1989021
0.0513456	309791.08	3.7732315	39.5319157	21.7898771	0.8433887	0.3565550	0.1870065

Table 35: Lambda UCAV U=40mph, h/b=0.3

Mach No.	Re No.	q_c	Uoo	alpha_c	C_L	C_D_c	Cm_cg_c_w
0.0499789	301545.07	3.5750332	38.4796556	-11.1033865	-0.5598594	0.0796875	-0.1868015
0.0498955	301042.12	3.5631175	38.4154753	-8.8676451	-0.4352694	0.0465462	-0.1364802
0.0499073	301112.90	3.5647933	38.4245079	-6.6114521	-0.2935486	0.0234374	-0.0863025
0.0499380	301298.49	3.5691890	38.4481910	-4.3522926	-0.1493429	0.0085745	-0.0419005
0.0499777	301537.61	3.5748563	38.4787036	-2.0904145	-0.0028601	0.0024306	-0.0011073
0.0500574	302018.42	3.5862658	38.5400593	0.1549576	0.1297969	0.0030148	0.0369847
0.0500702	302096.11	3.5881111	38.5499731	2.4186439	0.2777943	0.0087579	0.0752169
0.0500512	301981.30	3.5853844	38.5353227	4.5803138	0.4132135	0.0246242	0.1096569
0.0500050	301702.48	3.5787667	38.4997430	6.8279937	0.5478036	0.0476355	0.1398168
0.0499198	301188.69	3.5665881	38.4341794	8.9732387	0.6694649	0.0837265	0.1690096
0.0498043	300491.39	3.5500926	38.3451972	11.2068339	0.7922572	0.1268240	0.1970503
0.0497151	299953.43	3.5373928	38.2765494	12.3211407	0.8519858	0.1545599	0.2069844
0.0496373	299484.18	3.5263337	38.2166698	13.4472526	0.9207650	0.1872756	0.2188645
0.0495822	299151.67	3.5185076	38.1742385	14.5514453	0.9720218	0.2202391	0.2279976
0.0495445	298924.04	3.5131550	38.1451910	15.6383658	1.0079732	0.2522297	0.2354267
0.0495269	298817.61	3.5106537	38.1316090	16.7028871	1.0260001	0.2822791	0.2405351
0.0495724	299092.63	3.5171188	38.1667040	17.7477793	1.0267473	0.3099567	0.2413281
0.0495793	299133.80	3.5180873	38.1719583	18.7827304	1.0200054	0.3364271	0.2384204
0.0495173	298760.12	3.5093029	38.1242728	19.8039569	1.0009297	0.3618964	0.2328412
0.0495025	298670.77	3.5072044	38.1128718	20.8019821	0.9632575	0.3799871	0.2220250
0.0495065	298694.72	3.5077667	38.1159271	21.8847703	0.9228739	0.3941866	0.2120141

Table 36: Lambda UCAV U=40 mph, h/b=0.15

Mach No.	Re No.	q_c	Uoo	alpha_c	C_L	C_D_c	Cm_cg_c_w
0.0500449	301943.51	3.5844870	38.5304998	-11.2963575	-0.7214974	0.1014318	-0.2380583
0.0499510	301376.61	3.5710400	38.4581595	-9.0234041	-0.5657376	0.0575460	-0.1726088
0.0499545	301397.86	3.5715435	38.4608703	-6.7145128	-0.3798752	0.0269991	-0.1068817
0.0499955	301645.32	3.5774106	38.4924483	-4.4198521	-0.2059326	0.0087151	-0.0495493
0.0500255	301826.35	3.5817059	38.5155493	-2.1226221	-0.0298381	0.0015929	-0.0016039
0.0500842	302180.19	3.5901087	38.5607025	0.1504280	0.1260028	0.0020943	0.0389582
0.0501044	302302.07	3.5930055	38.5762561	2.3473780	0.2909737	0.0093029	0.0799982
0.0501028	302292.50	3.5927778	38.5750341	4.6078093	0.4362446	0.0256020	0.1158867
0.0500939	302238.61	3.5914969	38.5681571	6.8486024	0.5650661	0.0483885	0.1505304
0.0500609	302039.58	3.5867685	38.5427602	9.0085309	0.6990266	0.0882306	0.1797772
0.0499843	301577.72	3.5758076	38.4838230	11.2445654	0.8238622	0.1352178	0.2040131
0.0499197	301187.86	3.5665684	38.4340736	12.3768415	0.8986423	0.1663742	0.2149095
0.0498650	300857.99	3.5587601	38.3919788	13.4888902	0.9556419	0.1983410	0.2261328
0.0497983	300455.24	3.5492386	38.3405851	14.5856342	1.0006594	0.2294155	0.2367019
0.0497398	300102.64	3.5409131	38.2955906	15.6769449	1.0402881	0.2642980	0.2436153
0.0496701	299681.65	3.5309855	38.2418687	16.7326467	1.0509275	0.2949342	0.2492370
0.0496318	299450.73	3.5255459	38.2124009	17.7829374	1.0561968	0.3252571	0.2487694
0.0496089	299312.82	3.5222994	38.1948030	18.8075763	1.0408170	0.3508981	0.2427071
0.0495856	299171.79	3.5189807	38.1768052	19.8160174	1.0110319	0.3755596	0.2326929
0.0495633	299037.80	3.5158294	38.1597074	20.8298398	0.9865919	0.3951189	0.2277135
0.0495485	298948.47	3.5137293	38.1483088	21.9163405	0.9493181	0.4089464	0.2201509

Table 37: Lambda UCAV U=40 mph, h/b=0.10

Mach No.	Re No.	q_c	Uoo	alpha_c	C_L	C_D_c	Cm_cg_c_w
0.0499679	301478.60	3.5734573	38.4711735	-11.4717222	-0.8683878	0.1205407	-0.3333868
0.0498870	300990.81	3.5619030	38.4089277	-9.1652044	-0.6845135	0.0698891	-0.2256846
0.0498716	300897.39	3.5596923	38.3970066	-6.8214440	-0.4694437	0.0337181	-0.1349611
0.0498966	301048.43	3.5632670	38.4162809	-4.4771379	-0.2539168	0.0116097	-0.0612326
0.0499353	301282.15	3.5688019	38.4461059	-2.1627867	-0.0634811	0.0040212	-0.0027027
0.0499532	301389.80	3.5713527	38.4598430	0.1374925	0.1151676	0.0027615	0.0440680
0.0499290	301244.00	3.5678981	38.4412372	2.4356274	0.2920202	0.0085818	0.0875634
0.0499438	301333.05	3.5700079	38.4526012	4.6217691	0.4479377	0.0259560	0.1244376
0.0499454	301342.66	3.5702354	38.4538267	6.8717977	0.5844950	0.0509132	0.1600025
0.0498911	301014.99	3.5624754	38.4120138	9.0323556	0.7189829	0.0897703	0.1951594
0.0498399	300706.19	3.5551698	38.3726074	11.2722908	0.8470858	0.1382105	0.2210723
0.0498033	300485.38	3.5499507	38.3444313	12.3984552	0.9167466	0.1691125	0.2336652
0.0497839	300368.30	3.5471849	38.3294910	13.5193472	0.9811535	0.2023298	0.2437542
0.0497488	300156.86	3.5421926	38.3025091	14.6231975	1.0321234	0.2377493	0.2525168
0.0497219	299994.28	3.5383563	38.2817621	15.7048182	1.0636356	0.2726727	0.2577176
0.0496183	299369.59	3.5236356	38.2020469	16.7567100	1.0710837	0.3024781	0.2596625
0.0495023	298669.30	3.5071697	38.1126834	17.8080625	1.0772423	0.3345027	0.2595469
0.0494600	298414.10	3.5011788	38.0801177	18.8293773	1.0590782	0.3625876	0.2505862
0.0494347	298261.73	3.4976043	38.0606743	19.8365343	1.0282175	0.3879867	0.2405875
0.0493654	297843.36	3.4877993	38.0072877	20.8457348	0.9999060	0.4080458	0.2352796
0.0493349	297659.49	3.4834943	37.9838244	21.9726385	0.9964749	0.4330877	0.2345669

Table 38: Lambda UCAV U=40 mph, h/b=0.05

Mach No.	Re No.	q_c	Uoo	alpha_c	C_L	C_D_c	Cm_cg_c_w
0.0502762	303338.87	3.6176933	38.7085594	-4.4740818	-0.3242306	0.0194627	-0.0838707
0.0502678	303287.97	3.6164794	38.7020647	-2.2128810	-0.1054414	0.0070337	-0.0069954
0.0502790	303355.39	3.6180874	38.7106677	0.1144937	0.0959031	0.0050121	0.0488891
0.0502954	303454.32	3.6204477	38.7232928	2.3377748	0.2829297	0.0119785	0.0908509
0.0502926	303437.69	3.6200508	38.7211700	4.6115357	0.4393659	0.0246293	0.1281725
0.0502914	303430.68	3.6198837	38.7202762	6.8795456	0.5909850	0.0509287	0.1663732
0.0502974	303466.58	3.6207402	38.7248569	9.0666784	0.7477327	0.0907620	0.2000464
0.0502880	303410.20	3.6193949	38.7176618	10.1921041	0.8167747	0.1135030	0.2153432
0.0502248	303028.81	3.6103014	38.6689937	11.3112610	0.8797283	0.1394203	0.2320608
0.0501838	302781.38	3.6044081	38.6374198	12.4490875	0.9591576	0.1710920	0.2434490
0.0502005	302882.24	3.6068099	38.6502907	13.5737006	1.0266815	0.2047918	0.2547878

Table 39: Lambda UCAV U=60 mph, h/b=0.93 (OGE)

Mach No.	Re No.	q_c	Uoo	alpha_c	C_L	C_D_c	Cm_cg_c_w
0.0776734	468638.15	8.6347727	59.8021219	-10.9585824	-0.4385674	0.0619588	-0.1599142
0.0775824	468089.35	8.6145610	59.7320903	-8.7303866	-0.3202978	0.0369131	-0.1196698
0.0775045	467619.09	8.5972604	59.6720803	-6.4915244	-0.1930938	0.0195937	-0.0796986
0.0775067	467632.80	8.5977645	59.6738297	-4.2622828	-0.0739481	0.0110017	-0.0449288
0.0775813	468082.58	8.6143118	59.7312264	-2.0347297	0.0437831	0.0083064	-0.0117570
0.0776213	468323.77	8.6231913	59.7620036	0.2019923	0.1691945	0.0117369	0.0167927
0.0777004	468801.06	8.6407769	59.8229100	2.3501007	0.2932542	0.0197612	0.0482959
0.0778133	469482.30	8.6659079	59.9098419	4.5801897	0.4131096	0.0345274	0.0771982
0.0778885	469935.90	8.6826614	59.9677246	6.8063072	0.5296384	0.0555302	0.1080787
0.0779533	470326.87	8.6971148	60.0176160	8.9393551	0.6410831	0.0887845	0.1416933
0.0779733	470447.89	8.7015910	60.0330585	11.1526212	0.7468471	0.1315540	0.1690017
0.0779188	470118.84	8.6894230	59.9910701	12.2556901	0.7971626	0.1566752	0.1805738
0.0778579	469751.41	8.6758455	59.9441827	13.3608290	0.8483742	0.1843538	0.1912138
0.0778370	469625.17	8.6711829	59.9280726	14.4587151	0.8943484	0.2140804	0.2009088
0.0777924	469356.21	8.6612536	59.8937514	15.5466327	0.9311350	0.2454731	0.2077177
0.0777591	469155.31	8.6538405	59.8681146	16.6146163	0.9520620	0.2744700	0.2120042
0.0777292	468974.80	8.6471826	59.8450803	17.6758718	0.9665157	0.3034554	0.2150492
0.0776740	468641.96	8.6349131	59.8026078	18.7233503	0.9702669	0.3300311	0.2156436
0.0776474	468481.26	8.6289920	59.7821005	19.7468626	0.9531059	0.3533069	0.2092388
0.0776081	468244.39	8.6202684	59.7518741	20.7365093	0.9084156	0.3681276	0.1957749
0.0775418	467844.53	8.6055521	59.7008488	21.8308129	0.8776777	0.3844302	0.1865593

Table 40: Lambda UCAV U=60 mph, h/b=0.3

Mach No.	Re No.	q_c	Uoo	alpha_c	C_L	C_D_c	Cm_cg_c_w
0.0757250	456882.58	8.2070073	58.3020128	-11.0745945	-0.5357424	0.0744397	-0.1944406
0.0755488	455819.51	8.1688596	58.1663557	-8.8252873	-0.3997893	0.0436012	-0.1461118
0.0755631	455905.67	8.1719481	58.1773504	-6.5571523	-0.2480655	0.0222223	-0.0971334
0.0756208	456254.14	8.1844456	58.2218192	-4.3011136	-0.1064739	0.0116803	-0.0542499
0.0756996	456729.39	8.2015047	58.2824644	-2.0548807	0.0269041	0.0088291	-0.0145304
0.0757903	457276.80	8.2211764	58.3523190	0.1937262	0.1622705	0.0123665	0.0213939
0.0758317	457526.50	8.2301571	58.3841819	2.4499807	0.3040429	0.0205103	0.0559893
0.0758166	457435.22	8.2268735	58.3725341	4.6089405	0.4371922	0.0346695	0.0893307
0.0757413	456981.21	8.2105513	58.3145995	6.8573140	0.5723632	0.0599208	0.1222143
0.0755809	456013.07	8.1757988	58.1910557	9.0019429	0.6935083	0.0970342	0.1581329
0.0753983	454911.84	8.1363590	58.0505300	11.2325914	0.8138324	0.1440730	0.1873152
0.0752475	454001.53	8.1038288	57.9343669	12.3461609	0.8729434	0.1728620	0.2000662
0.0751880	453642.99	8.0910339	57.8886136	13.4528192	0.9254278	0.2023013	0.2123681
0.0751879	453642.22	8.0910065	57.8885157	14.5583327	0.9777909	0.2361749	0.2219927
0.0751667	453514.00	8.0864335	57.8721542	15.6471390	1.0153219	0.2699046	0.2295387
0.0751434	453373.50	8.0814239	57.8542252	16.7166534	1.0375311	0.3017399	0.2354492
0.0750850	453021.10	8.0688655	57.8092556	17.7735793	1.0483582	0.3328761	0.2382147
0.0750675	452915.91	8.0651191	57.7958334	18.8107876	1.0435069	0.3608254	0.2343426
0.0750815	453000.37	8.0681271	57.8066104	19.8312221	1.0237678	0.3862743	0.2253636
0.0750462	452787.00	8.0605286	57.7793828	20.8309474	0.9875197	0.4058588	0.2143406
0.0750732	452950.32	8.0663446	57.8002243	21.9222878	0.9542996	0.4228082	0.2061308

Table 41: Lambda UCAV U=60 mph, h/b=0.15

Mach No.	Re No.	q_c	Uoo	alpha_c	C_L	C_D_c	Cm_cg_c_w
0.0762491	460044.65	8.3210015	58.7055199	-11.2616906	-0.6924594	0.0969224	-0.2506158
0.0761437	459409.23	8.2980309	58.6244338	-8.9700686	-0.5210623	0.0555042	-0.1844693
0.0761355	459359.26	8.2962258	58.6180573	-6.6537162	-0.3289502	0.0272902	-0.1186787
0.0761677	459553.77	8.3032535	58.6428795	-4.3527712	-0.1497438	0.0133978	-0.0650355
0.0762673	460154.45	8.3249738	58.7195306	-2.0842203	0.0023284	0.0093525	-0.0173850
0.0763315	460541.76	8.3389939	58.7689545	0.1871500	0.1567622	0.0128623	0.0219702
0.0763171	460455.31	8.3358634	58.7579224	2.3706180	0.3104401	0.0216636	0.0598430
0.0763293	460528.79	8.3385242	58.7672997	4.6297633	0.4546339	0.0360805	0.0944588
0.0763249	460501.99	8.3375537	58.7638797	6.8899413	0.5996927	0.0644403	0.1265363
0.0762497	460048.63	8.3211454	58.7060273	9.0444150	0.7290842	0.1041010	0.1615516
0.0761605	459510.20	8.3016791	58.6373193	11.2792624	0.8529254	0.1533253	0.1904293
0.0760529	458861.29	8.2782485	58.5545123	12.3967017	0.9152779	0.1837932	0.2025663
0.0759699	458360.63	8.2601938	58.4906243	13.5114685	0.9745541	0.2161137	0.2157027
0.0759456	458213.58	8.2548947	58.4718597	14.6065962	1.0182177	0.2492704	0.2241152
0.0758701	457757.97	8.2384870	58.4137204	15.6933996	1.0540711	0.2847322	0.2311057
0.0757795	457211.59	8.2188317	58.3439975	16.7558323	1.0703485	0.3167472	0.2359974
0.0757029	456749.59	8.2022301	58.2850419	17.8067208	1.0761185	0.3484831	0.2365408
0.0756151	456219.72	8.1832105	58.2174260	18.8384619	1.0666876	0.3769381	0.2308746
0.0755461	455803.45	8.1682840	58.1643064	19.8494691	1.0390519	0.4013755	0.2193000
0.0755355	455739.22	8.1659822	58.1561105	20.8612491	1.0129012	0.4229396	0.2120500
0.0754836	455426.08	8.1547643	58.1161512	21.9572964	0.9836239	0.4411396	0.2043621

Table 42: Lambda UCAV U=60 mph, h/b=0.10

Mach No.	Re No.	q_c	Uoo	alpha_c	C_L	C_D_c	Cm_cg_c_w
0.0762546	460078.35	8.3222206	58.7098201	-11.1511319	-0.5998523	0.0966548	-0.1974063
0.0762151	459839.70	8.3135891	58.6793665	-10.3424329	-0.7969471	0.0896838	-0.3139364
0.0761622	459520.55	8.3020529	58.6386395	-10.3432606	-0.7976404	0.0900583	-0.3139908
0.0762443	460015.90	8.3199613	58.7018502	-9.1405060	-0.6638254	0.0648263	-0.2482471
0.0763958	460929.94	8.3530572	58.8184893	-6.7584531	-0.4166808	0.0298160	-0.1502415
0.0764314	461144.58	8.3608385	58.8458791	-4.4068598	-0.1950499	0.0125411	-0.0779374
0.0764247	461104.63	8.3593902	58.8407820	-2.1096491	-0.0189715	0.0078743	-0.0223862
0.0764547	461285.60	8.3659529	58.8638745	0.1901513	0.1592761	0.0117727	0.0202228
0.0764415	461205.69	8.3630546	58.8536773	2.4829002	0.3316172	0.0210139	0.0577794
0.0764294	461132.42	8.3603977	58.8443278	4.6701098	0.4884293	0.0388328	0.0918248
0.0764022	460968.30	8.3544478	58.8233850	6.9383210	0.6402169	0.0680437	0.1258788
0.0763725	460789.42	8.3479651	58.8005585	9.1041295	0.7791028	0.1104103	0.1612774
0.0763165	460451.64	8.3357304	58.7574539	11.3416237	0.9051609	0.1620599	0.1898896
0.0762296	459927.15	8.3167514	58.6905256	13.5744676	1.0273239	0.2277614	0.2124328
0.0761189	459259.13	8.2926096	58.6052805	14.6780584	1.0780765	0.2644445	0.2218742
0.0760313	458730.83	8.2735420	58.5378646	15.7624025	1.1118698	0.3015404	0.2270712
0.0759545	458267.39	8.2568336	58.4787261	16.8171166	1.1216819	0.3338417	0.2296408
0.0758614	457705.48	8.2365976	58.4070219	17.8611603	1.1217185	0.3659357	0.2272511
0.0757816	457224.07	8.2192803	58.3455896	18.8867584	1.1071422	0.3958095	0.2169531
0.0756870	456653.56	8.1987817	58.2727884	19.8921301	1.0747860	0.4198150	0.2060971
0.0755905	456071.34	8.1778883	58.1984913	20.9095202	1.0533345	0.4436126	0.2005376
0.0755438	455789.21	8.1677738	58.1624896	22.0445210	1.0566857	0.4732504	0.1986739

Table 43: Lambda UCAV U=60 mph, h/b=0.05

Mach No.	Re No.	q_c	Uoo	alpha_c	C_L	C_D_c	Cm_cg_c_w
0.0770126	464651.55	8.4884892	59.2933978	-4.4532705	-0.3067985	0.0209150	-0.1039468
0.0769766	464434.16	8.4805484	59.2656573	-2.1742931	-0.0731191	0.0121768	-0.0275031
0.0769433	464233.04	8.4732050	59.2399925	0.1612754	0.1350888	0.0132663	0.0260926
0.0769481	464262.34	8.4742748	59.2437320	2.3802661	0.3185216	0.0227937	0.0689664
0.0769465	464252.66	8.4739214	59.2424966	4.6628924	0.4823837	0.0369616	0.1028845
0.0768945	463938.61	8.4624606	59.2024210	6.9522146	0.6518545	0.0688305	0.1374797
0.0768628	463747.55	8.4554918	59.1780396	9.1263988	0.7977561	0.1116481	0.1741963
0.0768666	463770.70	8.4563362	59.1809945	10.2523525	0.8672405	0.1362855	0.1899429
0.0768402	463611.36	8.4505263	59.1606607	11.3742432	0.9324840	0.1637523	0.2036215
0.0768299	463549.35	8.4482658	59.1527476	12.5001290	1.0019115	0.1958820	0.2165373
0.0768204	463491.78	8.4461677	59.1454020	13.6254321	1.0700132	0.2319023	0.2278815

Table 44: Lambda UCAV U=80 mph, h/b=0.93 (OGE)

Mach No.	Re No.	q_c	Uoo	alpha_c	C_L	C_D_c	Cm_cg_c_w
0.1026153	619123.92	15.0706087	79.0053561	-10.9407128	-0.4235994	0.0572805	-0.1669016
0.1025246	618576.48	15.0439690	78.9354980	-8.7115261	-0.3044997	0.0332210	-0.1256668
0.1025145	618515.58	15.0410067	78.9277259	-6.4739461	-0.1783697	0.0167312	-0.0839062
0.1025199	618548.27	15.0425967	78.9318976	-4.2490192	-0.0628382	0.0096084	-0.0483749
0.1025621	618802.96	15.0549869	78.9643981	-2.0293633	0.0482782	0.0082370	-0.0132008
0.1025962	619008.99	15.0650138	78.9906895	0.1970754	0.1650759	0.0112141	0.0186588
0.1026822	619527.66	15.0902705	79.0568762	2.3469356	0.2906030	0.0185516	0.0513723
0.1028362	620456.54	15.1355550	79.1754086	4.5790621	0.4121651	0.0325740	0.0818564
0.1029548	621172.37	15.1704995	79.2667548	6.7981228	0.5227829	0.0543751	0.1148134
0.1029950	621414.81	15.1823438	79.2976922	8.9297089	0.6330032	0.0875307	0.1476143
0.1029705	621266.98	15.1751211	79.2788280	11.1515979	0.7459900	0.1317495	0.1772914
0.1029433	621102.76	15.1670998	79.2578724	12.2538155	0.7955923	0.1569141	0.1890686
0.1028903	620783.17	15.1514954	79.2170903	13.3593063	0.8470987	0.1851400	0.1988082
0.1028421	620492.35	15.1373025	79.1799791	14.4557378	0.8918544	0.2148462	0.2073826
0.1027897	620176.34	15.1218879	79.1396536	15.5440259	0.9289515	0.2465886	0.2131627
0.1027304	619818.25	15.1044300	79.0939580	16.6120279	0.9498938	0.2763389	0.2172271
0.1026721	619466.67	15.0872994	79.0490933	17.6719605	0.9632394	0.3047494	0.2203276
0.1026223	619165.88	15.0726514	79.0107101	18.7189659	0.9665944	0.3321566	0.2201676
0.1025631	618808.79	15.0552705	78.9651418	19.7396185	0.9470380	0.3529483	0.2144521
0.1025302	618610.19	15.0456089	78.9398000	20.7382368	0.9098627	0.3701720	0.2018834
0.1024903	618369.60	15.0339081	78.9090988	21.8332752	0.8797402	0.3872933	0.1912771

Table 45: Lambda UCAV U=80 mph, h/b=0.3

Mach No.	Re No.	q_c	Uoo	alpha_c	C_L	C_D_c	Cm_cg_c_w
0.1008926	608729.84	14.5688346	77.6789853	-11.0757238	-0.5366884	0.0731377	-0.2021286
0.1006944	607534.00	14.5116500	77.5263853	-8.8174828	-0.3932520	0.0424852	-0.1530179
0.1006481	607254.98	14.4983237	77.4907802	-6.5455973	-0.2383867	0.0210493	-0.1018019
0.1007188	607681.29	14.5186875	77.5451816	-4.2898758	-0.0970608	0.0116864	-0.0581698
0.1007827	608067.31	14.5371390	77.5944410	-2.0475367	0.0330555	0.0095832	-0.0166875
0.1008514	608481.27	14.5569387	77.6472652	0.2010135	0.1683746	0.0126189	0.0206090
0.1009179	608882.53	14.5761439	77.6984690	2.4654123	0.3169689	0.0207288	0.0568063
0.1008681	608582.18	14.5617672	77.6601418	4.6244042	0.4501450	0.0357019	0.0916434
0.1007415	607818.43	14.5252413	77.5626817	6.8602148	0.5747929	0.0601681	0.1288411
0.1005929	606921.95	14.4824259	77.4482832	9.0130770	0.7028346	0.0980740	0.1644739
0.1003881	605686.01	14.4235016	77.2905668	11.2509694	0.8292263	0.1476644	0.1956747
0.1002255	604705.03	14.3768183	77.1653855	12.3620413	0.8862453	0.1759251	0.2094504
0.1001696	604367.95	14.3607949	77.1223719	13.4750808	0.9440748	0.2077387	0.2204062
0.1000840	603851.65	14.3362690	77.0564875	14.5745674	0.9913895	0.2413117	0.2293665
0.1000148	603434.14	14.3164513	77.0032096	15.6696660	1.0341912	0.2776010	0.2360348
0.0999997	603342.72	14.3121134	76.9915429	16.7337412	1.0518444	0.3095981	0.2398457
0.1000084	603395.29	14.3146076	76.9982512	17.7887709	1.0610831	0.3402660	0.2412230
0.0999974	603328.79	14.3114530	76.9897663	18.8282997	1.0581755	0.3691986	0.2388700
0.0999429	602999.95	14.2958565	76.9478036	19.8416807	1.0325282	0.3924137	0.2296482
0.0999335	602943.49	14.2931793	76.9405983	20.8484229	1.0021577	0.4137082	0.2187877
0.0999794	603220.64	14.3063224	76.9759648	21.9482300	0.9760296	0.4341993	0.2100031

Table 46: Lambda UCAV U=80 mph, h/b=0.15

Mach No.	Re No.	q_c	Uoo	alpha_c	C_L	C_D_c	Cm_cg_c_w
0.1000407	603590.03	14.3238492	77.0231024	-11.2878964	-0.7144101	0.0983165	-0.2626218
0.0999666	603143.24	14.3026516	76.9660887	-8.9812106	-0.5303951	0.0548733	-0.1934094
0.1000001	603345.38	14.3122397	76.9918824	-6.6498522	-0.3257136	0.0262468	-0.1241449
0.1000185	603456.47	14.3175108	77.0060591	-4.3494951	-0.1469996	0.0131895	-0.0685463
0.1000812	603834.50	14.3354547	77.0542992	-2.0789776	0.0067198	0.0096229	-0.0200095
0.1001451	604220.25	14.3537764	77.1035238	0.1934181	0.1620124	0.0127879	0.0215853
0.1001211	604075.47	14.3468983	77.0850482	2.3896833	0.3264098	0.0211712	0.0604217
0.1000303	603527.71	14.3208913	77.0151492	4.6509887	0.4724129	0.0369698	0.0964486
0.0999562	603080.24	14.2996636	76.9580487	6.8953663	0.6042368	0.0638267	0.1349679
0.0998878	602668.00	14.2801212	76.9054440	9.0686917	0.7494191	0.1056965	0.1695812
0.0998471	602421.90	14.2684606	76.8740388	11.3046254	0.8741701	0.1570187	0.1991816
0.0996908	601479.13	14.2238364	76.7537339	12.4196776	0.9345231	0.1875464	0.2114352
0.0996001	600932.14	14.1979776	76.6839334	13.5398518	0.9983287	0.2217212	0.2237474
0.0995421	600581.88	14.1814316	76.6392375	14.6354467	1.0423838	0.2568013	0.2310768
0.0994654	600118.98	14.1595794	76.5801680	15.7235569	1.0793317	0.2933308	0.2371476
0.0993401	599362.92	14.1239237	76.4836878	16.7833137	1.0933677	0.3256214	0.2406075
0.0992494	598815.93	14.0981560	76.4138873	17.8305067	1.0960422	0.3569731	0.2396294
0.0991892	598452.55	14.0810511	76.3675177	18.8611119	1.0856600	0.3851071	0.2350009
0.0991958	598492.67	14.0829390	76.3726371	19.8690648	1.0554659	0.4094404	0.2229835
0.0991708	598341.46	14.0758236	76.3533411	20.8916115	1.0383336	0.4331947	0.2165404
0.0990774	597778.27	14.0493382	76.2814732	21.9925927	1.0131890	0.4538860	0.2094805

Table 47: Lambda UCAV U=80 mph, h/b=0.10

Mach No.	Re No.	q_c	Uoo	alpha_c	C_L	C_D_c	Cm_cg_c_w
0.0998654	602532.54	14.2737024	76.8881581	-10.3949110	-0.8409042	0.0951609	-0.3315795
0.0999067	602781.97	14.2855226	76.9199874	-9.1818946	-0.6984937	0.0678178	-0.2614432
0.0999532	603062.16	14.2988060	76.9557410	-6.7735132	-0.4292955	0.0299545	-0.1558090
0.0999806	603227.42	14.3066442	76.9768308	-4.4167954	-0.2033723	0.0131699	-0.0796992
0.0999906	603287.68	14.3095025	76.9845197	-2.1149111	-0.0233791	0.0081693	-0.0221072
0.1000686	603758.52	14.3318473	77.0446035	0.1873915	0.1569644	0.0107764	0.0225948
0.1001127	604024.50	14.3444776	77.0785448	2.4018869	0.3366318	0.0195615	0.0623189
0.1000993	603943.59	14.3406348	77.0682196	4.6766266	0.4938879	0.0364253	0.0993330
0.1000286	603517.51	14.3204072	77.0138476	6.9311310	0.6341943	0.0653995	0.1386978
0.0999891	603279.07	14.3090941	76.9834213	9.1106205	0.7845398	0.1090801	0.1752823
0.0998945	602708.38	14.2820344	76.9105959	11.3471214	0.9097660	0.1617618	0.2041767
0.0997975	602122.70	14.2542912	76.8358592	12.4691895	0.9759957	0.1939558	0.2166488
0.0997158	601629.99	14.2309726	76.7729854	13.5832906	1.0347143	0.2283761	0.2268401
0.0996128	601008.69	14.2015949	76.6937012	14.6836343	1.0827470	0.2660247	0.2337373
0.0994691	600141.80	14.1606559	76.5830790	15.7706462	1.1187750	0.3036625	0.2388708
0.0993060	599157.44	14.1142410	76.4574664	16.8229598	1.1265763	0.3360904	0.2405795
0.0991969	598499.43	14.0832572	76.3734999	17.8690068	1.1282910	0.3689017	0.2383983
0.0991176	598020.58	14.0607306	76.3123946	18.8889881	1.1090099	0.3972212	0.2287268
0.0990379	597539.72	14.0381276	76.2510327	19.9035748	1.0843724	0.4227242	0.2185846
0.0989300	596888.66	14.0075532	76.1679520	20.9328353	1.0728638	0.4490538	0.2134935
0.0988924	596661.85	13.9969096	76.1390086	22.0433830	1.0557324	0.4735952	0.2074880

Table 48: Lambda UCAV U=80, h/b=0.05

Mach No.	Re No.	q_c	Uoo	alpha_c	C_L	C_D_c	Cm_cg_c_w
0.1013017	611198.37	14.6872334	77.9939897	-4.4786482	-0.3280556	0.0211323	-0.1111524
0.1012621	610959.55	14.6757577	77.9635139	-2.1750269	-0.0737339	0.0117556	-0.0300190
0.1013509	611495.35	14.7015099	78.0318867	0.1700280	0.1424202	0.0132227	0.0254904
0.1013951	611762.17	14.7143424	78.0659353	2.4034276	0.3379224	0.0217443	0.0677119
0.1013738	611633.62	14.7081593	78.0495314	4.6880832	0.5034843	0.0376762	0.1047045
0.1013834	611691.38	14.7109373	78.0569020	6.9584834	0.6571055	0.0680160	0.1444599
0.1013993	611787.06	14.7155399	78.0691119	9.1468364	0.8148753	0.1131792	0.1806148
0.1014323	611986.21	14.7251216	78.0945242	10.2703786	0.8823397	0.1385499	0.1956606
0.1013918	611741.95	14.7133695	78.0633544	11.3969705	0.9515210	0.1676259	0.2094783
0.1013599	611549.80	14.7041283	78.0388354	12.5249420	1.0226956	0.2004149	0.2224216
0.1013122	611261.91	14.6902872	78.0020976	13.6498946	1.0905037	0.2374881	0.2335942

Table 49: Lambda UCAV U=100 mph, h/b=0.93 (OGE)

Mach No.	Re No.	q_c	Uoo	alpha_c	C_L	C_D_c	Cm_cg_c_w
0.1261694	761236.23	22.7831893	97.1400667	-10.9518828	-0.4329556	0.0570769	-0.1724558
0.1260348	760424.53	22.7346282	97.0364872	-8.7169223	-0.3090198	0.0324673	-0.1296161
0.1260287	760387.68	22.7324247	97.0317845	-6.4788904	-0.1825111	0.0163611	-0.0866714
0.1260531	760534.58	22.7412094	97.0505312	-4.2491676	-0.0629625	0.0092314	-0.0499278
0.1261023	760831.58	22.7589744	97.0884308	-2.0267019	0.0505074	0.0079098	-0.0128489
0.1261846	761328.26	22.7886985	97.1518106	0.2045380	0.1713268	0.0107237	0.0202784
0.1263191	762139.78	22.8373066	97.2553676	2.3605719	0.3020252	0.0186476	0.0548476
0.1264485	762920.46	22.8841166	97.3549893	4.5921537	0.4231310	0.0325870	0.0882014
0.1265386	763464.04	22.9167379	97.4243544	6.8164861	0.5381645	0.0551874	0.1228297
0.1265696	763650.82	22.9279521	97.4481886	8.9587437	0.6573235	0.0896974	0.1547233
0.1265518	763543.61	22.9215149	97.4345080	11.1812891	0.7708602	0.1331637	0.1836468
0.1265405	763475.18	22.9174066	97.4257759	12.2913231	0.8270097	0.1623096	0.1967434
0.1265132	763310.85	22.9075423	97.4048061	13.3916860	0.8742209	0.1912179	0.2050098
0.1264366	762848.64	22.8798082	97.3458244	14.4891768	0.9198639	0.2224589	0.2127813
0.1263697	762444.73	22.8555857	97.2942816	15.5759087	0.9556574	0.2548445	0.2187836
0.1262749	761872.59	22.8212969	97.2212719	16.6431502	0.9759628	0.2847502	0.2229005
0.1261685	761231.10	22.7828825	97.1394126	17.6986110	0.9855626	0.3130874	0.2252856
0.1261009	760823.29	22.7584784	97.0873727	18.7397558	0.9840087	0.3395613	0.2237830
0.1259924	760168.23	22.7193058	97.0037820	19.7543358	0.9593657	0.3600929	0.2157588
0.1259549	759942.09	22.7057903	96.9749244	20.7596225	0.9277759	0.3789351	0.2035979
0.1258753	759462.17	22.6771208	96.9136822	21.8629920	0.9046318	0.3982323	0.1947848

Table 50: Lambda UCAV U=100 mph, h/b=0.3

Mach No.	Re No.	q_c	Uoo	alpha_c	C_L	C_D_c	Cm_cg_c_w
0.1231209	742843.08	21.6955064	94.7929489	-11.0905563	-0.5491125	0.0728284	-0.2057823
0.1229331	741710.29	21.6293880	94.6483950	-8.8240406	-0.3987450	0.0412616	-0.1551430
0.1229431	741770.41	21.6328947	94.6560671	-6.5522790	-0.2439835	0.0204354	-0.1029270
0.1230230	742252.41	21.6610176	94.7175739	-4.2925516	-0.0993021	0.0112119	-0.0586090
0.1231005	742720.22	21.6883303	94.7772705	-2.0459994	0.0343433	0.0090375	-0.0161208
0.1231957	743294.43	21.7218784	94.8505442	0.2099916	0.1758949	0.0116329	0.0214650
0.1232323	743515.33	21.7347914	94.8787330	2.4723004	0.3227385	0.0202545	0.0598223
0.1231491	743013.24	21.7054464	94.8146616	4.6337763	0.4579953	0.0351147	0.0965974
0.1229496	741809.93	21.6351998	94.6611101	6.8716734	0.5843910	0.0600841	0.1343502
0.1227640	740690.23	21.5699357	94.5182264	9.0336815	0.7200935	0.0986584	0.1688131
0.1225367	739318.71	21.4901290	94.3432100	11.2788319	0.8525648	0.1492051	0.2017987
0.1223215	738020.16	21.4147039	94.1775037	12.3843127	0.9049005	0.1799188	0.2123533
0.1221843	737192.29	21.3666870	94.0718602	13.4985868	0.9637640	0.2126156	0.2232242
0.1221641	737070.41	21.3596229	94.0563082	14.5996026	1.0123597	0.2471577	0.2316304
0.1221074	736728.19	21.3397929	94.0126378	15.6864608	1.0482590	0.2822941	0.2373933
0.1220738	736525.99	21.3280808	93.9868353	16.7488709	1.0645174	0.3147895	0.2410338
0.1221025	736698.64	21.3380808	94.0088664	17.8048634	1.0745626	0.3456519	0.2429535
0.1221753	737138.33	21.3635593	94.0649747	18.8369076	1.0653857	0.3729655	0.2382908
0.1221442	736950.61	21.3526800	94.0410206	19.8566149	1.0450375	0.3978180	0.2297553
0.1220166	736180.55	21.3080788	93.9427535	20.8575192	1.0097770	0.4176584	0.2177033
0.1219444	735745.28	21.2828898	93.8872105	21.9633847	0.9887236	0.4391596	0.2111457

Table 51: Lambda UCAV U=100 mph, h/b=0.15

Mach No.	Re No.	q_c	Uoo	alpha_c	C_L	C_D_c	Cm_cg_c_w
0.1236492	746030.74	21.8821038	95.1997208	-11.3171557	-0.7389186	0.0997002	-0.2730910
0.1234927	745086.56	21.8267502	95.0792346	-9.0004386	-0.5465010	0.0548745	-0.2002914
0.1235561	745469.30	21.8491801	95.1280753	-6.6605906	-0.3347083	0.0256062	-0.1274368
0.1236836	746238.19	21.8942747	95.2261925	-4.3549330	-0.1515546	0.0126157	-0.0694846
0.1237563	746676.83	21.9200210	95.2821660	-2.0784147	0.0071913	0.0091994	-0.0199317
0.1237557	746673.41	21.9198206	95.2817304	0.2023676	0.1695088	0.0117143	0.0225449
0.1237189	746451.53	21.9067954	95.2534170	2.3985535	0.3338396	0.0205143	0.0637041
0.1236882	746266.27	21.8959223	95.2297752	4.6586153	0.4788011	0.0363509	0.1020198
0.1236413	745983.03	21.8793048	95.1936320	6.9082837	0.6150568	0.0638363	0.1409001
0.1235286	745303.14	21.8394416	95.1068729	9.0823861	0.7608899	0.1049228	0.1740406
0.1233191	744038.95	21.7654157	94.9455514	11.3312363	0.8964601	0.1607074	0.2054485
0.1231803	743201.79	21.7164641	94.8387224	12.4496364	0.9596174	0.1927399	0.2168752
0.1231167	742817.77	21.6940277	94.7897183	13.5601452	1.0153271	0.2267459	0.2270306
0.1230926	742672.47	21.6855416	94.7711770	14.6596540	1.0626605	0.2630258	0.2339644
0.1229829	742010.56	21.6469041	94.6867117	15.7394559	1.0926491	0.2992009	0.2385836
0.1228589	741262.49	21.6032787	94.5912517	16.7953271	1.1034304	0.3309934	0.2412774
0.1227251	740455.28	21.5562539	94.4882451	17.8369543	1.1014429	0.3603609	0.2400073
0.1225671	739502.14	21.5007939	94.3666169	18.8681209	1.0915309	0.3888956	0.2338688
0.1224623	738870.05	21.4640536	94.2859561	19.8734979	1.0591792	0.4123909	0.2218607
0.1224626	738871.37	21.4641306	94.2861254	20.8982095	1.0438603	0.4371382	0.2148703
0.1224468	738776.35	21.4586099	94.2739991	22.0134022	1.0306197	0.4614319	0.2099635

Table 52: Lambda UCAV U=100 mph, h/b=0.10

Mach No.	Re No.	q_c	Uoo	alpha_c	C_L	C_D_c	Cm_cg_c_w
0.1242016	749363.70	22.0780606	95.6250330	-9.2193216	-0.7298436	0.0708993	-0.2790077
0.1242111	749420.96	22.0814350	95.6323404	-6.7922669	-0.4450041	0.0310762	-0.1643810
0.1242289	749528.26	22.0877587	95.6460331	-4.4257667	-0.2108869	0.0138953	-0.0829112
0.1242835	749858.13	22.1072048	95.6881273	-2.1141141	-0.0227115	0.0090055	-0.0227053
0.1242857	749871.24	22.1079774	95.6897993	0.1958895	0.1640826	0.0115990	0.0229278
0.1243297	750136.36	22.1236134	95.7236320	2.4113928	0.3445943	0.0201997	0.0666408
0.1243692	750374.95	22.1376886	95.7540771	4.6809670	0.4975235	0.0366383	0.1065365
0.1243207	750082.07	22.1204110	95.7167037	6.9380492	0.6399892	0.0660781	0.1455342
0.1241803	749235.13	22.0704855	95.6086269	9.1177695	0.7905280	0.1083432	0.1796122
0.1240718	748580.87	22.0319568	95.5251379	11.3648597	0.9246241	0.1649325	0.2098447
0.1239876	748072.36	22.0020345	95.4602481	12.4866014	0.9905803	0.1977005	0.2208447
0.1238289	747115.12	21.9457625	95.3380962	13.6009541	1.0495097	0.2336436	0.2303271
0.1237344	746544.78	21.9122691	95.2653164	14.7014214	1.0976460	0.2716478	0.2367068
0.1236195	745851.90	21.8716136	95.1768989	15.7747928	1.1222483	0.3076864	0.2398986
0.1234345	744735.26	21.8061731	95.0344062	16.8244755	1.1278460	0.3393000	0.2408635
0.1232329	743518.92	21.7350011	94.8791905	17.8682430	1.1276512	0.3713398	0.2367564
0.1230959	742692.70	21.6867229	94.7737582	18.8862958	1.1067547	0.3992371	0.2272050
0.1229681	741921.41	21.6417030	94.6753357	19.9054008	1.0859019	0.4257217	0.2174303
0.1228607	741273.30	21.6039090	94.5926315	20.9363639	1.0758195	0.4515457	0.2121778
0.1227122	740377.78	21.5517418	94.4783556	22.0547431	1.0652479	0.4783273	0.2071604

Table 53: Lambda UCAV U=100 mph, h/b=0.05

Mach No.	Re No.	q_c	Uoo	alpha_c	C_L	C_D_c	Cm_cg_c_w
0.1253461	756268.97	22.4868273	96.5062033	−4.5074868	−0.3522117	0.0210381	−0.1188398
0.1252697	755807.93	22.4594187	96.4473708	−2.1808526	−0.0786136	0.0113573	−0.0301646
0.1253048	756019.93	22.4720199	96.4744239	0.1790432	0.1499717	0.0126609	0.0257886
0.1253036	756012.45	22.4715755	96.4734698	2.4174934	0.3497043	0.0211492	0.0720685
0.1252997	755988.99	22.4701809	96.4704761	4.7021111	0.5152345	0.0369477	0.1115659
0.1253091	756045.65	22.4735487	96.4777055	6.9828820	0.6775424	0.0692164	0.1503431
0.1252909	755935.97	22.4670291	96.4637101	9.1642653	0.8294742	0.1120351	0.1838936
0.1252593	755745.37	22.4557007	96.4393876	10.2998781	0.9070493	0.1422831	0.2007871
0.1252268	755549.34	22.4440532	96.4143732	11.4306974	0.9797716	0.1727759	0.2141875
0.1252144	755474.50	22.4396070	96.4048229	12.5590015	1.0512247	0.2066509	0.2263545
0.1251288	754958.04	22.4089366	96.3389174	13.6847537	1.1197027	0.2451491	0.2364538

Appendix D: MATLAB Data Reduction Program

```
%************************************************************************
%************************************************************************
%***************     Lt. Gebbie & Capt Anthony DeLuca    ******************
%********   Adapted for the Balance AFIT 1 by Lt. Rivera Parga    *********
%**************    Re-adapted by Troy Leveron, ENS, USNR    ***************
%**** Re-adapted by Brett Jones, ENS, USNR for UCAV Ground Effects Test****
%****** Re-adapted by Won In, Capt, USAF for UCAV Ground Efects Test ******
%******************** Calculation of Lift, Drag, Moments ********************
%************************************************************************
%************************************************************************

%This Code will transfer measured Forces and Moments on the AFIT-1 balance to Wind
%(earth) centered frame of reference by correcting for tare effects, balance
%interactions, and wind tunnel irregularities, then gives a file with all the
%corrected data

clear
clc
close all;
format long
%#########################################################################################
%INPUT DECK
%FIRST FILL THE FOLLOWING INFORMATION
%#########################################################################################

Masskg=1.235;                           % Mass of the UCAV in KGS (~3lbs for now until I weigh it)
T_room = mean([71.1 72.3 71.3 70.0]) + 459.67       %deg R  ****Changed for each day of
testing****
P_barro = mean([29.0636 28.8807 28.8818 28.9872]) * 0.4911541    %Psi   ****Changed for each
day of testing****

% INPUT DATA FILE AND INPUT DATA TARE FILE
load Chevron_P2_tarefile.txt;           %tarefile CHEVRON_tA-10to+20B0NP.txt
TareFile = Chevron_P2_tarefile(:,1:9);
load Chevron_P2_40mph_datafile.txt;       %datafile CHEVRON_40MA-10to+20B0NP.txt
DataFile = Chevron_P2_40mph_datafile(:,1:9);

%Offset distances from the Mounting Block to the Model C.G. (inches)
Y_cmb =  0;
X_cmb = 1.4975;                         %inches  (from origin @ balance center w/ + right)
Z_cmb = 0;



% Required for the Solid body blockage corrections due to wing
% and fuselage
Body_Volume = 63.39038 / 12^3 ;         %ft^3: From Solid Works "Mass Properties"
Wing_Area = 87.3958 / 12^2              %ft^2
```

```
%##########################################################################
%I.-   Room Conditions and Model Specifics :
%      UNITS are in Ft, Sec, lbm, Psf, Rankine, fps
%##########################################################################

Mass = (Masskg * 1000) * 0.0022046;                %lbm (UCAV)
Gas_Const = 1716;                                  %ft-lbf/Slug-R
Density = (P_barro * 144)/(1716 * T_room);         %lbm/ft^3 or lbf-s^2/ft^4
Root_Chord = 7.42/12;                              %ft
Span = 16 / 12;                                    %ft
Aspect_Ratio = Span^2 / Wing_Area;
Kinematic_Viscosity = .372e-6;                     %slug/ft-s
Speed_of_Sound = sqrt(1.4 * T_room * Gas_Const);    %fps

%Distances between sensors (inches) to calculate moments

D1 = (2.10 / 2); D2 = D1; D3 = (1.7 / 2); D4 = D3;

%##########################################################################
%II.-     Solid body blockage corrections due to wing and fuselage (Pope
%pg 369
%##########################################################################

K_1 = 1.04;                          % t/c=.15, 4 digit airfoil
delta = 0.3636;                      %boundary correction factor (b/B) (Ch. 10)
Tau_1 = 0.86;                        %factor from pg 369, fun. of tunnel shape and b/B
X_Section = (31/12)*(44/12);         %ft^2
Wing_Volume = Body_Volume;           %ft^3   Flying Wing UCAV
Epsilon_sb_w = (K_1*Tau_1*Wing_Volume) / X_Section^(3/2)
Epsilon_tunnel_correction = 0.983086;   %from Hot-wire data... ratio between hotwire and
transducer vel
Epsilon_sb_gp = 1.016092;            %Plane # Vel / Open Tunnel Vel as measured by the hot-
wire
Epsilon_tot = Epsilon_sb_w+ (Epsilon_sb_gp*Epsilon_tunnel_correction-1)

%##########################################################################
%VI.- CORRECT FORCES AND MOMENTS FOR BALANCE INTERACTIONS (body axis)
%##########################################################################

%Balance Interactions with off axis elements for the 100 lb balance
%Using average of the 100 lb calibration runs for N1 & N2 and the
%50 lb calibration for S1, S2 & A and 40 lb calibration for L then normalizing by the actual
%sensor (N1, N2,...) in question.  The sensor sequence in each row vector is:
%[N1 N2 S1 S2 A L]

N1_I = ([7.316 -0.735 0.195 0.018 -0.113 -0.073 ] + [7.207 -0.74 0.297 0.021 -0.062 0.021])/2;
   N11 = N1_I(1,1)/100;

N2_I = ([-0.109 7.64 0.015 0.118 0.043 -0.017] + [-0.173 7.481 0.041 0.151 0.064 0.02])/2;
   N22 = N2_I(1,2)/100;

S1_I = ([0.01 0.01  7.517 -0.439 0.058 -0.005] + [0.021 0.01 7.36 -0.443 0.053 0.048])/2;
```

```
   S11 = S1_I(1,3)/50;

S2_I = ([-0.005 -0.006 -0.108 7.286 -0.027 0.028] + [0 0 -0.132 7.015 -0.019 -0.031])/2;
   S22 = S2_I(1,4)/50;

A_I = ([0 0.004 -0.01 0.011 7.612 0.104] + [-0.05 0.042 -0.02 0.01 7.546 0.054])/2;
   A11 = A_I(1,5)/50;

L_I = ([-0.079 0.066 0.033 0.025 0.525 8.695] + [-0.09 0.04 0 -0.03 0.492 8.709])/2;
   L11 = L_I(1,6)/40;

N1_normalized = (N1_I/100)  .* [N11 N22 S11 S22 A11 L11].^(-1);
N2_normalized = (N2_I/100) .* [N11 N22 S11 S22 A11 L11].^(-1);
S1_normalized = (S1_I/50)  .* [N11 N22 S11 S22 A11 L11].^(-1);
S2_normalized = (S2_I/50)  .* [N11 N22 S11 S22 A11 L11].^(-1);
A_normalized = (A_I/50)    .* [N11 N22 S11 S22 A11 L11].^(-1);
L_normalized = (L_I/40)    .* [N11 N22 S11 S22 A11 L11].^(-1);

Interactions_Kij = [N1_normalized' N2_normalized' S1_normalized' S2_normalized'
A_normalized' L_normalized'];

%###########################################################################
% III.-  Load the static tare data for the alpha sweep w/o the wind ,
%        separate each force from the file, and fit a 4th order poly
%        as an x-y plot (AoA vs.Force) for each of the 6 force sensors.
%###########################################################################

%load tare1.txt;                    %Raw tare data file to be read in.
FILE=TareFile(:,1:9);                %GP42005tearA-10to+20B0model

j=1;
k=1;
L=length(FILE);

for i=1:L                          %Run for all data points # of rows
   if i~=L                         %if current row is not last row, go to next
      NEXT=i+1;                    %set next equal to the value of the next row
      VALUE2=FILE(NEXT,1);         %set value2 as next row column 1
   else if i==L                    %unless the it is the last value
      VALUE2=50;                   %value2 set to 50 to end the sequence
   end
   end
   A(j,:)=FILE(i,:);               %set row j of A equal to row i of FILE
   VALUE1=FILE(i,1);               %set value1 equal to row i column 1 of FILE
   if VALUE1==VALUE2               %if value1 equals value2, go to next row
      j=j+1;
   else if VALUE1~=VALUE2          %if value1 and value2 are different check
      if length(A(:,1))<5          %if less than 20 values, ignored due to angle change
         j=1;
         clear A;
      else if length(A(:,1))>5     %if more than 20 values
            C=length(A(:,1));      %find length of A
```

```
            for m=1:9              %Average all rows of the like values in A
               B(k,m)=mean(A(4:C,m));  %disregarding first 10 for vibrations
            end
            j=1;
            k=k+1;
            clear A
        end
        end

    end
    end
end

if B(k-1,1)<B((k-2),1)
    B=B(1:(k-2),:)
end

tare=[B];

%_____________________________________End of inserted code
[row,col] = size(tare);


for k = 1:row;

theta_tare(k,:,:)   = tare(k,1).* (pi/180);
N1_tare(k,:,:)      = tare(k,4);
N2_tare(k,:,:)      = tare(k,5);
S1_tare(k,:,:)      = tare(k,7);
S2_tare(k,:,:)      = tare(k,8);
A_tare(k,:,:)       = tare(k,6);
L_tare(k,:,:)       = tare(k,9);
end

N1_poly = polyfit(theta_tare,N1_tare,4);
N2_poly = polyfit(theta_tare,N2_tare,4);
S1_poly = polyfit(theta_tare,S1_tare,4);
S2_poly = polyfit(theta_tare,S2_tare,4);
A_poly  = polyfit(theta_tare,A_tare,4) ;
L_poly  = polyfit(theta_tare,L_tare,4) ;

clear ('B','C','D','L')
%##########################################################################
%IV.- Load the specific test run files,
%##########################################################################

%clear ('AA','B','C','L')

%load data1.txt;                    %Raw data file to be read in:
FILE=DataFile(:,:);                 %Same as above
```

```
j=1;
k=1;
L=length(FILE);

for i=1:L                          %Run for all data points # of rows
   if i~=L                         %if current row is not last row, go to next
      NEXT=i+1;                    %set next equal to the value of the next row
      VALUE2=FILE(NEXT,1);         %set value2 as next row column 1
   else if i==L                    %unless the it is the last value
      VALUE2=50;                   %value2 set to 50 to end the sequence
   end
   end
   A(j,:)=FILE(i,:);               %set row j of A equal to row i of FILE
   VALUE1=FILE(i,1);               %set value1 equal to row i column 1 of FILE
   if VALUE1==VALUE2               %if value1 equals value2, go to next row
      j=j+1;
   else if VALUE1~=VALUE2          %if value1 and value2 are different check
      if length(A(:,1))<5          %if less than 20 values, ignored due to angle change
         j=1;
         clear A;
      else if length(A(:,1))>5     %if more than 20 values
            C=length(A(:,1));      %find length of A
            for m=1:9              %Average all rows of the like values in A
               B(k,m)=mean(A(4:C,m));    %disregarding first 10 for vibrations
            end
            j=1;
            k=k+1;
            clear A
      end
      end
   end
   end
end

if B(k-1,1)<B((k-2),1)
   B=B(1:(k-2),:)
end

sample_data=[B];

%_____________________________________End of inserted code
[row2,col2] = size(sample_data);


for i = 1:row2;

%Angles of the model during test runs (Roll, Pitch {AoA}, Yaw {Beta}):

phi               = 0;
theta(i,:)        = sample_data(i,1) .* (pi/180);       %radians
si(i,:)           = sample_data(i,2) .* (pi/180);       %radians
Wind_Speed(i,:)   = sample_data(i,3) .* (5280/3600);    %fps
```

```
%Flight Parameters (Re#, Ma#, Dynamic Pressure):

q = (.5 * Density) .* Wind_Speed.^2;                    %lbf/ft^2
q_Corrected = q .* (1 + Epsilon_tot)^2;                 %lbf/ft^2
Wind_Speed_Corrected = Wind_Speed .* (1 + Epsilon_tot); %fps
Wind_Speed_Corrected_mph = Wind_Speed_Corrected.*(3600/5280);
Mach_Number = Wind_Speed_Corrected ./ Speed_of_Sound;   %NonDimensional
Reynolds_Number = ((Density * Root_Chord) .* Wind_Speed_Corrected) ./ Kinematic_Viscosity;
%NonDimensional
Flight_Parameters = [Mach_Number Reynolds_Number q_Corrected];

%individual forces and moments for each sensor:

%NEW NOTATION
N1_test(i,:,:)      = sample_data(i,4);
N2_test(i,:,:)      = sample_data(i,5);
S1_test(i,:,:)      = sample_data(i,7);
S2_test(i,:,:)      = sample_data(i,8);
A_test(i,:,:)       = sample_data(i,6);
L_test(i,:,:)       = sample_data(i,9);
%###########################################################################
%V.-   Subtract the effect of the static
%      weight with the tare polynominals above
%###########################################################################

%Evaluating the actual test theta angle (AoA) in the tare polynominal to
%determine the tare values for the angles tested in each run.

N1_eval = polyval(N1_poly,theta);
N2_eval = polyval(N2_poly,theta);
S1_eval = polyval(S1_poly,theta);
S2_eval = polyval(S2_poly,theta);
A_eval  = polyval(A_poly,theta);
L_eval  = polyval(L_poly,theta);

%The Time-Averaged (raw) forces and momentums NF,AF,SF,PM,YM AND RM measurd in the
wind
%tunnel (body axis) with the tare effect of the weight subtracted off.

N1_resolved = N1_test - (N1_eval);
N2_resolved = N2_test - (N2_eval);
S1_resolved = S1_test - (S1_eval);
S2_resolved = S2_test - (S2_eval);
A_resolved  = A_test -  (A_eval);
L_resolved  = L_test -  (L_eval);

%Forces_minus_tare = [NF_resolved, AF_resolved, PM_resolved, RM_resolved, YM_resolved,
SF_resolved]';
Forces_minus_tare = [N1_resolved N2_resolved S1_resolved S2_resolved A_resolved
L_resolved]';
```

```
%Forces N1, N2, S1, S2, A, & L corrected for the balance interactions (body axis)

Corrected_Data = (inv(Interactions_Kij) * Forces_minus_tare)

%#########################################################################
%VII.- Calculation of the Axial, Side, & Normal Forces from the corrected balance
%      forces in the Body Axis reference frame
%#########################################################################

Forces_b(:,i) = [Corrected_Data(5,i); Corrected_Data(3,i) + Corrected_Data(4,i);
Corrected_Data(1,i) + Corrected_Data(2,i)];

%Calculation of the Drag, Side, & Lift Forces in the Wind Axis reference
%frame

Forces_w =
[Forces_b(1,:).*cos(theta').*cos(si')+Forces_b(2,:).*sin(si')+Forces_b(3,:).*sin(theta').*cos(si');
          -Forces_b(1,:).*sin(si').*cos(theta')+Forces_b(2,:).*cos(si')-
Forces_b(3,:).*sin(theta').*sin(si');
          -Forces_b(1,:).*sin(theta')+Forces_b(3,:).*cos(theta')];

%First entry is the moments calculated by the balance or direct calculation
%in the Body Reference Frame.  Balance measures Roll (l), Yaw is about the
%z-axis (n), and Pitch is about the y-axis (m).  Distances from strain
%gages to C.G. are in INCHES.  Moments are in-lbf

m = Corrected_Data(1,i) * D1 - Corrected_Data(2,i) * D2;
n = Corrected_Data(3,i) * D3 - Corrected_Data(4,i) * D4;

Moments_b(:,i) = [Corrected_Data(6,i); m; n];

%Second entry is the conversion from the "Balance Centeric" moments to the
%Wind Reference monments with respect to the Balance Center (bc)


Moments_w_bc = [Moments_b(1,:).*cos(theta').*cos(si')-
Moments_b(2,:).*sin(si')+Moments_b(3,:).*sin(theta').*cos(si');

Moments_b(1,:).*sin(si').*cos(theta')+Moments_b(2,:).*cos(si')+Moments_b(3,:).*sin(theta').*sin(si'
);
          -Moments_b(1,:).*sin(theta')+Moments_b(3,:).*cos(theta')];


%Finally, the balance centered moments are converted to moments about the
%Model's Center of Mass (cm) or Center of Gravity (CG)

cgdist=sqrt((X_cmb)^2+(Z_cmb)^2);       %Obtaining the direct distance between the center of the
balance and %the center of mass
w=atan(-Z_cmb/X_cmb);                   %Obtaining the angle between cgdist and the x axes at zero
angle of %attack
```

```
X_cm(i,:)= cos(theta(i,:)+w)*cos(si(i,:))*(cgdist);
Y_cm(i,:) = Y_cmb + X_cm(i,:)*tan(si(i,:));
Z_cm(i,:)= -sin(theta(i,:)+w)*(cgdist);


Moments_w_cg_u = [Moments_w_bc(1,:) + Z_cm(i,:)*Forces_w(2,:) + Forces_w(3,:)* Y_cm(i,:);
            Moments_w_bc(2,:) - X_cm(i,:)*Forces_w(3,:) + Forces_w(1,:)* Z_cm(i,:);
            Moments_w_bc(3,:) - Y_cm(i,:)*Forces_w(1,:) - Forces_w(2,:)* X_cm(i,:)];

%#########################################################################

%VIII.- Calculation of the actual Lift and Drag nondimensional Coefficients, uncorrected for tunnel
effects, %(Cl and Cd)
%#########################################################################

C_D_u = Forces_w(1,:) ./ (q_Corrected' .* Wing_Area);
C_Y_u = Forces_w(2,:) ./ (q_Corrected' .* Wing_Area);
C_L_u = Forces_w(3,:) ./ (q_Corrected' .* Wing_Area);  %Keuthe & Chow pg 178
Coefficients = [C_L_u; C_D_u; C_Y_u]';
% Ave_Cl = mean(Coefficients(:,1));
% Ave_Cd = mean(Coefficients(:,2));

end

%#########################################################################
%IX          Drag Coefficient Correction
%#########################################################################

C_D_o = min(Coefficients(:,2));
C_L_u_sqrd = Coefficients(:,1).^2;
Delta_C_D_w = ((delta * Wing_Area) / X_Section) .* C_L_u_sqrd;
C_D_Corrected = C_D_u' + Delta_C_D_w;

%#########################################################################
%X.-  Angle of Attack due to upwash Correction
%#########################################################################

alpha = sample_data(:,1);
Delta_alpha_w = ((delta * Wing_Area) / X_Section) .* (57.3 * C_L_u);
alpha_Corrected = alpha + Delta_alpha_w';

%#########################################################################
%XI.-  Pitching Moment Correction
%#########################################################################

c_bar = (mean([7.42, 7.42, 7.42, 3.7442, 0])) / 12; %ft = Mean Chord of wing taken at five equal
stations

Cl_w_cg =   Moments_w_cg_u(1,:) ./ (q_Corrected' .* (Wing_Area * Span*12));
Cm_w_cg_u = Moments_w_cg_u(2,:) ./ (q_Corrected' .* (Wing_Area * c_bar*12));
Cn_w_cg =   Moments_w_cg_u(3,:) ./ (q_Corrected' .* (Wing_Area * Span*12));
```

```
Cm_w_cg_corrected = Cm_w_cg_u;         %No Tail
Corrected_Moment_Coefficients = [Cl_w_cg' Cm_w_cg_corrected' Cn_w_cg'];

%OBTAINING THE MOMENTS COEFFICIENTS CORRECTED ABOUT THE CENTER OF THE
%BALANCE

Cl_w_bc =   Moments_w_bc(1,:) ./ (q_Corrected' .* (Wing_Area * Span*12));
Cm_w_bc_u = Moments_w_bc(2,:) ./ (q_Corrected' .* (Wing_Area * c_bar*12));
Cn_w_bc =   Moments_w_bc(3,:) ./ (q_Corrected' .* (Wing_Area * Span*12));

Cm_w_bc_corrected = Cm_w_bc_u;
Corrected_Moment_Coefficients_bc = [Cl_w_bc' Cm_w_bc_corrected' Cn_w_bc'];

%##########################################################################
%XII.- OUTPUT VARIABLES FORMATING
%##########################################################################

alpha = sample_data(:,1);

fprintf('   Mach Number Reynolds Number Dynamic Pressure(Psf)\r')
Flight_Parameters
fprintf(' \r');
fprintf(' Loads are in lbf and arranged [D S L] across the top and increments of alpha down the
side \r')
Forces_w'
fprintf(' \r')
fprintf(' Moments are in in-lbf and arranged [L M N] down the side and increments of alpha along
the top \r')
Moments_w_cg_u
fprintf(' \r')
fprintf('      Cl_u          Cd_u           CY_u \r');
Coefficients
fprintf(' \r')
fprintf('    Del_CD_w       CD_u     CD_Corrected \r');
Compare_CD = [Delta_C_D_w C_D_u' C_D_Corrected]
fprintf(' \r')
fprintf('    Del_alpha_w    alpha_g     alpha_Corrected \r');
Compare_alpha = [Delta_alpha_w' alpha alpha_Corrected ]
fprintf(' \r')
fprintf('    Cl_cg_wind    Cm_cg_corrected_w     Cn_cg_wind \r');
Corrected_Moment_Coefficients
fprintf(' \r')
fprintf('      M#          Re#          q_c          Uoo        alpha_c       C_L       C_D_c      Cl_cg_w
Cm_cg_c_w    Cn_cg_w       C_Y\r');
YY=[Flight_Parameters (Wind_Speed_Corrected .* (3600/5280)) alpha_Corrected C_L_u'
C_D_Corrected Corrected_Moment_Coefficients C_Y_u']%pressure]
%XX=['M#' 'Re#' 'q_c'  'Uoo' 'alpha_c' 'C_L' 'C_D_c' 'Cl_cg_w' 'Cm_cg_c_w' 'Cn_cg_w \r'];

%ZZ=[XX; YY];
wk1write('output.xls',YY,2,1)
```

Bibliography

1. Jones, Brett L. *Experimental Investigation into the Aerodynamic Ground Effect of a Tailless Chevron-shaped UCAV.* MS thesis, AFIT/GAE/ENY/05-J04, Department of Aeronautics and Astronautics, Air Force Institute of Technology (AU), Wright-Patterson AFB, OH, June 2005.

2. Pendleton, Linda D. "Ground Effect." *AV Web.* Aviation Publishing Group, 2005. 2 April 2005 http://www.avweb.com/news/airman/185905-1.html.

3. Wyatt, Earl C. and Michael J. Hirschberg. "Transforming the Future Battlefield: The DARPA / Air Force Unmanned Combat Air Vehicle (UCAV) Program," *AIAA/ICAS International Air and Space Symposium and Exposition: The Next 100 Years*, AIAA 2003-2616: 1-8 (July 2003).

4. "Joint Unmanned Combat Air Systems." Excerpt from unpublished article. n.pag. 6 April 2005 http://www.darpa.mil/j-ucas/.

5. Curry, Robert E. *Dynamic Ground Effect for a Cranked Arrow Wing Airplane*. NASA TM 4799, 1997.

6. Tirpak, John A. "The Robotic Air Force," *Journal of the Air Force Association,* 80 (9) (September 1997) n.pag. 4 April 2005 http://www.afa.org/magazine/sept1997/0997robot.asp.

7. Reed, Shad A. *Subsonic Aerodynamic Stability and Control Assessment of Advanced Aerial Vehicle Configurations*. MS thesis, School of Graduate Studies, Wright State University, Dayton, OH, March 1998.

8. Wieselsberger, C. *Wing Resistance Near the Ground.* NACA TM 77, 1922.

9. Fink, Marvin P. and James L. Lastinger. *Aerodynamic Characteristics of Low-Aspect-Ratio Wings in Close Proximity to the Ground.* NASA TN D-926, 1961.

10. Le Sueur, Maurice. *Ground Effect on the Take-off and Landing of Airplanes.* NACA TM 771, 1934.

11. McCormick, Barnes W. *Aerodynamics, Aeronautics, and Flight Mechanics.* New York: John Wiley and Sons, Inc, 1995.

12. Baker, Paul A., William G. Schweikhard, and William R. Young. *Flight Evaluation of Ground Effect on Several Low-Aspect-Ratio Airplanes.* NASA TN D-6053, 1970.

13. Lee, Pai Hung, C. Edwards Lan, and Vincent U. Muirhead. *An Experimental Investigation of Dynamic Ground Effect.* NASA CR 4105, 1987.

14. Curry, Robert E. and Lewis R. Owens. *Ground-Effect Characteristics of the Tu-144 Supersonic Transport Airplane.* NASA TM 2003-212035, 2003.

15. Raymond, Arthur E. *Ground Influence on Aerofoils.* NACA TN 67, 1921.

16. Schweikhard, William. "A Method for In-Flight Measurement of Ground Effect on Fixed-Wing Aircraft," *Journal of Aircraft,* 4 (2): 101-104 (March-April 1967).

17. Chang, Ray Chung and Vincent U. Muirhead. "Effect of Sink Rate on Ground Effect of Low-Aspect-Ratio Wings," *Journal of Aircraft,* 24 (3): 176-180 (March 1986).

18. Corda, Stephen and others. *Dynamic Ground Effects Flight Test of an F-15 Aircraft.* NASA TM 4604, 1994.

19. McDonnell Douglas Corporation, *USAF Stability and Control DATCOM,* U.S. Air Force Flight Dynamics Laboratory, Wright-Patterson AFB, OH, Oct. 1960 (Revised Apr. 1976).

20. Turner, Thomas R. "Endless-belt Technique for Ground Simulation," *Proceedings of Conference on VTOL/STOL Aircraft,* NASA SP 116, Paper 25: 445, (1966).

21. Kemmerly, Guy T. and John W. Paulson, Jr. *Investigation of a Moving-Model Technique for Measuring Ground Effects.* NASA TM 4080, 1989.

22. Gebbie, David A. *Experimental Study of the Subsonic Aerodynamics of a Blended Wing Body Air Vehicle with a Focus on Rapid Technology Assessment.* MS thesis, AFIT/GAE/ENY/05-M09, Department of Aeronautics and Astronautics, Air Force Institute of Technology (AU), Wright-Patterson AFB, OH, March 2005.

23. DeLuca, Anthony M. *Experimental Investigation into the Aerodynamic Performance of Both Rigid and Flexible Wing Structured Micro-Air-Vehicles.* MS thesis, AFIT/GAE/ENY/04-M06, Department of Aeronautics and Astronautics, Air Force Institute of Technology (AU), Wright-Patterson AFB, OH, March 2004.

24. Barlow, Jewel B. and others. *Low-Speed Wind Tunnel Testing* (3rd Edition). New York: John Wiley and Sons, 1999.

25. Rivera Parga, Jose R. *Wind Tunnel Investigation of the Static Stability and Control Effectiveness of a Rotary Tail in a Portable UAV.* MS thesis, AFIT/GAE/ENY/04-D02, Department of Aeronautics and Astronautics, Air Force Institute of Technology (AU), Wright-Patterson AFB, OH, December 2004.

26. *Eden 333.* Technical Specifications. Stratasys Inc. © 2003. 3 May 2005 http://www.stratasys.com/NA/pdfs/PS_eden333.pdf.

27. *FullCure™ 700 Series.* Technical Specifications. Stratasys Inc. © 2005. 25 March 2005 http://www.stratasys.com/NA/pdfs/Eden_FullCure700.pdf.

28. Westfall, James T. *Aero 543 Final.* MS Aero 543 Class Report, Department of Aeronautics and Astronautics, Air Force Institute of Technology (AU), Wright-Patterson AFB, OH, December 2005.

29. Adamczak, D. W. "Experimental Investigation of a Lambda Wing Configuration," WL-TR-96-3148, February 1996.

30. Gatlin, G. M., McGrath, B. E. "Low-Speed Longitudinal Aerodynamic Characteristics Through Poststall for Twenty-One Novel Planform Shapes," NASA-TP-3503, August 1995.

31. Fears, S. P., Ross, H. M., Moul, T. M. "Low-Speed Wind-Tunnel Investigation of the Stability and Control Characteristics of a Series of Flying Wings with Sweep Angles of 50°," NASA-TM-4640, June 1995.

32. Ross, H. M., Fears, S. P., Moul, T. M. "Low-Speed Wind-Tunnel Investigation of the Stability and Control Characteristics of a Series of Flying Wings with Sweep Angles of 60°," NASA-TM-4641, June 1995.

33. Moul, T. M., Fears, S. P., Ross, H. M. "Low-Speed Wind-Tunnel Investigation of the Stability and Control Characteristics of a Series of Flying Wings with Sweep Angles of 70°," NASA-TM-4642, June 1995.

Vita

Won In was born in Kimpo, South Korea. His family immigrated to the United States in 1979 and Won grew up in College Park, Maryland. He graduated from High Point High School in 1987. He attended the University of Maryland, College Park campus and received a BS in Mechanical Engineering in 1994. He originally joined the United States Air Force in Novermber 1990 and finished his technical training as a Korean Cryptologic Linguist at the Goodfellow AFB. His first assignment as a linguist was at the Osan AB, South Korea where he served two one-year tours in 1991 and 1995. He also served as a linguist at the National Security Agency from 1992 to1994, where he was accepted to the Bootstrap program to finish his BS degree at the University of Maryland. His last tour as a linguist was at the Davis Monthan AFB with the 43rd Electronic Combat Squadron flying in the backend of an EC-130H, Compass Call. After serving as a linguist for seven years, he worked as a civilian controls engineer in San Diego, California. After working three years as a civilian, he was accepted to the OTS class 0107 and received his Air Force commission in August 2001. His first assignment as an officer was at the Tinker AFB as a propulsion engineer. During his duty at the Tinker AFB, he was deployed during the Operation Iraqi Freedom as an Air Battle Damage Repair engineer to design repairs for damaged KC-135 tankers for their safe flight back home. After Tinker AFB, he was accepted to the Air Force Institute of Technology for masters program in Astronautical Engineering. Won enjoys golf, snowboarding and spending quality time with his two boysand his wife of 14 yearsas much as his duty permits. Most of all he enjoys serving God and his country, the USA.

REPORT DOCUMENTATION PAGE

Form Approved
OMB No. 074-0188

1. REPORT DATE *(DD-MM-YYYY)*	**2. REPORT TYPE**	**3. DATES COVERED** *(From – To)*
17 Mar 06	**Master's Thesis**	28 Jul 04 – 17 Mar 06

4. TITLE AND SUBTITLE
Experimental Investigation Into the Aerodynamic Ground Effect of a Tailless Chevron and Lambda-shaped UCAVs

5a. CONTRACT NUMBER

5b. GRANT NUMBER

5c. PROGRAM ELEMENT NUMBER

6. AUTHOR(S)

IN, WON, Captain, USAF

5d. PROJECT NUMBER

5e. TASK NUMBER

5f. WORK UNIT NUMBER

7. PERFORMING ORGANIZATION NAMES(S) AND ADDRESS(S)
Air Force Institute of Technology
Graduate School of Engineering and Management (AFIT/ENY)
2950 Hobson Way
WPAFB OH 45433-7765

8. PERFORMING ORGANIZATION REPORT NUMBER

AFIT/GAE/ENY/06-M16

9. SPONSORING/MONITORING AGENCY NAME(S) AND ADDRESS(ES)
AFRL/VAAA
Attn: Mr. Dieter Multhopp
3550 Aberdeen Rd. SE
WPAFB OH 45433 DSN: 246-2871

10. SPONSOR/MONITOR'S ACRONYM(S)

11. SPONSOR/MONITOR'S REPORT NUMBER(S)

12. DISTRIBUTION/AVAILABILITY STATEMENT
APPROVED FOR PUBLIC RELEASE; DISTRIBUTION UNLIMITED.

13. SUPPLEMENTARY NOTES

14. ABSTRACT As future aircraft migrate toward tailless, blended wing body configurations, aircraft designers are faced with a lack of experimental data that represent these types of configurations. A wind tunnel investigation was conducted to identify the ground effect region of two unmanned combat air vehicle (UCAV) models. The AFIT low-speed wind tunnel (LSWT) and ground plane were used to study the forces and moments on the UCAV models in ground effect. The Chevron and Lambda planforms used in this study were originally tested in full-scale for stability and control without ground effects. A static ground plane was used in this study. Hot-wire results showed a minimal difference between the transducer velocity and the hot-wire measured velocity and these differences were accounted for as wind tunnel blockage. In addition to hot-wire results, flow visualization results revealed the AFIT LSWT had an adequate testing environment for the use of the ground plane.
The ground effect region for the Chevron and Lambda UCAVs was characterized by an increase in lift, drag, and a decrease in lift-to-drag ratio. These trends were also noted in previous studies of similar aspect ratio and wing sweep.

15. SUBJECT TERMS
Ground Effect, Ground Plane Flow Analysis, Chevron and Lambda UCAVs

16. SECURITY CLASSIFICATION OF:			**17. LIMITATION OF ABSTRACT**	**18. NUMBER OF PAGES**	**19a. NAME OF RESPONSIBLE PERSON**
REPORT	**ABSTRACT**	**c. THIS PAGE**			MILTON E. FRANKE
U	**U**	**U**	**UU**	147	**19b. TELEPHONE NUMBER** *(Include area code)* (937) 255-6565, e-mail: MILTON.FRANKE@afit.edu

Standard Form 298 (Rev: 8-98)
Prescribed by ANSI Std. Z39-18